



HAL
open science

Target identification using electroreception

Chun-Hsiang Tsou

► **To cite this version:**

Chun-Hsiang Tsou. Target identification using electroreception. Modeling and Simulation. Université Grenoble Alpes, 2017. English. NNT : 2017GREAM099 . tel-01887572

HAL Id: tel-01887572

<https://theses.hal.science/tel-01887572>

Submitted on 4 Oct 2018

HAL is a multi-disciplinary open access archive for the deposit and dissemination of scientific research documents, whether they are published or not. The documents may come from teaching and research institutions in France or abroad, or from public or private research centers.

L'archive ouverte pluridisciplinaire **HAL**, est destinée au dépôt et à la diffusion de documents scientifiques de niveau recherche, publiés ou non, émanant des établissements d'enseignement et de recherche français ou étrangers, des laboratoires publics ou privés.

THÈSE

Pour obtenir le grade de

DOCTEUR DE LA COMMUNAUTÉ UNIVERSITÉ GRENOBLE ALPES

Spécialité : Mathématiques Appliquées

Arrêté ministériel : 25 mai 2016

Présentée par

Chun-Hsiang TSOU

Thèse dirigée par **Faouzi TRIKI**
et codirigée par **Eric BONNETIER**, Université Grenoble Alpes
préparée au sein du **Laboratoire Laboratoire Jean Kuntzmann**
dans **l'École Doctorale Mathématiques, Sciences et
technologies de l'information, Informatique**

Identification d'une cible par l'électro- localisation

Target identification using electroreception

Thèse soutenue publiquement le **22 décembre 2017**,
devant le jury composé de :

Monsieur ERIC BONNETIER

PROFESSEUR, UNIVERSITE GRENOBLE ALPES, Co-directeur de
thèse

Monsieur JIN CHENG

PROFESSEUR, UNIVERSITE DE FUDAN A SHANGHAI - CHINE,
Rapporteur

Monsieur PAUL SACKS

PROFESSEUR, UNIVERSITE DE L'IOWA - ETATS-UNIS, Rapporteur

Monsieur LAURENT DESBAT

PROFESSEUR, UNIVERSITE GRENOBLE ALPES, Président

Madame FLORENCE HUBERT

PROFESSEUR, UNIVERSITE AIX-MARSEILLE, Examineur

Monsieur FAOUZI TRIKI

MAITRE DE CONFERENCES, UNIVERSITE GRENOBLE ALPES,
Directeur de thèse



UNIVERSITÉ GRENOBLE-ALPES

Doctoral School ED MSTII 217

University Department **Laboratoire Jean Kuntzmann**

Thesis defended by **Chun-Hsiang TSOU**

Defended on **22nd December, 2017**

In order to become Doctor from Université Grenoble-Alpes

Academic Field **Applied Mathematics**

Thesis Title

Target identification using electroreception

Thesis supervised by Faouzi TRIKI Supervisor
Eric BONNETIER Co-Supervisor

Committee members

<i>Referees</i>	Jin CHENG	Professor at Fudan University
	Paul SACKS	Professor at Iowa Stat University
<i>Examiners</i>	Laurent DESBAT	Professor at Université Grenoble-Alpes
	Florence HUBERT	Professor at Université Aix-Marseille
<i>Supervisors</i>	Faouzi TRIKI	HDR Associate Professor at Université Grenoble-Alpes
	Eric BONNETIER	Professor at Université Grenoble-Alpes

The Université Grenoble-Alpes neither endorse nor censure authors' opinions expressed in the theses: these opinions must be considered to be those of their authors.

Keywords: inverse problem, conduction equation, electroreception

Mots clés : problème inverse, équation de conduction, électro-localisation

This thesis has been prepared at

Laboratoire Jean Kuntzmann

Bâtiment IMAG

Université Grenoble Alpes

700 Avenue Centrale

38401 Domaine Universitaire de Saint-Martin-
d'Hères

France

☎ +33 4 57 42 17 36

Web Site <https://www-ljk.imag.fr/>



TARGET IDENTIFICATION USING ELECTRORECEPTION**Abstract**

Electrolocation is the name given to the sensor ability for certain electric fish robots, which are able to detect electrostatic perturbations caused to the presence of some objects in their neighborhood. This ability to interpret an electrical signal to locate itself in space opens important perspectives, including in the field of biologically inspired robotics. Mathematically, electrolocation is linked to the electric impedance tomography: so it's about a non-linear inverse problem, particularly ill-posed problem. We will, in this Phd, study some methods of reconstruction, which could be obtain robustly some characteristic of the obstacle's shape, rather all of their geometry details. So, it's about to study the stability between the observable part of the obstacles and the errors of measurements.

Keywords: inverse problem, conduction equation, electroreception

IDENTIFICATION D'UNE CIBLE PAR L'ÉLECTRO-LOCALISATION**Résumé**

L'électro-localisation est le nom donné aux capacités sensorielles de certains poissons électriques, vivant en eaux troubles, capables de détecter les perturbations électrostatiques dues à la présence d'objets dans leurs voisinages. Cette aptitude à interpréter un signal électrique pour se repérer dans l'espace ouvre l'importance perspectives, notamment dans le domaine de la robotique bio-inspiré. Mathématiquement, l'électro-localisation est proche de la tomographie d'impédance électrique : il s'agit donc d'un problème inverse non linéaire, notoirement mal posé. Nous proposons dans cette thèse d'étudier des méthodes de reconstruction qui permettraient d'obtenir de manière robuste certaines caractéristiques de la forme des obstacles, plutôt que l'ensemble des détails de leurs géométries. Il s'agit donc d'étudier la stabilité de la partie observable des obstacles par rapport à des erreurs dans les mesures.

Mots clés : problème inverse, équation de conduction, électro-localisation

Laboratoire Jean Kuntzmann

Bâtiment IMAG – Université Grenoble Alpes – 700 Avenue Centrale – 38401
Domaine Universitaire de Saint-Martin-d'Hères – France

Remerciements

Après avoir effectué des efforts pendant ces trois ans, j'ai finalement atteint à la dernière phase de la thèse en octobre 2017. Au fond, je n'avait pas cru que j'aurai terminer les travaux recherches du sujet au bout de trois ans comme prévu. Il ne serais pas possible que cette thèse, bien que mon nom apparaisse sur le champs auteur, soit réalisable aujourd'hui sans les contributions des personnes suivantes que je vais remercier ici.

Tout d'abord, je remercie mon directeur de thèse Eric Bonnetier. Malgré qu'il était très occupé par son travail de directeur du laboratoire Jean Kuntzmann, il m'a guidé beaucoup sur les sujets mathématiques et aussi sur la rédaction des articles scientifiques. Je suis très impressionné par sa gentillesse, son enthousiasme et sa façon d'explication très pédagogique. J'espère que j'aurai encore des opportunités de le rejoindre dans l'avenir.

Je dois également remercier à Faouzi Triki, mon co-directeur de thèse. Il m'a déjà pris en contact quand j'étais en deuxième année à l'école des mines. Faouzi et Eric étaient également les encadrants de mon stage du master. Pendant la période de la thèse, j'avais discuté régulièrement avec Faouzi sur les difficultés mathématiques. A part les sujets mathématiques, Faouzi m'a aidé aussi pour trouver le financement de la thèse, pour valoriser les travaux recherches, pour développer le réseau au sein de la communauté scientifique.

Mazen Alamir, mon co-encadrant de thèse en Gipsa-lab, m'a enrichi un point de vu différent que les mathématiciens concernent. Il m'a inspiré des applications potentielles de ce sujet au monde industriel.

Je n'oublierais pas mes collègues au LJK. Je me sentais très agréable de travail avec eux. Nous avons partagé les expériences de la recherche, d'enseignements ou justement des échanges amicaux. Je souligne ici les doctorants passés et présents dans l'équipe EDP, notamment ce qui travail en problèmes inverses. Merci à Qui Xue, Margaux Vauthrin, Abdelfettah Gtet, Lionel Salesses, Tao Yin, Arnaud Sengers, Baptiste Trey et François Generau.

Regardant en derrière mon parcours scolaire, je devrais remercier particulièrement au Bureau Français de Taipei et au Bureau de Représentation de Taipei en France. Grâce aux collaborations entre la France et Taïwan par

l'intermédiaire de ces deux organismes, j'ai obtenu l'opportunité de poursuivre mes études en France. En même temps, je remercie à Jih-Huang Li, Hung-Ling Chen et Hsueh-Yung Lin, qui étaient les étudiants taiwanais démarrant ses études en France en ensemble avec moi. Pendant les premières années d'étude en France, ce sont eux qui m'ont supporté le plus à surmonter les difficultés.

Je voudrais mentionner ici quelques gens qui m'ont aidé beaucoup dans ma vie. Merci à Antoine Henrot et Marius Tucsnack, professeurs de mathématiques en université de Lorraine, qui ont trouvé le stage au LJK pour moi. Il n'y aura plus mes histoires au LJK sans eux, y compris cette thèse. Merci à Chi-Ting Wu, ma camarade taiwanais à Nancy. Merci à Arnaud Pinguet, professeur à la classe préparatoire, qui m'a sollicité des très bonnes connaissances mathématiques basiques. Merci aux étudiants taiwannais résidant sur Grenoble, Ting-Ting Wu, Chien-ju Chen, Hao-Cheng Wang et Chun-Mei Chen. Nous avons passé des bons moments en soirées ou en montagnes.

En fin, je remercie mes parents et mes deux soeurs qui m'accompagnaient tout le long dans ma vie, m'encourageaient de façon constante et me supportaient tous les choix que j'ai eu fait. Sans doute, le soutien de ma famille est le facteur le plus important qui m'amène à la réussite de la thèse.

Avertissement

This work has been partially supported by the LabEx PERSYVAL-Lab (ANR-11-LABX-0025-01) funded by the French program Investissements d'avenir.

Sommaire

Abstract	xiii
Remerciements	xv
Avertissement	xvii
Sommaire	xix
List of Tables	xxi
List of Figures	xxiii
Introduction	1
1 Determination of a disk in a two dimensional plane	7
2 Numerical determination of disks	23
3 Determination of inclusions using multifrequency measurements	31
4 Mathematical model of electroreception	53
5 Numerical identification of the target fish	73
6 Spectrum of Neumann-Poincaré operator for two close-to-touching inclusions	89
Conclusion	105
Bibliography	107
Contents	113

List of Tables

2.1	Hölder exponents in different cases	30
3.1	Errors between $u_{0reconstruct}$ and u_0	49
3.2	Reconstructs conductivity coefficients	49
3.3	Relative symmetric difference	49
5.1	Errors between $\tilde{u}_{0reconstruct}$ and \tilde{u}_0	84
5.2	Relative symmetric difference	84

List of Figures

2.1	Numerical solutions of (2)	28
2.2	Decay of $\log(J)$ during iterations	28
2.3	Case $X_0 = (2, 0.8)$, $R = 1$	29
2.4	Case $X_0 = (-0.3, 0.5)$, $R = 0.7$	29
2.5	Case $X_0 = (2.4, -1.2)$, $R = 0.3$	30
3.1	Example: ellipse	50
3.2	Example: square	50
3.3	Example: a near boundary concave domain	51
3.4	Example: a centered small domain	51
3.5	Example: The case in Ω_2	52
5.1	Interior solution to the equation (5.1)	81
5.2	Solutions to (5.1) in the presence/absence of inclusion	82
5.3	Different positions of the electric fish	83
5.4	Reconstruction of an ellipse	85
5.5	Reconstruction of a triangle	86
5.6	Reconstruction of a star-shape domain	87
5.7	Reconstruction of a displaced disk	88
6.1	The touching and non-touching configurations.	90
6.2	Mesh refinement zone.	99
6.3	Mesh for $\delta = 1/16$.	99
6.4	Mesh refinement near the contact point.	99
6.5	$\log b_{1,N}^{\delta,+}$ as function of $\log \delta$.	100
6.6	The effect of the dimension of V_N on the values of $b_{1,N}^{\delta,+}$.	101
6.7	Domains D_1 and D_2	102

Introduction

Electroreception or electrolocalization is the name given to the sensor ability for certain electric fish. There exist many species of electric fish, which belong principally to the two orders, Gymnotiforms in South America and Mormyri-forms in Africa [57]. They are able to detect electrostatic perturbations caused by the presence of some objects in their neighborhood. This ability to interpret an electrical signal to locate itself in space opens important perspectives for applications, in particular in the field of biologically inspired robotics. From the point view of mathematics, electroreception leads to an inverse conductivity problem.

Inverse conductivity problems, also called Calderón problems, are the prototypical models of mathematical inverse problems. They have been studied with the purpose of deriving some nondestructive imaging methods such as Electrical Impedance Tomography(EIT). This technique has a main application in medical imaging, but variants are used in geophysics and other domains. The principal purpose of Calderón problems is to determine the conductivity at each point in a conductive medium from some total or partial measurements of the voltage and the current on its boundary.

The mathematical model of Calderón problems is described as follows. Let Ω be a bounded smooth domain in \mathbb{R}^n for $n \geq 2$, $\gamma \in L_{loc}^\infty(\Omega)$ be the unknown positive conductivity, and u be the solution to the Dirichlet problem,

$$\begin{cases} \operatorname{div}(\gamma(x)\nabla u(x)) = 0 & x \in \Omega, \\ u(x) = f & x \in \partial\Omega. \end{cases} \quad (1)$$

Since γ is positive, existence and uniqueness of the solution $u \in H^1(\Omega)$ for any

Dirichlet data $f \in H^{1/2}(\Omega)$ can be derived from standard arguments. The inverse problem is formulated as follows: Given the Dirichlet to Neumann map $\Lambda : H^{1/2}(\partial\Omega) \rightarrow H^{-1/2}(\partial\Omega)$ (or given partial information on λ), can we reconstruct the conductivity γ ? In general, the inverse problem is non-linear and ill-posed. Calderón published his seminal paper [31] in 1980. Since then, developments on this problem have been focused on three perspectives: uniqueness, stability and reconstruction algorithms.

The general theories on Calderón problems assume that an infinite number of measurements are available. The essential tool is the Dirichlet to Neumann operator (DtN operator), which is defined for any function $f \in H^{1/2}(\Omega)$ maps to the normal derivative $\gamma \frac{\partial u}{\partial \nu}$ where u is the solution to (1). The uniqueness of γ for smooth conductivity coefficients was proven by Sylvester and Uhlmann [44], which showed that if two Dirichlet to Neumann operators, associated to conductivity coefficients γ_1 and γ_2 , are equal, then $\gamma_1 = \gamma_2$ in Ω . Moreover, the uniqueness results in two dimensions were generalized by Astala and Päivärinta [22], which states that all conductivity coefficients in $L^\infty(\Omega)$ can be determined by Dirichlet to Neumann map. A general stability estimate is given by Alessandrini [3]. This is a logarithmic stability estimate, which is valid for the C^∞ conductivity coefficients in three dimensions. Precisely speaking, there exists constants C and σ such that

$$\|\gamma_1 - \gamma_2\|_{L^\infty(\Omega)} \leq C(|\log(\|\Lambda_{\gamma_1} - \Lambda_{\gamma_2}\|_{1/2,-1/2})|^{-\sigma} + \|\Lambda_{\gamma_1} - \Lambda_{\gamma_2}\|_{1/2,-1/2}),$$

where $\|\cdot\|_{1/2,-1/2}$ refers the operator norm from $H^{1/2}(\partial\Omega)$ to $H^{-1/2}(\partial\Omega)$. Nachman [58] proved firstly the uniqueness result in dimension two and convergence for an algorithm to reconstruct γ from the associated Dirichlet to Neumann operator in dimensions two.

We call inverse inclusion problems the particular case when the conductivity has the form $\gamma = k_0 + (k - k_0)\chi_D$, where k_0 is the conductivity in the neighboring environment, $k > 0$, $k \neq k_0$ and $D \subset\subset \Omega$ a bounded, smooth inclusion in Ω .

As it is not possible in any concrete experiment to have the access to infinitely many measurements, we are also interested in the inverse conductivity problem

under a finite number of measurements. The question whether one measurement uniquely determines D has already been addressed in several papers, when D is a ball or a convex polyhedron in 3d (see [24], [38], [43], [46]). The question of stability has been investigated in the case of disks in [37] and [47]. Kwon [50] has established a real-time scheme to locate the unknown inclusion with the hypothesis that its size is small compared with that of Ω . Other works concern the case of inclusions of small sizes, while knowledge about their number, location and conductivity may be derived from the knowledge of a certain number of generalized polarization tensors (Ammari and Kang [8]).

In this Phd thesis, we present three main achievements and an auxiliary result on the inverse inclusion problems, which we briefly introduce below.

Identification of disks in a two dimensional plane

Let $D = B_R(X_0) \subset \Omega_0$ be the disk of radius R centered at X_0 , where $\Omega_0 := \{x \in \Omega \mid \text{dist}(x, \partial\Omega) > \delta_0\}$ with the constant $\delta_0 > 0$. We assume that the electrical conductivity $\gamma \equiv 1$ in $\Omega \setminus \bar{D}$ and $\gamma \equiv k$ in D . We inject a current with density g and measure the voltage f on $\partial\Omega$. The inverse inclusion problem consists in determining the unknown domain D from the data g and f . As we assume D is a disk, we only need to determine its center X_0 and its radius R . Let u be the electrostatic potential in Ω , solution to the following conductivity problem

$$\begin{cases} \operatorname{div}((1 + (k - 1)\chi_D)\nabla u) = 0 & \text{in } \Omega, \\ \frac{\partial u}{\partial \nu} = g & \text{on } \partial\Omega, \end{cases} \quad (2)$$

where u is normalized by $\int_{\partial\Omega} u = 0$.

The first result in this work is that the solution to (2) admits the following representation

$$\begin{cases} u(x) = H(x) + \frac{1-k}{1+k}(H(x) - H(X_0)) & x \in \bar{D}, \\ u(x) = H(x) + \frac{1-k}{1+k}(H(X_0 + \frac{R^2(x-X_0)}{\|x-X_0\|^2}) - H(X_0)) & x \in \Omega \setminus \bar{D}, \end{cases} \quad (3)$$

where H is a harmonic function, which can be directly calculated from the Cauchy data.

Concerning the uniqueness and stability to the inverse problem, Kang and Seo [37], have established a Hölder-type stability estimate under a well-chosen current density for the same problem. In this work, we drop the last assumption i.e. we derive a new, more precise, Hölder type stability estimate for all non zero Neumann data $g \in H_0^{-1/2}(\Omega)$. These theoretical results are given in chapter 1.

In chapter 2, we give a numerical scheme, which is based on the gradient method to reconstruct the disk. We compare the symmetric differences between the target disk and its numerical approximation during the iterations to illustrate the stability estimates.

Determination of inclusions using multifrequency measurements

In the next chapter, we again consider the inverse inclusion problem with a Neumann boundary condition on $\partial\Omega$. We adopt a new mathematical model of EIT [19] by injecting an electric current at different frequencies. In this model, the conductivity γ and solution u depend on the frequency ω . We consider the conductivity in this form,

$$\gamma(x, \omega) = k_0 + (k(\omega) - k_0)\chi_D(x)$$

and the electrical voltages on $\partial\Omega$ are measured for the frequencies in certain interval, $\omega \in [\underline{\omega}, \bar{\omega}]$. In this work, we assume that the conductivity profile $\omega \mapsto k(\omega)$ inside the inclusion is given by a empirical law, which we present later.

Using the eigenfunctions of the Neumann-Poincaré operator on D , we prove the solution u admits the following spectral decomposition

$$u(x, \omega) = k_0^{-1}u_0(x) + u_f(x, \omega),$$

where u_0 is independent of the frequency. On the other hand, u_0 is also the

solution to an inverse boundary problem, which can be considered as an asymptotic case of the Calderón problem, and for which optimal stability estimates on inverse boundary problems have already been derived, see for example [4].

We then introduce our numerical methods to reconstruct the inclusion. This method is divided into two main steps. The first consists in reconstructing the frequency profile $k(\omega)$ and the frequency independent part u_0 . Once the reconstructed u_0 has been determined, we reconstruct the inclusion D from the Cauchy data of u_0 using an optimization scheme in the next step. To derive the optimization scheme, we need to calculate the shape derivative, and we use the asymptotic expansions of layer potentials to derive the shape derivatives. Those results are presented in chapter 3.

Determination of inclusions in the model of electric fish

Instead of working in a bounded domain Ω , the mathematical model of electrical fish concerns the domain $\Omega_e = \mathbb{R}^d \setminus \Omega$ exterior of the fish. Precisely speaking, we consider the following equation [6],

$$\begin{cases} \Delta u = J_s & \text{in } \Omega, \\ \operatorname{div}[\gamma(x, \omega)\nabla u] = 0 & \text{in } \Omega_e, \\ \frac{\partial u}{\partial \nu}|_- = 0 & \text{on } \partial\Omega, \\ u|_+ - u|_- = \xi \frac{\partial u}{\partial \nu}|_+ & \text{on } \partial\Omega, \\ |u| = O(|x|^{1-d}) & \text{as } |x| \rightarrow \infty. \end{cases} \quad (4)$$

Here, the constant $\xi > 0$ is the effective thickness of the fish skin. The function J_s represents the electric current source generated by the fish's organs. We assume that J_s can be written as the sum of Dirac functions,

$$J_s = \sum_{j=1}^M \alpha_j \delta_{x_s^{(j)}}. \quad (5)$$

In chapter 4, we introduce the weighted Sobolev space $\mathcal{W}^{1,-1}(\Omega_e)$ to define the

weak solution to (4.1) in an unbounded domain. Then we prove the uniqueness and the existence of a solution to the forward problem. We also prove that the solution of (4.1) admits a spectral decomposition of the same form as the solution of the conductive equation in the case Ω is bounded (cf chapter 3). In chapter 5, we present numerical simulations of electroreception. Using similar ideas as those of chapter 3, we give our method to reconstruct the frequency independent function u_0 and the inclusion D , using multifrequency measurements. In order to simulate the solution in an unbounded domain, we will consider the equation posed in a truncated domain, and we will show that the solution in the truncated domain admits a similar spectral decomposition.

Eigenvalues of Neumann-Poincaré operator for two close-to-touching inclusions

In our analysis on inverse inclusion problems, the representation formula in layer potentials plays an essential role, especially the Neumann-Poincaré operator or the variational Poincaré operator. We have observed in the case of two close-to-touching inclusions, the pointwise values of the gradient of the voltage potential ∇u may blow up as the distance δ between some inclusions tends to 0 and as the conductivity contrast degenerates. In [27], we showed that the blow-up rate of the gradient is related to how the eigenvalues of the associated Neumann-Poincaré operator converge to $\pm 1/2$ as $\delta \rightarrow 0$, and on the regularity of the contact.

In chapter 6, we consider two connected 2-D inclusions, at a distance $\delta > 0$ from each other. When $\delta = 0$, the contact between the inclusions is of order $m \geq 2$. We propose an original numerical method to determine the eigenvalues of the Neumann-Poincaré operator. We at first prove the equivalence relation between the problem in unbounded domain and the problem in a truncated domain. Our original numerical method consists in projecting functions in $\mathcal{W}^{1,-1}(\mathbb{R}^2)$ on a vector space formed by the polynomial harmonics. We then numerically determine the asymptotic behavior of the first eigenvalue of the Neumann-Poincaré operator, in terms of δ and m , and we check that we recover the estimates obtained in [26].

Determination of a disk in a two dimensional plane

1.1 Introduction

Let $D = B_R(X_0) \subset \Omega_0$ be the disk of radius R centered at X_0 , where $\Omega_0 := \{x \in \Omega \mid \text{dist}(x, \partial\Omega) > \delta_0\}$ with the constant $\delta_0 > 0$. We assume that the electrical conductivity $\sigma \equiv 1$ in $\Omega \setminus \bar{D}$ and $\sigma \equiv k$ in D . We inject a current with density $g \in H_0^{-1/2}(\Omega)$ and measure the voltage f on $\partial\Omega$. The inverse conductivity problem consists in determining the unknown domain D from the data g and f . As we assume D is a disk, we only need to determine its center X_0 and its radius R . Let u be the electrostatic potential in Ω , solution to the inverse conductivity problem (2).

Denoting respectively the solution in the interior of the disk D by u^i , and the solution in the exterior by u^e , the equation (2) can also be formulated as follows:

$$\left\{ \begin{array}{ll} \Delta u^e = 0 & \text{in } \Omega \setminus \bar{D} \\ \Delta u^i = 0 & \text{in } D \\ u^e = u^i & \text{on } \partial D \\ \frac{\partial u^e}{\partial \nu} = k \frac{\partial u^i}{\partial \nu} & \text{on } \partial D \\ \frac{\partial u}{\partial \nu} = g & \text{on } \partial\Omega. \end{array} \right. \quad (1.1)$$

In fact, Fabes, Kang and Seo [37], have established a Hölder-type stability estimate under a well-chosen current density for the same problem. In this work, we drop the last assumption i.e. we derive a new, more precise, also Hölder type stability estimate for all non zero Neumann data $g \in H_0^{-1/2}(\Omega)$. Moreover, we give in this work a reconstruction method from two linearly independent measurement and a minimizing scheme for recovery from a single measurement.

1.2 Main Results

1.2.1 Generalities

We introduce the fundamental solution of the Laplace operator in all \mathbb{R}^2

$$\Gamma(x) = \frac{1}{2\pi} \ln|x|,$$

and the single and double layer potentials defined for $\phi \in L^2(\partial D)$ by

$$\begin{aligned} \mathcal{S}_D \phi(x) &= \int_{\partial D} \Gamma(x-y) \phi(y) d\sigma_y & x \in \mathbb{R}^2, \\ \mathcal{D}_D \phi(x) &= \int_{\partial D} \frac{\partial}{\partial \nu_y} \Gamma(x-y) \phi(y) d\sigma_y & x \in \mathbb{R}^2 \setminus \partial D. \end{aligned}$$

Using integration by parts, for $x \in \Omega \setminus \bar{D}$, the solution to (1.1) can be represented in the form:

$$\begin{aligned} u^e(x) &= \int_{\partial \Omega} u(y) \frac{\partial}{\partial \nu_y} \Gamma(x-y) - \frac{\partial u}{\partial \nu}(y) \Gamma(x-y) d\sigma_y \\ &\quad - \int_{\partial D} u(y) \frac{\partial}{\partial \nu_y} \Gamma(x-y) - \frac{\partial u}{\partial \nu}(y) \Gamma(x-y) d\sigma_y \\ &= H(x) + \mathcal{S}_D \frac{\partial u^e}{\partial \nu}(x) - \mathcal{D}_D u^e(x), \end{aligned} \tag{1.2}$$

and, for $x \in D$

$$\begin{aligned} u^i(x) &= \int_{\partial D} u(y) \frac{\partial}{\partial \nu_y} \Gamma(x-y) - \frac{\partial u}{\partial \nu}(y) \Gamma(x-y) d\sigma_y \\ &= -\mathcal{S}_D \frac{\partial u^i}{\partial \nu}(x) + \mathcal{D}_D u^i(x), \end{aligned} \quad (1.3)$$

where the harmonic function H is entirely determined by the Cauchy data (f, g)

$$H(x) = \int_{\partial \Omega} u(y) \frac{\partial}{\partial \nu_y} \Gamma(x-y) - \frac{\partial u}{\partial \nu}(y) \Gamma(x-y) d\sigma_y = \mathcal{D}_\Omega f - \mathcal{S}_\Omega g. \quad (1.4)$$

Theorem 1.2.1. *The solution to (1.1) admits the following representation*

$$\begin{cases} u^i(x) = H(x) + \frac{1-k}{1+k}(H(x) - H(X_0)) & x \in \bar{D} \\ u^e(x) = H(x) + \frac{1-k}{1+k}(H(X_0 + \frac{R^2(x-X_0)}{\|x-X_0\|^2}) - H(X_0)), & x \in \Omega \setminus \bar{D} \end{cases} \quad (1.5)$$

Proof. With the jump condition on ∂D , we have [8],[33]

$$\mathcal{D}_D \phi(x)|_{\pm} = (\mp \frac{1}{2} I + \mathcal{K}_D) \phi(x) \quad x \in \partial D,$$

where \mathcal{K} is the Neumann-Poincaré operator defined on $L^2(\partial \Omega)$ by

$$\mathcal{K}_D \phi(x) = \frac{1}{2\pi} \int_{\partial D} \frac{\langle y-x, \nu_y \rangle}{|x-y|^2} \phi(y) d\sigma_y.$$

When D is a disk in \mathbb{R}^2 of radius R , the operator \mathcal{K} has a very simple form [8]

$$\mathcal{K}_D \phi(x) = \frac{1}{4\pi R} \int_{\partial D} \phi(y) d\sigma_y \quad \forall x \in \partial D.$$

Using the jump conditions, it follows from (1.2) and (1.3) that

$$u^e(x) = H(x) + \mathcal{S}_D \frac{\partial u^e}{\partial \nu}(x) + (\frac{1}{2} I - \mathcal{K}_D) u^e(x), \quad (1.6)$$

and

$$u^i(x) = -\mathcal{S}_D \frac{\partial u^i}{\partial \nu}(x) + \left(\frac{1}{2}I + \mathcal{K}_D\right)u^i(x). \quad (1.7)$$

Adding (1.6) to k times (1.7), and using the mean value propriety for harmonic functions, we obtain for $x \in \partial D$,

$$u(x) = \frac{2}{k+1}H(x) + \frac{2(k-1)}{k+1}\mathcal{K}_D u(x) = \frac{2}{k+1}H(x) + \frac{k-1}{k+1}u^i(X_0).$$

As H is harmonic in D , it follows that u^i coincides with the above right-hand side in \bar{D} :

$$u^i(x) = \frac{2}{k+1}H(x) + \frac{k-1}{k+1}u^i(X_0).$$

And, at X_0 ,

$$u^i(X_0) = \frac{2}{k+1}H(X_0) + \frac{k-1}{k+1}u^i(X_0),$$

which implies $u^i(X_0) = H(X_0)$. Then we have the representation of u^i ,

$$u^i(x) = H(x) + \frac{1-k}{1+k}(H(x) - H(X_0)) \quad x \in \bar{D} \quad (1.8)$$

We represent each point $x \in \Omega$ as $x = X_0 + r \begin{pmatrix} \cos \theta \\ \sin \theta \end{pmatrix}$, with $\theta \in [0, 2\pi)$ and $r > 0$,

and we write the function H as a sum of harmonic functions $r^n \cos(n\theta)$ and $r^n \sin(n\theta)$:

$$H(x) = H(X_0) + \sum_{n=1}^{\infty} r^n (a_n \cos(n\theta) + b_n \sin(n\theta)). \quad (1.9)$$

By (1.8) and the transmission conditions, we immediately have:

$$u^i(x) = H(X_0) + \frac{2}{k+1} \sum_{n=1}^{\infty} r^n (a_n \cos(n\theta) + b_n \sin(n\theta)), \quad x \in D, \quad (1.10)$$

$$u^e(x) = H(X_0) + \sum_{n=1}^{\infty} \left(r^n + \frac{1-k}{1+k} \left(\frac{R^2}{r}\right)^n\right) (a_n \cos(n\theta) + b_n \sin(n\theta)), \quad x \in \Omega \setminus \bar{D}. \quad (1.11)$$

Let $\Psi_D(x)$ denote the point obtained by reflecting x over ∂D

$$\Psi_D(x) = X_0 + \frac{R^2(x - X_0)}{\|x - X_0\|^2} \quad x \in \mathbb{R}^2 \setminus \{X_0\}.$$

We can thus write

$$u^e(x) = H(x) + \frac{1-k}{1+k}(H(\Psi_D(x)) - H(X_0)) \quad x \in \Omega \setminus \bar{D}, \quad (1.12)$$

which concludes the proof. \square

1.2.2 Analysis in complex variables

Using the representation (1.5) of u^e and u^i , we study our problem in the complex plane \mathbb{C} . We introduce a harmonic conjugate G of the harmonic function H , so that the function

$$F := H + iG \quad (1.13)$$

is holomorphic in Ω . Also, the reflection has an explicit expression in terms of complex variables:

$$\Psi_D(z) = Z_0 + \frac{R^2}{\bar{z} - \bar{Z}_0} \quad z \in \mathbb{C} \setminus \{Z_0\}.$$

By (1.12) and (1.1), the function $H \circ \Psi_D$ is harmonic in $\Omega \setminus \bar{D}$. We can also express its harmonic conjugate \tilde{G} for $x \in \Omega \setminus \bar{D}$ as

$$\begin{aligned} \nabla \tilde{G}(x) &= A \nabla H \circ \Psi_D(x) \\ &= A \mathcal{D}\Psi_D(x) \nabla H(\Psi_D(x)), \end{aligned} \quad (1.14)$$

where $A = \begin{pmatrix} 0 & -1 \\ 1 & 0 \end{pmatrix}$,

and where

$$\mathcal{D}\Psi_D(x) = \frac{R^2}{\|x - X_0\|^2} \begin{pmatrix} (x - X_0)_2^2 - (x - X_0)_1^2 & -2(x - X_0)_1(x - X_0)_2 \\ -2(x - X_0)_1(x - X_0)_2 & (x - X_0)_1^2 - (x - X_0)_2^2 \end{pmatrix}.$$

Notice that

$$\mathcal{D}\Psi_D = -\mathcal{D}\Psi_D A,$$

combined with (1.14), which yield:

$$\begin{aligned} \nabla \tilde{G}(x) &= A \nabla H \circ \Psi_D(x) \\ &= A \mathcal{D}\Psi_D(x) \nabla H(\Psi_D(x)) \\ &= -\mathcal{D}\Psi_D(x) A \nabla H(\Psi_D(x)) \\ &= -\mathcal{D}\Psi_D(x) \nabla G(\Psi_D(x)) \\ &= -\nabla G \circ \Psi_D(x). \end{aligned}$$

Thus, the function $-G \circ \Psi_D$ is a harmonic conjugate of the function $H \circ \Psi_D$, and therefore the function $z \mapsto H \circ \Psi_D(z) - iG \circ \Psi_D(z) = \bar{F} \circ \Psi_D(z)$ is holomorphic and its real part is equal to $H \circ \Psi_D$.

Assuming that F is analytic in Ω , we can write F as a sum

$$F(z) = \sum_{n=0}^{\infty} c_n (z - Z_0)^n, \quad z \in \Omega.$$

Also, the holomorphic function $\bar{F} \circ \Psi_D$ admits the following development:

$$\bar{F} \circ \Psi_D(z) = \sum_{n=0}^{\infty} \bar{c}_n \frac{R^{2n}}{(z - Z_0)^n}, \quad z \in \Omega \setminus \bar{D}. \quad (1.15)$$

Therefore, denoting by v^e a harmonic conjugate of u^e , and given any $C \in \mathbb{R}$, the function:

$$h(z) := u^e(z) + i v^e(z) = F(z) + \frac{1-k}{1+k} (\bar{F} \circ \Psi_D(z) - H(Z_0) + iC), \quad z \in \Omega \setminus \bar{D},$$

is holomorphic.

Remark 1.2.1. *We can calculate directly from the measurements (f, g) the values of the function h on $\partial\Omega$.*

1.2.3 Stability estimate

We next establish a Hölder-type stability estimate for the center and radius of the disk. Let D_1, D_2 denote 2 disks centered at the points z_1, z_2 and with radii R_1, R_2 . For $i = 1, 2$, let u_i be the solutions of the problem (1.1). We assume that the two solutions satisfy the same non-zero Neumann data g on $\partial\Omega$, and that the L^∞ - norm of the difference between their traces on $\partial\Omega$ (the Dirichlet data) is a small quantity ε . We denote by Ω_1, Ω_2 the images of $\mathbb{C} \setminus \bar{\Omega}$ by the reflections Ψ_{D_1}, Ψ_{D_2} .

Theorem 1.2.2 (Uniqueness of the inverse problem). *If $u_1 = u_2$ on $\partial\Omega$ then $D_1 = D_2$.*

Proof. From (1.4), the function H linked to each solution of (1.1) depends uniquely on the Cauchy data. As u_1 and u_2 have the same Cauchy data, their functions H are the same, and we will note this function by H in this proof.

Using the unique continuation propriety, we have: $u_1 = u_2$ in $\Omega \setminus (D_1 \cup D_2)$.

Case 1: $D_1 \cap D_2 = \emptyset$. In this case, u_1^e has a harmonic continuation in D_1 , which coincides with u_2^e i.e. $u_2^e = u_1^e$ in D_1 . Then, on ∂D_1 , we have:

$$\frac{\partial u_1^i}{\partial \nu} = \frac{\partial u_2^e}{\partial \nu} = \frac{\partial u_1^e}{\partial \nu} = k \frac{\partial u_1^i}{\partial \nu}, \quad (1.16)$$

which implies $\frac{\partial u_1^i}{\partial \nu} = 0$ on ∂D_1 , so that $u_1^i = 0$, and thus $u_1 = 0$ and $g = 0$.

Hence the contradiction.

Let z^* and Z^* be defined as (1.25).

Case 2: $\partial D_1 \cap \partial D_2 \neq \emptyset$. In this case, from (1.25), $\partial D_1 \cap \partial D_2 = \{z^*, Z^*\}$. Then, from the continuity of the solutions, we have:

$$u_1^i(z^*) = u_1^e(z^*) = u_2^e(z^*) = u_2^i(z^*) \quad (1.17)$$

Using (Theorem 1.2.1), we have $H(z_1) = H(z_2)$ and $u_1^i = u_2^i$ in $D_1 \cap D_2$.

So, on $\partial(D_1 - D_2)$, $u_1 - u_2 = 0$, which implies $u_1^i = u_2^e$ in $D_1 - D_2$. Then, on the arc $D_1 \cap \partial D_2$, we have:

$$\frac{\partial u_2^i}{\partial \nu} = \frac{\partial u_1^i}{\partial \nu} = \frac{\partial u_2^e}{\partial \nu} = k \frac{\partial u_2^i}{\partial \nu}, \quad (1.18)$$

which implies $\frac{\partial u_1^i}{\partial \nu} = \frac{\partial u_2^i}{\partial \nu} = 0$. For the same reason, we also have: $\frac{\partial u_1^i}{\partial \nu} = \frac{\partial u_2^i}{\partial \nu} = 0$ on the arc $D_2 \cap \partial D_1$. It follows that, $\frac{\partial u_1^i}{\partial \nu} = \frac{\partial u_2^i}{\partial \nu} = 0$ in $\partial(D_1 \cap D_2)$. This also implies $u_1^i = 0$ and then $g = 0$.

Hence the contradiction.

Case 3: $D_1 \subset D_2$. In this case, we have: $z^* \in D_1$ and $Z^* \in \mathbb{C} \setminus D_2$. The functions $u_j^e - H$, $j = 1, 2$ have a harmonic extension in $\mathbb{C} \setminus D_2$, and they are equal in $\Omega \setminus D_1$, so from (1.2.1), we have:

$$H(\Psi_1(z)) - H(z_1) = H(\Psi_2(z)) - H(z_2) \quad (1.19)$$

in $\mathbb{C} \setminus D_2$.

Applying (1.19) on z^* , we have $H(z_1) = H(z_2)$ and then $u_1 = u_2$ in $D_1 \cap D_2 = D_1$. The rest of the proof follows the same argument as in the previous cases.

That completes the proof \square

Lemma 1.2.1. *Let f be a non-zero holomorphic function in Ω , and assuming that $D_1 \neq D_2$, then there exist $0 < \beta < 1$, which only depends on f , such that*

$$\int_{\partial\Omega} \frac{|\Psi_1(z) - \Psi_2(z)|}{|f(\Psi_1(z)) - f(\Psi_2(z))|^\beta} ds < \infty. \quad (1.20)$$

Proof. We first show that the set $\mathcal{Z} := \{z \in \partial\Omega | f(\Psi_1(z)) - f(\Psi_2(z)) = 0\}$ is finite. Indeed, assume that \mathcal{Z} has infinitely many elements. Then by an argument of compactness, \mathcal{Z} has a limit point. As the functions $f \circ \Psi_i$, $i = 1, 2$ are anti-holomorphic, it follows that $f(\Psi_1(z)) = f(\Psi_2(z))$ on $\mathbb{C} \setminus (D_1 \cup D_2)$. Thus, from the explicit formula of solutions, we can construct two solutions to (1.1) related to D_1 and D_2 , which have the same Cauchy data on $\partial\Omega$. This contradicts the uniqueness of the inverse problem (Theorem 1.2.2).

As the function $\mathcal{F}(z) := \overline{f(\Psi_1(z)) - f(\Psi_2(z))}$ is holomorphic in $\mathbb{C} \setminus (D_1 \cup D_2)$, if $\tilde{z} \in \mathcal{Z}$, there is $m(\tilde{z}) \in \mathbb{N}$ such that, in a neighborhood of \tilde{z} ,

$$\mathcal{F}(z) = \sum_{n \geq m(\tilde{z})} q_n(z - \tilde{z})^n,$$

with $q_{m(\tilde{z})} \neq 0$.

Let $\gamma \in C^1([a, b])$ be a parametrization of $\partial\Omega$, and set $\tilde{z} = \gamma(\tilde{t})$. Then, in a neighborhood of \tilde{t} , we have

$$\mathcal{F}(\gamma(t)) = \sum_{n \geq m(\tilde{z})} q'_n(t - \tilde{t})^n,$$

with $q'_{m(\tilde{z})} \neq 0$.

We choose $0 < \beta < \frac{1}{m}$ where $m := \max_{\tilde{z} \in \mathcal{Z}} m(\tilde{z})$. Then, for $\tilde{t} - \delta < t < \tilde{t} + \delta$ we have,

$$\frac{1}{|\mathcal{F}(\gamma(t))|^\beta} \leq \tilde{C}|t - \tilde{t}|^{-\beta m(\tilde{z})},$$

with $0 < \beta m(\tilde{z}) < 1$.

Therefore,

$$\int_{\tilde{t}-\delta}^{\tilde{t}+\delta} \frac{1}{|\mathcal{F}(\gamma(t))|^\beta} dt < \infty.$$

Thus,

$$\begin{aligned} & \int_{\partial\Omega} \frac{|\Psi_1(z) - \Psi_2(z)|}{|f(\Psi_1(z)) - f(\Psi_2(z))|^\beta} ds \\ &= \int_a^b \frac{|\Psi_1(\gamma(t)) - \Psi_2(\gamma(t))|}{|\mathcal{F}(\gamma(t))|^\beta} |\gamma'(t)| dt < \infty. \end{aligned}$$

and (1.20) follows. □

Theorem 1.2.3. *Assume that*

$$\|u_1|_{\partial\Omega} - u_2|_{\partial\Omega}\|_{L^\infty(\partial\Omega)} = \varepsilon. \quad (1.21)$$

Then there exists constants $0 < \alpha, \beta < 1$ and $C > 0$, such that

$$|z_1 - z_2| \leq C\varepsilon^{\alpha\beta}, \quad (1.22)$$

and

$$|R_1 - R_2| \leq C\varepsilon^{\alpha\beta}, \quad (1.23)$$

where $\alpha := \omega(z^\star) > 0$, and where ω and z^\star are given by the following equations

$$\begin{cases} \Delta\omega = 0 & \text{in } \Omega \setminus \overline{\Omega_1 \cup \Omega_2} \\ \omega = 1 & \text{on } \partial\Omega \\ \omega = 0 & \text{on } \partial(\Omega_1 \cup \Omega_2), \end{cases} \quad (1.24)$$

$$z_1 + \frac{R_1^2}{\bar{z}^\star - \bar{z}_1} = z_2 + \frac{R_2^2}{\bar{z}^\star - \bar{z}_2} = Z^\star \in \mathbb{C}, \quad (1.25)$$

where β only depend on the Cauchy data.

Remark 1.2.2. We remark that z^\star and Z^\star are uniquely determined by (1.25), and we observe that

- Z^\star is the image of z^\star by the reflection with respect to ∂D_1 and with respect to ∂D_2 .
- in the case where $\partial D_1 \cap \partial D_2 \neq \emptyset$, $z^\star = Z^\star$ is one of the intersection points.
- in the case where $D_1 \cap D_2 = \emptyset$, then either $z^\star \in D_1$ and $Z^\star \in D_2$ or $z^\star \in D_2$ and $Z^\star \in D_1$.
- in the case where $D_1 \subset D_2$ (resp. $D_2 \subset D_1$), then $z^\star \in D_1$ (resp. $z^\star \in D_2$) and $Z^\star \in \mathbb{C} \setminus D_2$ (resp. $Z^\star \in \mathbb{C} \setminus D_1$).
- at least one of the points z^\star and Z^\star is in Ω . We can always assume that $z^\star \in \Omega$.

Proof. According to the position of the point Z^\star , we distinguish two cases:

Case 1: both z^\star and Z^\star are in Ω .

Because Z^\star is the image of z^\star by Ψ_{D_1} and vice-versa, one of z^\star or Z^\star is in \bar{D}_1 , the other lies in $\Omega \setminus D_1$. We may assume that $z^\star \in \Omega \setminus D_1$.

We define

$$\tilde{h}_i(z) = h_i(z) - h_i(z^\star) = F_i(z) - F_i(z^\star) + \frac{1-k}{1+k} \left(\overline{F_i\left(z_i + \frac{R_i^2}{\bar{z} - \bar{z}_i}\right)} - \overline{F_i(Z^\star)} \right). \quad (1.26)$$

By construction, the function $h_1 - h_2$ can be holomorphically extended in

$\Omega \setminus \overline{\Omega_1 \cup \Omega_2}$ and from the standard elliptic estimation, this function satisfies

$$M := \sup\{|h_1 - h_2| : z \in \Omega \setminus \overline{\Omega_1 \cup \Omega_2}\} \leq C\|g\|_{L^2(\partial\Omega)}, \quad (1.27)$$

$$|h_1 - h_2| \leq \varepsilon \quad \text{on } \partial\Omega. \quad (1.28)$$

Consequently, for $z \in \partial\Omega$,

$$\begin{aligned} & \tilde{h}_1(z) - \tilde{h}_2(z) \\ &= h_1(z) - h_2(z) - [h_1(z^\star) - h_2(z^\star)] \\ &= F_1(z) - F_2(z) + F_1(z^\star) - F_2(z^\star) \\ &+ \frac{1-k}{1+k} \left(\overline{F_1\left(z_1 + \frac{R_1^2}{\bar{z} - \bar{z}_1}\right)} - \overline{F_2\left(z_2 + \frac{R_2^2}{\bar{z} - \bar{z}_2}\right)} + \overline{F_2(Z^\star)} - \overline{F_1(Z^\star)} \right). \end{aligned} \quad (1.29)$$

Let ω be the solution to the Dirichlet problem (1.24), the function $\omega \log \varepsilon + (1 - \omega) \log M$ is therefore harmonic in $\Omega \setminus \overline{\Omega_1 \cup \Omega_2}$. On the other hand, $\log|h_1 - h_2| = \Re(\log(h_1 - h_2))$ is also a harmonic function in $\Omega \setminus \overline{\Omega_1 \cup \Omega_2}$. From (1.27) and (1.28), we have

$$\log|h_1(z) - h_2(z)| \leq \omega(z) \log \varepsilon + (1 - \omega(z)) \log M, \quad z \in \partial(\Omega \setminus \overline{\Omega_1 \cup \Omega_2}) \quad (1.30)$$

Then, by the maximum principle,

$$\log|h_1(z^\star) - h_2(z^\star)| \leq \omega(z^\star) \log \varepsilon + (1 - \omega(z^\star)) \log M \quad (1.31)$$

Hence,

$$|h_1(z^\star) - h_2(z^\star)| \leq C\varepsilon^\alpha, \quad (1.32)$$

with $\alpha := \omega(z^\star)$.

Using the assumption (1.21) and the definition (1.4) of H , we have

$$\forall z \in \bar{\Omega}, |F_1(z) - F_2(z)| \leq C\varepsilon. \quad (1.33)$$

Further, from (1.29) we have that for all $z \in \partial\Omega$,

$$\begin{aligned} & \overline{F_1(z_1 + \frac{R_1^2}{\bar{z} - \bar{z}_1})} - \overline{F_1(z_2 + \frac{R_2^2}{\bar{z} - \bar{z}_2})} \\ &= \overline{F_1(Z^*)} - \overline{F_2(Z^*)} + \frac{1+k}{1-k} [F_2(z) - F_1(z) + F_2(z^*) - F_1(z^*) \\ &+ h_1(z) - h_2(z) + h_2(z^*) - h_1(z^*)]. \end{aligned} \quad (1.34)$$

Applying (1.28), (1.32) and (1.33), we obtain:

$$\left| \overline{F_1(z_1 + \frac{R_1^2}{\bar{z} - \bar{z}_1})} - \overline{F_1(z_2 + \frac{R_2^2}{\bar{z} - \bar{z}_2})} \right| \leq C\varepsilon^\alpha, \quad \forall z \in \partial\Omega. \quad (1.35)$$

Then, using (1.35) and (1.20), we have the following estimate:

$$\begin{aligned} & \int_{\partial\Omega} |\Psi_1(z) - \Psi_2(z)| ds \\ &= \int_{\partial\Omega} \frac{|\Psi_1(z) - \Psi_2(z)|}{|F_1(\Psi_1(z)) - F_1(\Psi_2(z))|^\beta} |F_1(\Psi_1(z)) - F_1(\Psi_2(z))|^\beta ds \\ &\leq \int_{\partial\Omega} \frac{|\Psi_1(z) - \Psi_2(z)|}{|F_1(\Psi_1(z)) - F_1(\Psi_2(z))|^\beta} ds \times C\varepsilon^{\alpha\beta} \\ &\leq C'\varepsilon^{\alpha\beta}. \end{aligned} \quad (1.36)$$

On the other hand, we have:

$$\begin{aligned} & \int_{\partial\Omega} |\Psi_1(z) - \Psi_2(z)| ds \\ &= \int_{\partial\Omega} |\overline{\Psi_1(z) - \Psi_2(z)}| ds \\ &\geq \left| \int_{\partial\Omega} \overline{\Psi_1(z) - \Psi_2(z)} dz \right| \\ &= \left| \int_{\partial\Omega} \bar{z}_1 - \bar{z}_2 + \frac{R_1^2}{z - z_1} - \frac{R_2^2}{z - z_2} dz \right| \\ &= |R_1^2 - R_2^2|. \end{aligned}$$

So, we have:

$$|R_1 - R_2| \leq C\varepsilon^{\alpha\beta}. \quad (1.37)$$

Using (1.37), we have: for all $z \in \partial\Omega$,

$$|\Psi_1(z) - \Psi_2(z)| = |\bar{z}_1 - \bar{z}_2 + R_1^2 \frac{z_1 - z_2}{(z - z_1)(z - z_2)}| + O(\varepsilon^{\alpha\beta}).$$

So, from (1.36),

$$\begin{aligned} & C\varepsilon^{\alpha\beta} \\ & \geq \int_{\partial\Omega} |\bar{z}_1 - \bar{z}_2 + R_1^2 \frac{z_1 - z_2}{(z - z_1)(z - z_2)}| ds \\ & = |z_1 - z_2| \int_{\partial\Omega} |e^{-2i \arg(z_1 - z_2)} + \frac{R_1^2}{(z - z_1)(z - z_2)}| ds \end{aligned}$$

with $\int_{\partial\Omega} |e^{-2i \arg(z_1 - z_2)} + \frac{R_1^2}{(z - z_1)(z - z_2)}| ds > 0$.

Thus,

$$|z_1 - z_2| \leq C\varepsilon^{\alpha\beta}. \quad (1.38)$$

Case 2: $z^* \in \Omega$, $Z^* \in \mathbb{C} \setminus \bar{\Omega}$. We define

$$\tilde{h}_i(z) = h_i(z) - (h_i(Z^*) - f_i(Z^*)) = f_i(z) + \frac{1-k}{1+k} \left(\overline{F_i(z_i + \frac{R_i^2}{\bar{z} - \bar{z}_i})} - \overline{F_i(Z^*)} \right). \quad (1.39)$$

By (1.15), the holomorphic functions $h_i - F_i$, $i = 1, 2$ can be extended to $\mathbb{C} \setminus \bar{D}_i$ and they vanish as $|z| \rightarrow \infty$. Let $\tilde{\Omega}$ be an open set containing Ω and the point Z^* , and consider a harmonic function ω solution to the following equation

$$\begin{cases} \Delta\omega = 0 & \text{in } \tilde{\Omega} \setminus \bar{\Omega} \\ \omega = 1 & \text{on } \partial\Omega \\ \omega = 0 & \text{on } \partial\tilde{\Omega}. \end{cases} \quad (1.40)$$

Define $\alpha = \omega(Z^*)$.

Thus, from (1.28) and (1.33) we have

$$|(h_1 - F_1) - (h_2 - F_2)| \leq C\varepsilon \quad \text{on } \partial\Omega. \quad (1.41)$$

We apply the maximum principle on $\tilde{\Omega} \setminus \Omega$ to the harmonic function $\omega \log \varepsilon + (1 - \omega) \log M - \log |(h_1 - F_1) - (h_2 - F_2)|$ to obtain:

$$\log |(h_1 - F_1)(Z^\star) - (h_2 - F_2)(Z^\star)| \leq \omega(Z^\star) \log \varepsilon + (1 - \omega(Z^\star)) \log M, \quad (1.42)$$

so that

$$|(h_1 - F_1)(Z^\star) - (h_2 - F_2)(Z^\star)| \leq C\varepsilon^\alpha. \quad (1.43)$$

In fact, we can choose, $\tilde{\Omega} = \mathcal{B}_\rho(z_1)$ with ρ as large as we want. We denote ω_ρ the solution to the associated equation (1.40) and we also consider the harmonic function $\tilde{\omega}_\rho$ solution to

$$\begin{cases} \Delta \tilde{\omega}_\rho = 0 & \text{in } \mathcal{B}(z_1, \rho) \setminus \mathcal{B}(z_1, R_1) \\ \tilde{\omega}_\rho = 1 & \text{on } \partial\mathcal{B}(z_1, R_1) \\ \tilde{\omega}_\rho = 0 & \text{on } \partial\mathcal{B}(z_1, \rho). \end{cases} \quad (1.44)$$

The function $\tilde{\omega}_\rho$ has the explicit expression

$$\tilde{\omega}_\rho(r) = \frac{\ln(r) - \ln(\rho)}{\ln(R) - \ln(\rho)}, \quad (1.45)$$

with $r := |z - z_1|$.

By the maximum principle, $\tilde{\omega}_\rho \leq \omega_\rho$ in $\mathcal{B}(z_1, \rho) \setminus \Omega$. So, we have

$$1 > \omega_\rho(Z^\star) \geq \tilde{\omega}_\rho(Z^\star) = \frac{\ln(r) - \ln(\rho)}{\ln(R) - \ln(\rho)} \xrightarrow{\rho \rightarrow \infty} 1. \quad (1.46)$$

From (1.43), we have

$$|(h_1(Z^\star) - F_1(Z^\star)) - (h_2(Z^\star) - F_2(Z^\star))| \leq C\varepsilon^\beta, \quad 0 < \beta < 1. \quad (1.47)$$

Thus,

$$|(h_1(Z^*) - F_1(Z^*)) - (h_2(Z^*) - F_2(Z^*))| \leq C\varepsilon. \quad (1.48)$$

The rest of the proof follows the same argument as that of *case 1*. \square

1.2.4 Reconstruction from two measurements

It follows from the analysis of section 1.2.2, we can obtain some geometric elements of the disk from a simple contour integration. Thus, we can reconstruct the center, the radius and the conductivity k if we have two distinct measurements under the assumption that $\nabla u \neq 0$ in Ω . The method of reconstruction is described as follows.

We calculate the following integral:

$$I := \frac{1}{2\pi i} \int_{\partial\Omega} h(z) dz. \quad (1.49)$$

Using the representation (1.15) and the Residue Theorem on Ω , we have

$$\begin{aligned} I &:= \frac{1}{2\pi i} \int_{\partial\Omega} h(z) dz \\ &= \frac{1}{2\pi i} \int_{\partial\Omega} F(z) + \frac{1-k}{1+k} (\bar{F} \circ \Psi_D(z) - H(Z_0) + iC) dz \\ &= \frac{1}{2\pi i} \left[\int_{\partial\Omega} F(z) dz + \frac{1-k}{1+k} \left(\int_{\partial\Omega} \sum_{n=0}^{\infty} \bar{c}_n \frac{R^{2n}}{(z-Z_0)^n} dz + \int_{\partial\Omega} -H(Z_0) + iC dz \right) \right] \\ &= \frac{1}{2\pi i} \frac{1-k}{1+k} \sum_{n=1}^{\infty} \bar{c}_n R^{2n} \int_{\partial\Omega} \frac{1}{(z-Z_0)^n} dz \\ &= \frac{1-k}{1+k} \bar{c}_1 R^2 = \frac{1-k}{1+k} \overline{F'(Z_0)} R^2. \end{aligned} \quad (1.50)$$

Using the same arguments, we can also calculate the following integral

$$\begin{aligned}
\frac{1}{2\pi i} \int_{\partial\Omega} zh(z)dz &= \frac{1}{2\pi i} \int_{\partial\Omega} zF(z) + \frac{1-k}{1+k} z(\bar{F} \circ \Psi_D(z) - H(Z_0) + iC)dz \\
&= \frac{1}{2\pi i} \left[\int_{\partial\Omega} zF(z)dz + \frac{1-k}{1+k} \left(\int_{\partial\Omega} \sum_{n=0}^{\infty} \bar{c}_n \frac{zR^{2n}}{(z-Z_0)^n} dz + \int_{\partial\Omega} z(-H(Z_0) + iC)dz \right) \right] \\
&= \frac{1}{2\pi i} \frac{1-k}{1+k} \sum_{n=1}^{\infty} \bar{c}_n R^{2n} \int_{\partial\Omega} \frac{z}{(z-Z_0)^n} dz \\
&= \frac{1}{2\pi i} \frac{1-k}{1+k} \sum_{n=1}^{\infty} \bar{c}_n R^{2n} \int_{\partial\Omega} \frac{1}{(z-Z_0)^{n-1}} + \frac{Z_0}{(z-Z_0)^n} dz \\
&= \frac{1-k}{1+k} (Z_0 \bar{c}_1 R^2 + \bar{c}_2 R^4). \tag{1.51}
\end{aligned}$$

Denoting by f_1, f_2 two functions f corresponding to two distinct measurements, from (1.50) we have

$$\frac{\bar{I}_1}{\bar{I}_2} = \frac{F'_1(Z_0)}{F'_2(Z_0)}. \tag{1.52}$$

We remind that the holomorphic functions F_j above are defined by (1.13), $F_j = H_j + iG_j$, where G_j are the harmonic conjugate of H_j , and $H_j = \mathcal{D}_\Omega f_j - \mathcal{S}_\Omega g$.

So, Z_0 is a zero of the holomorphic function $z \mapsto \frac{F'_1(z)}{F'_2(z)} - \frac{\bar{I}_1}{\bar{I}_2}$ ($F'_2(z) \neq 0 \forall z \in \Omega$ as we supposed that $\nabla u \neq 0$). Once Z_0 is determined, R and k can be easily found from (1.50) and (1.51).

Chapter 2

Numerical determination of disks

2.1 Optimization algorithm

In this section, we consider a numerical scheme to reconstruct a disk contained in a subset $\Omega_0 \subset \Omega$ with $dist(\partial\Omega_0, \partial\Omega) \geq \delta_0 > 0$, using a single measurement. The scheme is based on minimizing the functional

$$J(u) = \frac{1}{2} \int_{\partial\Omega} |u - u_{meas}|^2 d\sigma,$$

where u_{meas} is the measured Dirichlet data and where u is the solution to (2) associated to a disk $D = \mathcal{B}(X_0, R) \subset \Omega_0$.

Given $(c_1, c_2, R) \in \mathbb{R}^3$, where we suppose $X_0 = (c_1, c_2)$, the gradient of the functional J at this point can be calculated as follows.

Theorem 2.1.1. *Let u be the solution to the problem (2) associated to a disk and let w be the solution to the following problem*

$$\begin{cases} \operatorname{div}((1 + (k-1)\chi_D)\nabla w) = 0 & \text{in } \Omega, \\ \frac{\partial w}{\partial \nu} = u - u_{meas} & \text{on } \partial\Omega. \end{cases} \quad (2.1)$$

Then

$$\frac{\partial J}{\partial c_1} = (k-1) \int_D \frac{\partial}{\partial x_1} (\nabla u \nabla w) dX \quad (2.2)$$

$$\frac{\partial J}{\partial c_2} = (k-1) \int_D \frac{\partial}{\partial x_2} (\nabla u \nabla w) dX \quad (2.3)$$

$$\frac{\partial J}{\partial R} = \frac{k-1}{R} \int_D 2 \nabla u \nabla w + \sum_{i=1,2} (x_i - c_i) \frac{\partial}{\partial x_i} (\nabla u \nabla w) dX. \quad (2.4)$$

Proof. Let $(c_1, c_2, R) \in \mathbb{R}^3$, such that the disk D centered at (c_1, c_2) , with radius R is included in Ω_0 . Denote u (receptively \tilde{u}) the solutions to (2) associated to the disk $\mathcal{B}_R(c_1, c_2)$ (respectively $\mathcal{B}_R(c_1 + dx_1, c_2)$). Then we have

$$\begin{aligned} J(c_1 + dc_1, c_2, R) - J(c_1, c_2, R) &= \frac{1}{2} \int_{\partial\Omega} |\tilde{u} - u_{meas}|^2 d\sigma - \frac{1}{2} \int_{\partial\Omega} |u - u_{meas}|^2 d\sigma \\ &= \frac{1}{2} \int_{\partial\Omega} (\tilde{u} - u)(\tilde{u} + u - 2u_{meas}) d\sigma \\ &= \frac{1}{2} \int_{\partial\Omega} (\tilde{u} - u)(\tilde{u} - u + 2(u - u_{meas})) d\sigma \\ &= \int_{\partial\Omega} (u - u_{meas}) v dc_1 d\sigma + O(|dc_1|^2). \end{aligned}$$

Therefore,

$$\frac{\partial J}{\partial c_1} = \int_{\partial\Omega} (u - u_{meas}) v d\sigma, \quad (2.5)$$

where $v := \lim_{dc_1 \rightarrow 0} \frac{\tilde{u} - u}{dc_1}$.

Combining the variational forms of (2) for u and for \tilde{u} , we have that for all $\phi \in H^1(\Omega)$,

$$\int_{\Omega} (1 + (k-1)\chi_{\bar{D}}) \nabla \tilde{u} \nabla \phi dX - \int_{\partial\Omega} g \phi d\sigma = 0, \quad (2.6)$$

and

$$\int_{\Omega} (1 + (k-1)\chi_D) \nabla u \nabla \phi dX - \int_{\partial\Omega} g \phi d\sigma = 0. \quad (2.7)$$

By applying a result of shape derivative (see [5]), (2.6)-(2.7) give us:

$$\begin{aligned}
0 &= \frac{1}{dc_1} \left[\int_{\Omega} (1 + (k-1)\chi_{\bar{D}}) \nabla \bar{u} \nabla \phi dX - \int_{\Omega} (1 + (k-1)\chi_D) \nabla u \nabla \phi dX \right] \\
&= \int_{\Omega} \nabla v \nabla \phi dX + \frac{k-1}{dc_1} \left(\int_{\bar{D}} \nabla \bar{u} \nabla \phi dX - \int_D \nabla u \nabla \phi dX \right) \\
&= \int_{\Omega} (1 + (k-1)\chi_D) \nabla v \nabla \phi dX + \frac{k-1}{dc_1} \left(\int_{\bar{D}} \nabla u \nabla \phi dX - \int_D \nabla u \nabla \phi dX \right) + O(|dc_1|) \\
&= \int_{\Omega} (1 + (k-1)\chi_D) \nabla v \nabla \phi dX + (k-1) \int_{\partial D} e_1 \cdot \nu \nabla u \nabla \phi d\sigma + O(|dc_1|).
\end{aligned}$$

It follows that v satisfies, for all $\phi \in H^1(\Omega)$,

$$\int_{\Omega} (1 + (k-1)\chi_D) \nabla v \nabla \phi dX + (k-1) \int_{\partial D} e_1 \cdot \nu \nabla u \nabla \phi d\sigma. \quad (2.8)$$

Introducing the function w defined by (2.1), and taking w as ϕ in (2.8) we get

$$0 = \int_{\Omega} (1 + (k-1)\chi_D) \nabla v \nabla w dX + (k-1) \int_{\partial D} e_1 \cdot \nu \nabla u \nabla w d\sigma. \quad (2.9)$$

On the other hand,

$$\begin{aligned}
0 &= \int_{\Omega} \operatorname{div}[(1 + (k-1)\chi_D) \nabla w] v dX \\
&= \int_{\partial \Omega} v (u - u_{meas}) d\sigma + \int_{\Omega} (1 + (k-1)\chi_D) \nabla v \nabla w dX.
\end{aligned}$$

Consequently,

$$\frac{\partial J}{\partial c_1} = \int_{\partial \Omega} (u - u_{meas}) v d\sigma \quad (2.10)$$

$$= (k-1) \int_{\partial D} e_1 \cdot \nu \nabla u \nabla w d\sigma \quad (2.11)$$

$$= (k-1) \int_{\partial D} \frac{\partial x_1}{\partial \nu} \nabla u \nabla w d\sigma \quad (2.12)$$

$$= (k-1) \int_D \frac{\partial}{\partial x_1} (\nabla u \nabla w) dX, \quad (2.13)$$

and (2.2) follows. By the same argument, we can obtain (2.3) and

$$\frac{\partial J}{\partial R} = (k-1) \int_{\partial D} \nabla u \nabla w d\sigma.$$

As D is a disk, we have $\nu = \frac{x-X_0}{R}$ so that the previous integral becomes

$$\begin{aligned} \int_{\partial D} \nabla u \nabla w d\sigma &= \int_{\partial D} \nu \cdot \nu \nabla u \nabla w d\sigma \\ &= \int_{\partial D} \frac{x-X_0}{R} \cdot \nu \nabla u \nabla w d\sigma \\ &= \frac{1}{2R} \int_{\partial D} \frac{\partial |x-X_0|^2}{\partial \nu} \nabla u \nabla w d\sigma \\ &= \frac{1}{2R} \left(\int_D \nabla |x-X_0|^2 \nabla (\nabla u \nabla w) dX + \int_D \Delta(|x-X_0|^2) \nabla u \nabla w dX \right) \\ &= \frac{1}{R} \int_D 2\nabla u \nabla w + \sum_{i=1,2} (x_i - c_i) \frac{\partial}{\partial x_i} (\nabla u \nabla w) dX, \end{aligned}$$

and (2.4) follows. □

The expression of the shape derivative is the basis of the following iterative algorithm:

1. Chose an initial disk $D = \mathcal{B}(X_0, R_0)$.
2. For each iteration, $i > 0$:
 - (a) Calculate the solution to (2) u_i , associated to the disk $D_i = \mathcal{B}(X_i, R_i)$.
 - (b) Calculate the shape derivatives $\frac{\partial J}{\partial c_1}$, $\frac{\partial J}{\partial c_2}$, $\frac{\partial J}{\partial R}$
 - (c) Update the parameters of the disk $(X_{i+1}, R_{i+1}) = (X_i, R_i) - \delta \nabla J(X_i, R_i)$ with $\delta > 0$.
 - (d) If the updated disk is not entirely in Ω or if R becomes negative, reduce the size δ .
3. When $J(X_i, R_i)$ becomes smaller than a fixed threshold, we stop.

2.2 Numerical examples

The setting of all numerical tests is as follows:

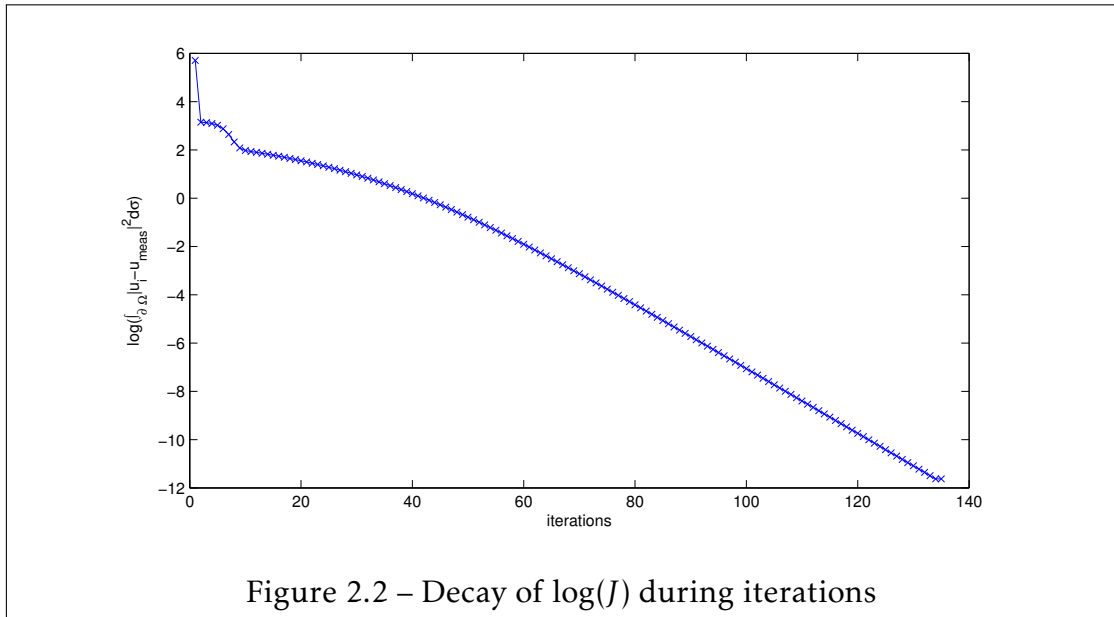
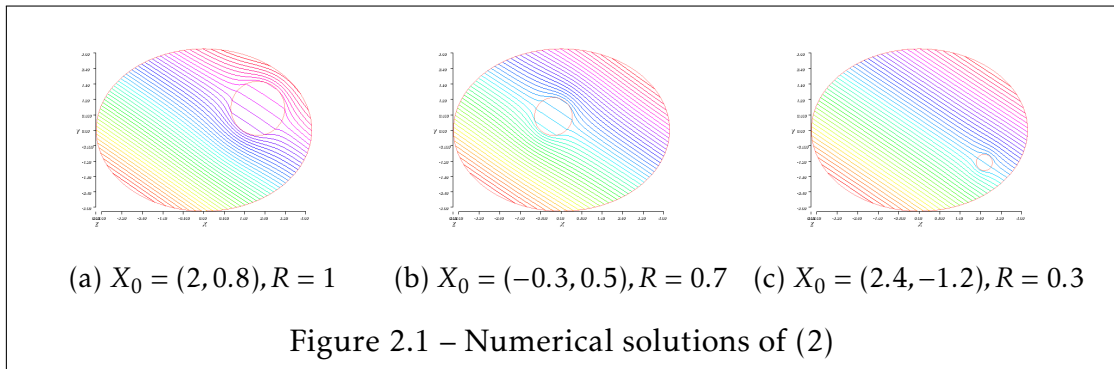
- We use FreeFem++ for our numerical experiments.
- Ω is a centered ellipse defined by the equation: $\frac{x_1^2}{4^2} + \frac{x_2^2}{3^2} \leq 1$.
- the conductivity k is a fixed constant, here we set $k = 5$.
- the Neumann data $g := \frac{\partial u}{\partial \nu}$ is defined by: $g = \langle e, \nu \rangle$ on $\partial\Omega$ where $e = \begin{pmatrix} 2 \\ 3 \end{pmatrix}$.
- We use P1 finite elements for the numerical resolution of the PDEs.
- At each iteration, we remesh the domain to adapt to the new predicted position of the disk.

In this subsection, we show three examples according to the disk's size, and its distance to the boundary $\partial\Omega$,

1. The target is close to the boundary $\partial\Omega$. Figure 2.1a shows the solution to (2) when the target disk is centered at $X_0 = \begin{pmatrix} 2 \\ 0.8 \end{pmatrix}$ and has radius $R = 1$.
2. The target is apart from the boundary $\partial\Omega$. Figure 2.1b shows the solution to (2) when the target disk is centered at $X_0 = \begin{pmatrix} 0.5 \\ 0.5 \end{pmatrix}$ and has radius $R = 0.7$.
3. The target has a small size. Figure 2.1c shows the solution to (2) when the target disk is centered at $X_0 = \begin{pmatrix} 2.4 \\ -1.2 \end{pmatrix}$ and has radius $R = 0.3$.

In these three cases, we exercise our algorithm with the same initial guess: the disk centered at $\begin{pmatrix} 0 \\ 0 \end{pmatrix}$ with radius 2.5.

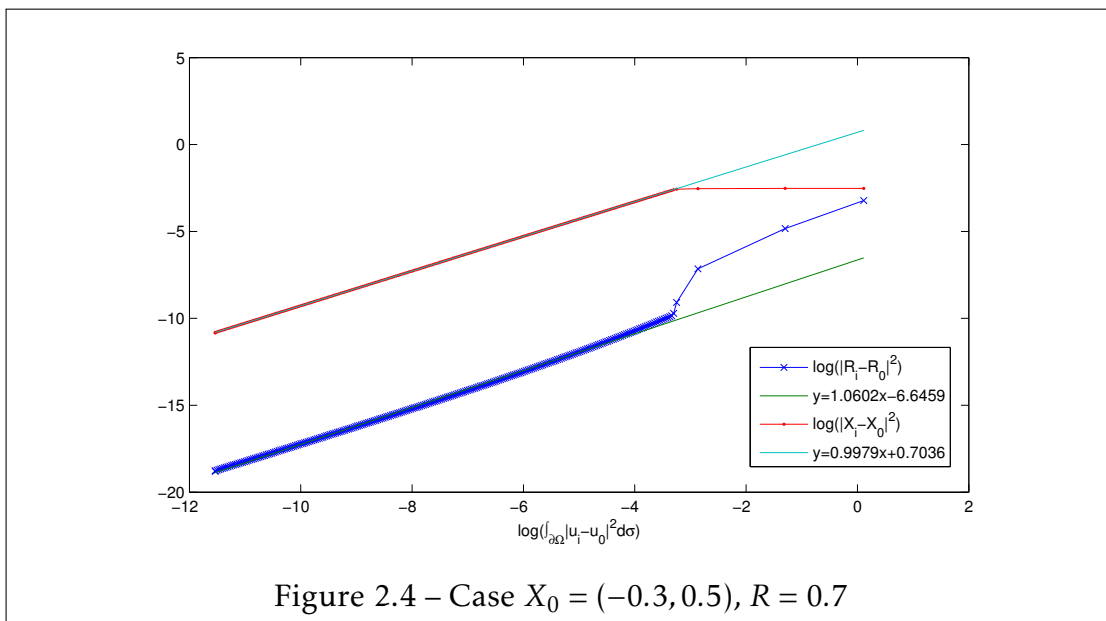
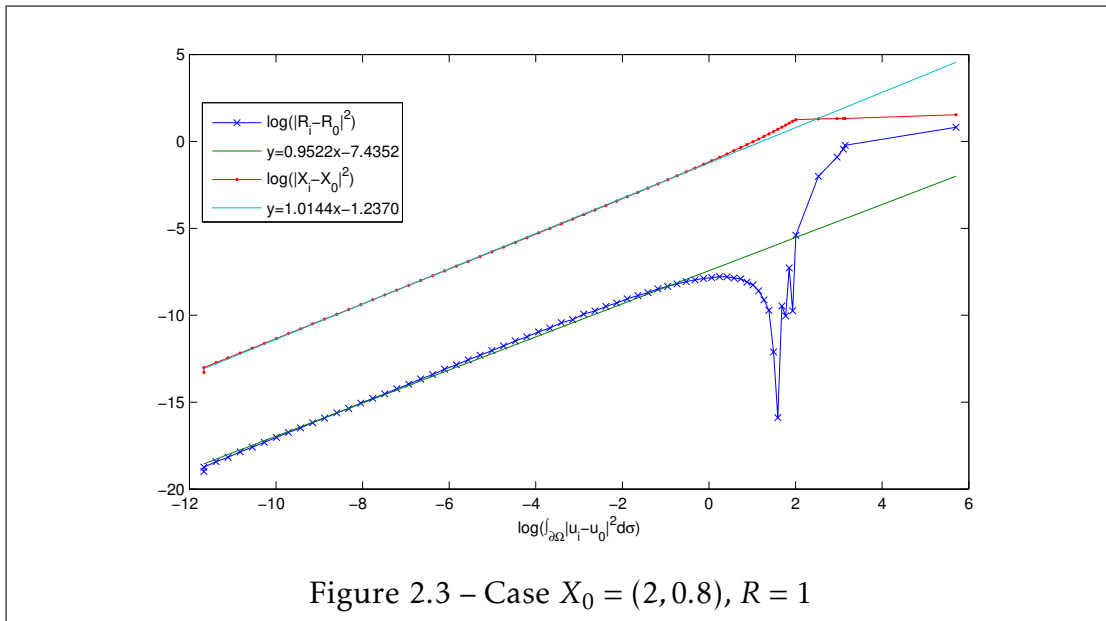
Figure 2.2 shows the decay of $\log(J)$ during the iterations in the first case. We can observe that J decays exponentially to 0. To illustrate the dependence between the geometric characteristics of the disk and J , we draw $\log(|X_i - X_0|^2)$ and



$\log(|R_i - R_0|^2)$ in terms of $\log(J)$ (Figures 2.3, 2.4, 2.5), where X_i and R_i denote the center and radius of the disk at the i -th iteration. In order to show the Hölder-type stability, it is also interesting to draw linear regression lines to each of these curves. Thus, the inclination of the linear regression lines present a numerical estimation of the Hölder exponent.

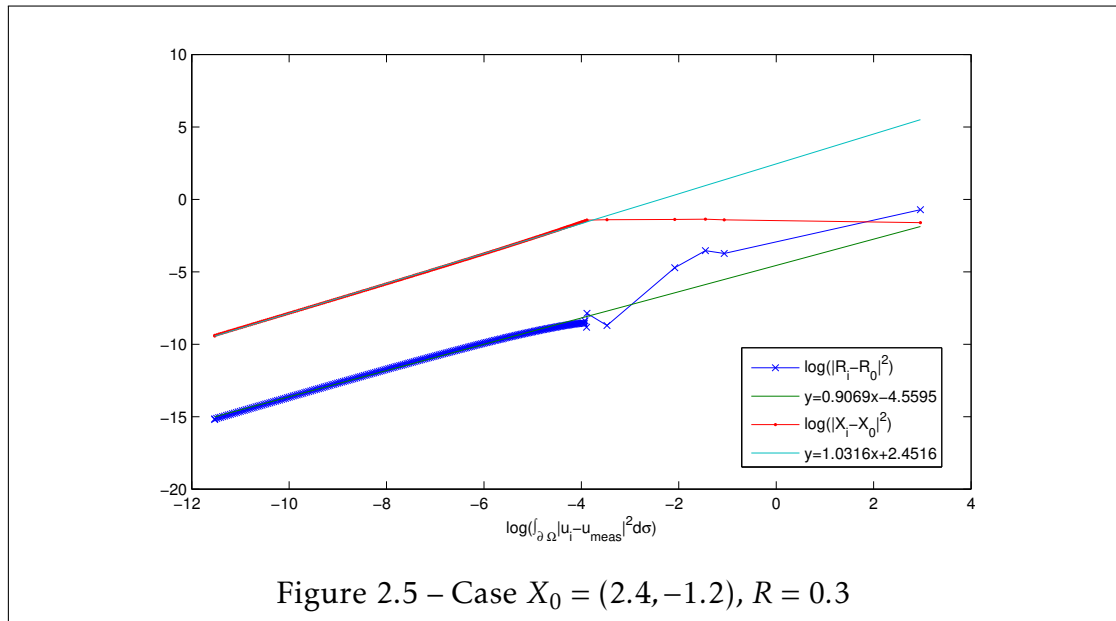
Finally, we conclude the numerical results of these three cases by the following remark.

Remark 2.2.1. • *Figures 2.3, 2.4, 2.5 show the asymptotic behaviors of $|X_i - X_0|$ and $|R_i - R_0|$ when J becomes small. We can observe from the left side of those*



figures that the data points are very close to a line. That numerically justify the theoretical prediction Theorem 1.2.3.

- The inclination of the linear regression lines present a numerical estimation of the Hölder exponent. The values in those three examples are presented in the table 2.1. These results show, the Hölder exponents are all close to 1.



- *There is no clear evidence of a relation between the Hölder exponents α and the distance between the target disk and $\partial\Omega$.*
- *We always choose δ near 0.1. Roughly speaking, when δ exceed 0.5, J does not decay during the iterations.*
- *For the same target, different initial guesses do not change the number of iterations to reach convergence.*
- *Exceptionally, if the center of the initial guess coincide with the target's center, only about 10 iterations are needed to reach the target.*
- *When the target disk is too small, more iterations are needed.*

•	inclination $\log X_i - X_0 /\log J$	inclination $\log R_i - R_0 /\log J$
example 1	1.0144	0.9522
example 2	0.9979	1.0602
example 3	1.0316	0.9069

Table 2.1 – Hölder exponents in different cases

Determination of inclusions using multifrequency measurements

3.1 Introduction

In this work, we introduce a new approach to analyze the inverse inclusion problem, the multifrequency measurements, we consider the following equation,

$$\begin{cases} \operatorname{div}(\gamma(x, \omega)\nabla u(x, \omega)) = 0 & \text{in } \Omega, \\ \gamma(x, \omega)\partial_\nu u(x, \omega) = f(x) & \text{on } \partial\Omega, \\ \int_{\partial\Omega} u(x, \omega) = 0, \end{cases} \quad (3.1)$$

where ω denotes the frequency, $\nu_\Omega(x)$ is the outward normal vector to $\partial\Omega$, $\gamma(x, \omega)$ is the conductivity coefficient, and $f \in H_\diamond^{-1/2}(\partial\Omega) := \{g \in H^{-1/2}(\partial\Omega) : \int_{\partial\Omega} g d\sigma = 0\}$ is the input current.

In this work we are interested in the case where the frequency dependent conductivity distribution takes the form

$$\gamma(x, \omega) = k_0 + (k(\omega) - k_0)\chi_D(x) \quad (3.2)$$

with $\chi_D(x)$ being the characteristic function of a C^2 domain D in Ω ($D \subset\subset \Omega$), k_0 being a fixed strictly positive constant, and $k(\omega) : \mathbb{R}_+ \rightarrow \mathbb{C} \setminus \mathbb{R}_-$, being a continuous complex-valued function. Here k_0 representing the conductivity of

the background medium, is known, and $k(\omega)$ is the conductivity of the biological tissue, given by the empirical model

$$k(\omega) := \kappa_1 - \frac{\kappa_2}{\omega^2 + i\omega\kappa_3}, \quad (3.3)$$

where $\kappa_p > 0, p = 1, 2, 3$, are constants that only depend on the biological tissue properties (see for instance [19]). The frequency profile $k(\omega)$ is somehow a meromorphic approximation with a single pole of the graph of experimental measurements for a given biological tissue [19]. It also appears as a homogenized model for periodically distributed biological cells in the dilute limit [19], and is similar to Drude models that describes the frequency dependence of the electric permittivity of a real metal within the visible frequency range [55].

3.2 Spectral decomposition

We first introduce an operator whose spectral decomposition will be later the cornerstone of the identification of the anomaly D . Let $H_\diamond^1(\Omega)$ be the space of functions v in $H^1(\Omega)$ satisfying $\int_{\partial\Omega} v d\sigma = 0$.

For $u \in H_\diamond^1(\Omega)$, we infer from the Riesz theorem that there exists a unique function $Tu \in H_\diamond^1(\Omega)$ such that for all $v \in H_\diamond^1(\Omega)$,

$$\int_{\Omega} \nabla Tu \nabla v dx = \int_D \nabla u \nabla v dx. \quad (3.4)$$

The variational Poincaré operator $T : H_\diamond^1(\Omega) \rightarrow H_\diamond^1(\Omega)$ is easily seen to be self-adjoint and bounded with norm $\|T\| \leq 1$.

The spectral problem for T reads as: Find $(\lambda, w) \in \mathbb{R} \times H_\diamond^1(\Omega)$, $w \neq 0$ such that $\forall v \in H_\diamond^1(\Omega)$,

$$\lambda \int_{\Omega} \nabla w \nabla v dx = \int_D \nabla w \nabla v dx.$$

Integrating by parts, one immediately obtains that any eigenfunction w is harmonic in D and in $D' = \Omega \setminus \overline{D}$, and satisfies the transmission and boundary

conditions

$$w|_{\partial D}^+ = w|_{\partial D}^-, \quad \partial_\nu w|_{\partial D}^+ = \left(1 - \frac{1}{\lambda}\right) \partial_\nu w|_{\partial D}^-, \quad \partial_{\nu_\Omega} w = 0,$$

where $w|_{\partial D}^\pm(x) = \lim_{t \rightarrow 0} w(x \pm t\nu_D(x))$ for $x \in \partial D$. In other words, w is a solution to (3.1) for $k = k_0(1 - \frac{1}{\lambda})$ and $f = 0$.

Let \mathfrak{H}_\diamond be the space of harmonic functions in D and D' , with zero mean $\int_{\partial\Omega} u d\sigma = 0$, and zero normal derivative $\partial_{\nu_\Omega} u = 0$ on $\partial\Omega$, and with finite energy semi-norm

$$\|u\|_{\mathfrak{H}_\diamond} = \int_{\Omega} |\nabla u|^2 dx.$$

Since the functions in \mathfrak{H}_\diamond are harmonic in D' , the space \mathfrak{H}_\diamond is a closed subspace of $H^1(\Omega)$. Later on, we will give a new characterization of the space \mathfrak{H}_\diamond in terms of the single layer potential on ∂D associated with the Neumann function of Ω .

We remark that $Tu = 0$ for all u in $H_0^1(D')$, and $Tu = u$ for all u in $H_0^1(D)$ (the set of functions $H^1(D)$ with trace zero).

We also remark that $T\mathfrak{H}_\diamond \subset \mathfrak{H}_\diamond$ and hence the restriction of T to \mathfrak{H}_\diamond defines a linear bounded operator. Since we are interested in harmonic functions in D and D' , we only consider the action of T on the closed space \mathfrak{H}_\diamond . We further keep the notation T for the restriction of T to \mathfrak{H}_\diamond . We will prove later that T has only isolated eigenvalues with an accumulation point $1/2$. We denote by $(\lambda_n^-)_{n \geq 1}$ the eigenvalues of T repeated according to their multiplicity, and ordered as follows

$$0 < \lambda_1^- \leq \lambda_2^- \leq \dots < \frac{1}{2},$$

in $(0, 1/2]$ and, similarly,

$$0 > \lambda_1^+ \geq \lambda_2^+ \geq \dots > \frac{1}{2}.$$

the eigenvalues in $[1/2, 1)$. The eigenvalue $\lambda_\infty = 1/2$ is the unique accumulation point of the spectrum. To ease the notation we further denote the orthogonal spectral projector on the eigenspace associated to $1/2$, by $\int_{\partial\Omega} w_\infty^\pm d\sigma w_\infty^\pm(x)$. Next, we will characterize the spectrum of T via the mini-max principle.

Proposition 3.2.1. [10] *The variational Poincaré operator has the following decom-*

position

$$T = \frac{1}{2}I + K, \quad (3.5)$$

where K is a compact self-adjoint operator. Let w_n^\pm , $n \geq 1$ be the eigenfunctions associated to the eigenvalues $(\lambda_n^\pm)_{n \geq 1}$. Then

$$\begin{aligned} \lambda_1^- &= \min_{0 \neq w \in \mathfrak{H}_\circ} \frac{\int_D |\nabla w(x)|^2 dx}{\int_{\Omega_e} |\nabla w(x)|^2 dx} \\ \lambda_n^- &= \min_{0 \neq w \in \mathfrak{H}_\circ, w \perp w_1^-, \dots, w_{n-1}^-} \frac{\int_D |\nabla w(x)|^2 dx}{\int_{\Omega_e} |\nabla w(x)|^2 dx} \\ &= \min_{F_n \subset \mathfrak{H}_\circ, \dim(F_n) = n} \max_{w \in F_n} \frac{\int_D |\nabla w(x)|^2 dx}{\int_{\Omega_e} |\nabla w(x)|^2 dx}, \end{aligned} \quad (3.6)$$

and similarly

$$\begin{aligned} \lambda_1^+ &= \max_{0 \neq w \in \mathfrak{H}_\circ} \frac{\int_D |\nabla w(x)|^2 dx}{\int_{\Omega_e} |\nabla w(x)|^2 dx} \\ \lambda_n^+ &= \min_{0 \neq w \in \mathfrak{H}_\circ, w \perp w_1^+, \dots, w_{n-1}^+} \frac{\int_D |\nabla w(x)|^2 dx}{\int_{\Omega_e} |\nabla w(x)|^2 dx} \\ &= \max_{F_n \subset \mathfrak{H}_\circ, \dim(F_n) = n} \min_{w \in F_n} \frac{\int_D |\nabla w(x)|^2 dx}{\int_{\Omega_e} |\nabla w(x)|^2 dx}. \end{aligned} \quad (3.7)$$

We have the following decomposition of $u(x, \omega)$ in the basis of the eigenfunctions of the variational Poincaré operator T .

Theorem 3.2.1. [10] *Let $u(x, \omega)$ be the unique solution to the system (3.1). Then, the following decomposition holds:*

$$u(x, \omega) = k_0^{-1} u_0(x) + \sum_{n=1}^{\infty} \frac{\int_{\partial\Omega} f(z) w_n^\pm(z) ds(z)}{k_0 + \lambda_n^\pm(k(\omega) - k_0)} w_n^\pm(x), \quad x \in \Omega, \quad (3.8)$$

where $u_0 \in H_\diamond^1(\Omega)$ depends only on f and D , and is the unique solution to

$$\left\{ \begin{array}{l} \Delta v = 0 \quad \text{in } D', \\ \nabla v = 0 \quad \text{in } D, \\ \partial_{\nu_\Omega} v = f \quad \text{on } \partial\Omega, \\ \int_{\partial\Omega} v d\sigma = 0. \end{array} \right. \quad (3.9)$$

Proof. We first observe that frequency dependent part

$$u_f = u - k_0^{-1} u_0,$$

lies in \mathfrak{H}_\diamond . Since the eigenfunctions $w^\pm(x)$ form an orthonormal basis of \mathfrak{H}_\diamond , the frequency part u_f posses the following spectral decomposition:

$$u_f(x) = \sum_{n=1}^{\infty} \int_{\Omega} \nabla u_f(z) \nabla w_n^\pm(z) dz w_n^\pm(x) \quad x \in \Omega.$$

A straightforward computation leads to

$$\int_{\Omega} \nabla u_f(z) \nabla w_n^\pm(z) dz = \int_{\Omega} \nabla u(z) \nabla w_n^\pm(z) dz.$$

On the other hand, since $u \in H_\diamond^1(\Omega)$, we obtain

$$\begin{aligned} \int_{\Omega} \nabla u(z) \nabla w_n^\pm(z) dz &= \lambda_n^\pm \int_D \nabla u(z) \nabla w_n^\pm(z) dz \\ &= \frac{k_0}{k(\omega)} \lambda_n^\pm \int_{\partial D} \partial_{\nu_D} u(z) |^+ w_n^\pm(z) d\sigma(z) \\ &= \frac{k_0}{k(\omega)} \lambda_n^\pm \int_{D'} \nabla u(z) \nabla w_n^\pm(z) dz - \frac{k_0}{k(\omega)} \lambda_n^\pm \int_{\partial\Omega} f(z) w_n^\pm(z) d\sigma(z). \end{aligned}$$

Using the simple fact that

$$\int_{\Omega} \nabla u(z) \nabla w_n^\pm(z) dz = \int_D \nabla u(z) \nabla w_n^\pm(z) dz + \int_{D'} \nabla u(z) \nabla w_n^\pm(z) dz,$$

we obtain the desired decomposition. \square

3.3 Retrieval the frequency part

In this section, we will try to reconstruct the constants κ_1 , κ_2 and κ_3 in the model (3.3) and the function u_0 in the spectral decomposition (3.8) of the solution $u(x, \omega)$ from the multifrequency measurements by using an optimization algorithm.

We consider the M frequencies of measurements $\omega_1, \omega_2, \dots, \omega_M$ corresponding to the values of conductivity $k(\omega_1), k(\omega_2), \dots, k(\omega_M)$, and the associated solutions $u(x, \omega_1), u(x, \omega_2), \dots, u(x, \omega_M)$. As $\frac{1}{2}$ is the unique accumulation point of the eigenvalues $(\lambda_n^\pm)_{n \in \mathbb{N}}$, we only consider the N_f first eigenvalues as unknown variables, and we approximate the others eigenvalues by $\frac{1}{2}$. That means, we make the following approximation, for $x \in \Omega$, $1 \leq p \leq M$,

$$u(x, \omega_p) \approx k_0^{-1} u_0(x) + \sum_{n=1}^{N_f} \frac{1}{k_0 + \lambda_n^\pm (k(\omega_p) - k_0)} v_n^\pm(x) + \frac{2}{k(\omega_p) + k_0} v_{N_f+1}(x), \quad (3.10)$$

where

$$v_n^\pm(x) = \int_{\partial\Omega} f(z) w_n^\pm(z) ds(z) w_n^\pm(x),$$

and

$$v_{N_f+1}(x) = \sum_{n>N_f} \int_{\partial\Omega} f(z) w_n^\pm(z) ds(z) w_n^\pm(x).$$

Using a simple integration by parts, we have, for all $n \in \mathbb{N}$,

$$\int_{\partial\Omega} f(z) w_n^\pm(z) ds(z) = \int_{\Omega} \nabla f(x) \nabla w_n^\pm(x) dx, \quad (3.11)$$

where f is the unique solution in $H_\diamond^1(\Omega)$ to

$$\begin{cases} \Delta f = 0 & \text{in } \Omega, \\ \partial_\nu f = f & \text{on } \partial\Omega. \end{cases} \quad (3.12)$$

So, the function $\sum_{n=1}^{\infty} v_n^\pm$ is the orthogonal projection of the function f on the

space \mathfrak{H}_\diamond . Moreover, u_0 satisfies, for all $n \in \mathbb{N}$,

$$\begin{aligned}
& \int_{\Omega} \nabla u_0(x) \nabla w_n^\pm(x) dx = \int_{\Omega \setminus \bar{D}} \nabla u_0(x) \nabla w_n^\pm(x) dx \\
& = \int_{\partial\Omega} u_0(x) \frac{\partial}{\partial \nu} w_n^\pm(x) ds(x) - \int_{\partial D} u_0(x) \frac{\partial}{\partial \nu} w_n^\pm(x) ds(x) \\
& = 0 - C \int_{\partial D} \frac{\partial}{\partial \nu} w_n^\pm(x) ds(x) \\
& = 0
\end{aligned} \tag{3.13}$$

As $\mathfrak{f} - u_0 \in \mathfrak{H}_\diamond$, the orthogonal projection of \mathfrak{f} on the space \mathfrak{H}_\diamond is $\mathfrak{f} - u_0$.

The formula (3.10) becomes,

$$\begin{aligned}
u(x, \omega_p) & \approx \frac{k(\omega_p) - k_0}{k_0(k(\omega_p) + k_0)} u_0(x) + \frac{2}{k(\omega_p) + k_0} \mathfrak{f}(x) \\
& + \sum_{n=1}^{N_f} \left(\frac{1}{k_0 + \lambda_n^\pm(k(\omega_p) - k_0)} - \frac{2}{k(\omega_p) + k_0} \right) v_n^\pm(x).
\end{aligned} \tag{3.14}$$

Now we want to reconstruct $\kappa_1, \kappa_2, \kappa_3$ and $u_0(x)$ by an optimization algorithm. In order to do so, we need an *a priori* estimation of the eigenvalues $\widetilde{\lambda}_n^\pm \in [0, 1]$ for $1 \leq n \leq N_f$. We will not recover the eigenvalues λ_n^\pm for the reason that they all vary in a relatively narrow interval such that the reconstruction of u_0 is not very sensitive to the variations of those eigenvalues.

Let $(x_j)_{1 \leq j \leq N_d} \in \partial\Omega$ be a discretization of the boundary $\partial\Omega$, and define, for $1 \leq j \leq N_d$,

$$\begin{aligned}
& F_j(U_0^{(j)}, V_1^{\pm(j)}, \dots, V_{N_f}^{\pm(j)}, \omega, \kappa_1, \kappa_2, \kappa_3) := \\
& \frac{k(\omega, \kappa_1, \kappa_2, \kappa_3) - k_0}{k_0(k(\omega, \kappa_1, \kappa_2, \kappa_3) + k_0)} U_0^{(j)} + \frac{2}{k(\omega, \kappa_1, \kappa_2, \kappa_3) + k_0} \mathfrak{f}(x_j) \\
& + \sum_{n=1}^{N_f} \left(\frac{1}{k_0 + \widetilde{\lambda}_n^\pm(k(\omega, \kappa_1, \kappa_2, \kappa_3) - k_0)} - \frac{2}{k(\omega, \kappa_1, \kappa_2, \kappa_3) + k_0} \right) V_n^{\pm(j)}.
\end{aligned} \tag{3.15}$$

where $(U_0^{(j)})_{1 \leq j \leq N_d}, (V_n^{\pm(j)})_{1 \leq j \leq N_d}$ are vectors in \mathbb{R}^{N_d} .

The scheme consists in minimizing the functional,

$$J_m(U_0, V_1^\pm, \dots, V_{N_f}^\pm, \kappa_1, \kappa_2, \kappa_3) := \frac{1}{2} \sum_{p=1}^M \sum_{j=1}^{N_d} |u(x_j, \omega_p) - F_j(U_0^{(j)}, V_1^{\pm(j)}, \dots, V_{N_f}^{\pm(j)}, \omega_p, \kappa_1, \kappa_2, \kappa_3)|^2. \quad (3.16)$$

We can easily calculate its gradient from (3.15) and (3.3), for $i = 1, 2, 3$, $1 \leq l \leq N_d$ and $1 \leq n \leq N_f$,

$$\frac{\partial J_m}{\partial \kappa_i} = \sum_{p=1}^M \sum_{j=1}^{N_d} \overline{(u(x_j, \omega_p) - F_j(\cdot, \omega_p))} \frac{\partial F_j}{\partial \kappa_i}(\cdot, \omega_p), \quad (3.17)$$

$$\frac{\partial J_m}{\partial U_0^{(l)}} = \sum_{p=1}^M \overline{(u(x_j, \omega_p) - F_l(\cdot, \omega_p))} \frac{\partial F_l}{\partial U_0^{(l)}}(\cdot, \omega_p), \quad (3.18)$$

$$\frac{\partial J_m}{\partial V_n^{\pm(l)}} = \sum_{p=1}^M \overline{(u(x_j, \omega_p) - F_l(\cdot, \omega_p))} \frac{\partial F_l}{\partial V_n^{\pm(l)}}(\cdot, \omega_p), \quad (3.19)$$

where we denote here $F_j(U_0^{(j)}, V_1^{\pm(j)}, \dots, V_{N_f}^{\pm(j)}, \omega_p, \kappa_1, \kappa_2, \kappa_3)$ by $F_j(\cdot, \omega_p)$ in order to simplify the notations.

The algorithm then follows the standard gradient method for $3 + N_d(1 + 2N_f)$ variables. Once we have reconstructed the conductivity profile, i.e. the approximate values of $\kappa_1, \kappa_2, \kappa_3$, we can use (3.14) again to calculate the approximate conductivity $\tilde{k}(\omega)$ by (3.3) and the approximate u_0 . Letting $x \in \partial\Omega$, we define,

$$\tilde{U}(x, \omega_1, \dots, \omega_M) = \begin{pmatrix} \tilde{u}(x, \omega_1) \\ \tilde{u}(x, \omega_2) \\ \vdots \\ \tilde{u}(x, \omega_M) \end{pmatrix},$$

$$L(\widetilde{\lambda}_1^\pm, \dots, \widetilde{\lambda}_{N_f}^\pm, \omega_1, \dots, \omega_M) = \begin{pmatrix} q_0(\omega_1) & q(\widetilde{\lambda}_1^+, \omega_1) & q(\widetilde{\lambda}_1^-, \omega_1) & \cdots & q(\widetilde{\lambda}_{N_f}^-, \omega_1) \\ q_0(\omega_2) & q(\widetilde{\lambda}_1^+, \omega_2) & q(\widetilde{\lambda}_1^-, \omega_2) & \cdots & q(\widetilde{\lambda}_{N_f}^-, \omega_2) \\ \vdots & \vdots & \vdots & \ddots & \vdots \\ q_0(\omega_M) & q(\widetilde{\lambda}_1^+, \omega_M) & q(\widetilde{\lambda}_1^-, \omega_M) & \cdots & q(\widetilde{\lambda}_{N_f}^-, \omega_M) \end{pmatrix},$$

$$V(x) = \begin{pmatrix} u_0(x) \\ v_1^+(x) \\ v_1^-(x) \\ \vdots \\ v_{N_f}^-(x) \end{pmatrix},$$

where $\tilde{u}(x, \omega) = u(x, \omega) - \frac{2}{\bar{k}(\omega) + k_0} \Gamma(x)$, $q_0(\omega) = \frac{\bar{k}(\omega) - k_0}{k_0(\bar{k}(\omega) + k_0)}$, and $q(\widetilde{\lambda}, \omega) = \frac{1}{k_0 + \widetilde{\lambda}(\bar{k}(\omega) - k_0)} - \frac{2}{\bar{k}(\omega) + k_0}$. Then, the approximate relation (3.14) becomes

$$\tilde{U}(x, \omega_1, \omega_2, \dots, \omega_M) \approx L(\widetilde{\lambda}_1^\pm, \dots, \widetilde{\lambda}_{N_f}^\pm, \omega_1, \dots, \omega_M) V(x). \quad (3.20)$$

We can therefore calculate the vector V from the following formula,

$$V(x) \approx (L^T L)^{-1} L^T \tilde{U}(x, \omega_1, \dots, \omega_M). \quad (3.21)$$

The approximate $u_0(x)$ is the first coefficient of the vector $V(x)$.

We sum up our method to reconstruct u_0 by the following algorithm:

1. Give an *a priori* estimation of eigenvalues $(\lambda_n^\pm)_{1 \leq n \leq N_f}$.
2. Chose a step length α_m .
3. Initialize the vectors $U_0|_0, V_1|_0, \dots, V_n|_0$ and the coefficients $\kappa_1|_0, \kappa_2|_0, \kappa_3|_0$.
4. While $|\nabla J_m|$ is larger then a threshold, we do
 - (a) Calculate the values of the functions F_j by (3.15), and ∇J_m by (3.17), (3.18), (3.19).
 - (b) Update the parameters $\kappa_i|_{k+1} = \kappa_i|_k - \alpha \frac{\partial J_m}{\partial \kappa_i}$, $U_0^{(l)}|_{k+1} = U_0^{(l)}|_k - \alpha \frac{\partial J_m}{\partial U_0^{(l)}}$, and $V_n^{\pm(l)}|_{k+1} = V_n^{\pm(l)}|_k - \alpha \frac{\partial J_m}{\partial V_n^{\pm(l)}}$.

5. When $|\nabla J_m|$ is smaller than the threshold, we stop the iterations.
6. Use (3.21) with the approximate coefficients κ_i obtained in the previous step to calculate the approximate value of $u_0(x)$ for every $x \in \partial\Omega$.

3.4 Asymptotic expansion

Let $\Omega \subset \mathbb{R}^2$ be a bounded domain with a \mathcal{C}^2 boundary $\partial\Omega$. The inclusion to determine $D \subset \Omega$ is also a \mathcal{C}^2 domain. We assume that the inclusion D has a positive distance from $\partial\Omega$: $\text{dist}(D, \partial\Omega) \geq \delta > 0$. Assuming $f \in H_0^{-1/2}(\Omega)$, we consider the following equation,

$$\begin{cases} \Delta u = 0 & \text{in } \Omega \setminus \overline{D}, \\ \nabla u = 0 & \text{in } D, \\ \frac{\partial u}{\partial \nu} = f & \text{on } \partial\Omega, \\ \int_{\partial\Omega} u d\sigma = 0. \end{cases} \quad (3.22)$$

Let D_ε be the perturbed domain, which is given by

$$\partial D_\varepsilon = \{\tilde{x} : \tilde{x} = x + \varepsilon h(x)\nu(x), x \in \partial D\}, \quad (3.23)$$

where $h \in \mathcal{C}^1(\partial D)$ and ν denotes the unit outward normal vector. And we consider the perturbed equation,

$$\begin{cases} \Delta u_\varepsilon = 0 & \text{in } \Omega \setminus \overline{D_\varepsilon}, \\ \nabla u_\varepsilon = 0 & \text{in } D_\varepsilon, \\ \frac{\partial u_\varepsilon}{\partial \nu} = f & \text{on } \partial\Omega, \\ \int_{\partial\Omega} u_\varepsilon d\sigma = 0 \end{cases} \quad (3.24)$$

From the representation formula, the solution u can be written as

$$u(x) = \mathcal{S}_D \phi(x) + \mathcal{S}_\Omega \psi(x) \quad x \in \Omega, \quad (3.25)$$

where $\phi = \frac{\partial u}{\partial \nu}|_+ \in L_0^2(\partial D)$ and $\psi \in L_0^2(\partial \Omega)$. From the same reason, we have,

$$u_\varepsilon(x) = \mathcal{S}_{D_\varepsilon} \phi_\varepsilon(x) + \mathcal{S}_\Omega \psi_\varepsilon(x) \quad x \in \Omega. \quad (3.26)$$

Using the jump relation and the facts that $\frac{\partial u}{\partial \nu}|_- = 0$ on ∂D and $\frac{\partial u}{\partial \nu}|_- = f$ on $\partial \Omega$, the densities ϕ and ψ satisfy the following system,

$$\begin{cases} (-\frac{1}{2}I + \mathcal{K}_D^*)\phi(x) + \frac{\partial}{\partial \nu} \mathcal{S}_\Omega \psi(x) = 0 & \text{on } \partial D, \\ \frac{\partial}{\partial \nu} \mathcal{S}_D \phi(x) + (-\frac{1}{2}I + \mathcal{K}_\Omega^*)\psi(x) = f & \text{on } \partial \Omega. \end{cases} \quad (3.27)$$

This system can be also represented in a matrix form:

$$M \begin{pmatrix} \phi \\ \psi \end{pmatrix} := \begin{pmatrix} (-\frac{1}{2}I + \mathcal{K}_D^*) & \frac{\partial}{\partial \nu} \mathcal{S}_\Omega \\ \frac{\partial}{\partial \nu} \mathcal{S}_D & (-\frac{1}{2}I + \mathcal{K}_\Omega^*) \end{pmatrix} \begin{pmatrix} \phi \\ \psi \end{pmatrix} = \begin{pmatrix} 0 \\ f \end{pmatrix}. \quad (3.28)$$

From the same reason, we have the following equation for the perturbed domain,

$$M_\varepsilon \begin{pmatrix} \phi_\varepsilon \\ \psi_\varepsilon \end{pmatrix} := \begin{pmatrix} (-\frac{1}{2}I + \mathcal{K}_{D_\varepsilon}^*) & \frac{\partial}{\partial \nu_\varepsilon} \mathcal{S}_\Omega \\ \frac{\partial}{\partial \nu} \mathcal{S}_{D_\varepsilon} & (-\frac{1}{2}I + \mathcal{K}_\Omega^*) \end{pmatrix} \begin{pmatrix} \phi_\varepsilon \\ \psi_\varepsilon \end{pmatrix} = \begin{pmatrix} 0 \\ f \end{pmatrix}. \quad (3.29)$$

3.4.1 Expansions of layer potentials

Let $a, b \in \mathbb{R}$, $a < b$ and $X(t) : [a, b] \rightarrow \mathbb{R}^2$ be a parametrization of ∂D , which satisfies $X \in \mathcal{C}^2([a, b])$ and $|X'(t)| = 1$ for all $t \in [a, b]$, then

$$\partial D = \{x = X(t), t \in [a, b]\}. \quad (3.30)$$

Then the outward unit normal vector $\nu(x)$ is given by $\nu(x) = R_{-\frac{\pi}{2}} T(x)$, where $R_{-\frac{\pi}{2}}$ is the rotation with the angle $-\frac{\pi}{2}$ and $T(x) = X'(t)$ denotes the tangential normal vector. Also the curvature $\gamma(x)$ satisfies

$$X''(t) = \gamma(x)\nu(x). \quad (3.31)$$

Then, the perturbed boundary ∂D_ε can be parametrized by

$$\partial D_\varepsilon = \{\tilde{x} = \tilde{X}(t) = X(t) + \varepsilon h(x)\nu(x), t \in [a, b]\}. \quad (3.32)$$

We denote the outward unit normal vector to ∂D_ε at \tilde{x} by $\tilde{\nu}(\tilde{x})$. Then we have,

$$\tilde{\nu}(\tilde{x}) = \nu(x) - \varepsilon h'(t)T(x) + O(\varepsilon^2), \quad (3.33)$$

where $h'(t) = \frac{d}{dt}h(X(t))$ - we use also sometimes $h'(x)$ to denote this quantity. We can also obtain the length element $d\sigma_\varepsilon(\tilde{y})$,

$$d\sigma_\varepsilon(\tilde{y}) = d\sigma(y)(1 - \varepsilon\gamma(y)h(y) + O(\varepsilon^2)) \quad (3.34)$$

Let Ψ_ε be the diffeomorphism from ∂D onto ∂D_ε given by $\Psi_\varepsilon(x) = x + \varepsilon h(x)\nu(x)$. From [12], we have the asymptotic expansion of \mathcal{K}_D^* ,

$$(\mathcal{K}_{D_\varepsilon}^* \tilde{\phi}) \circ \Psi_\varepsilon = \mathcal{K}_D^* \phi + \varepsilon \mathcal{K}_D^{(1)} \phi + O(\varepsilon^2), \quad (3.35)$$

where $\tilde{\phi} = \phi \circ \Psi_\varepsilon^{-1}$. The operator $\mathcal{K}_D^{(1)}$ is defined as:

$$\begin{aligned} \mathcal{K}_D^{(1)} \phi(x) = \int_{\partial D} & \left[\left(\frac{1}{|x-y|^2} - \frac{2\langle x-y, \nu(x) \rangle^2}{|x-y|^4} \right) h(x) - \frac{\langle x-y, T(x) \rangle}{|x-y|^2} h'(x) \right. \\ & - \frac{\nu(x), \nu(y)}{|x-y|^2} h(y) + \frac{2\langle x-y, \nu(x) \rangle \langle x-y, \nu(y) \rangle}{|x-y|^4} h(y) \\ & \left. - \frac{\langle x-y, \nu(x) \rangle}{|x-y|^2} \gamma(y) h(y) \right] \phi(y) d\sigma(y) \end{aligned} \quad (3.36)$$

Now we calculate the asymptotic expansion of the operators $\frac{\partial}{\partial \nu} \mathcal{S}_\Omega$ on ∂D and $\frac{\partial}{\partial \nu} \mathcal{S}_D$ on $\partial \Omega$. Let $\psi \in L_0^2(\partial \Omega)$ and $x \in \partial D$, then $\tilde{x} = x + \varepsilon h(x)\nu(x) \in \partial D_\varepsilon$, and we have:

$$\begin{aligned} \frac{\partial}{\partial \nu_\varepsilon} \mathcal{S}_\Omega \psi(\tilde{x}) &= \int_{\partial \Omega} \frac{\langle \tilde{x} - y, \tilde{\nu}(\tilde{x}) \rangle}{|\tilde{x} - y|^2} \psi(y) d\sigma(y), \\ &= \int_{\partial \Omega} \frac{\langle x + \varepsilon h(x)\nu(x) - y, \nu(x) - \varepsilon h'(x)T(x) \rangle}{|x + \varepsilon h(x)\nu(x) - y|^2} \psi(y) d\sigma(y) + O(\varepsilon^2), \\ &= \frac{\partial}{\partial \nu} \mathcal{S}_\Omega \psi(x) + \varepsilon (-h'(x)) \frac{\partial}{\partial T} \mathcal{S}_\Omega \psi(x) + h(x) \mathcal{S}_\Omega^{(1)} \psi(x) + O(\varepsilon^2), \end{aligned}$$

where $\frac{\partial}{\partial T}$ denotes the tangential derivative and $\mathcal{S}_\Omega^{(1)}$ is defined by: for $x \in \partial D$,

$$\mathcal{S}_\Omega^{(1)} \psi(x) = \int_{\partial\Omega} \left[\frac{1}{|x-y|^2} - \frac{2\langle x-y, \nu(x) \rangle^2}{|x-y|^4} \right] \psi(y) d\sigma(y). \quad (3.37)$$

By the similar method, we obtain the asymptotic expansion of $\frac{\partial}{\partial \nu} \mathcal{S}_D$. Let $\phi \in L_0^2(\partial D)$ and $x \in \Omega$,

$$\begin{aligned} \frac{\partial}{\partial \nu} \mathcal{S}_{D_\varepsilon} \tilde{\phi}(x) &= \int_{D_\varepsilon} \frac{\langle x - \tilde{y}, \nu(x) \rangle}{|x - \tilde{y}|^2} \tilde{\phi}(\tilde{y}) d\sigma_\varepsilon(\tilde{y}), \\ &= \int_D \frac{\langle x - y - \varepsilon h(y) \nu(y), \nu(x) \rangle}{|x - y - \varepsilon h(y) \nu(y)|^2} \phi(y) (1 - \varepsilon \gamma(y) h(y)) d\sigma + O(\varepsilon^2), \\ &= \frac{\partial}{\partial \nu} \mathcal{S}_D \phi(x) + \varepsilon \left\{ \int_{\partial D} \left[-\frac{\langle \nu(x), \nu(y) \rangle}{|x-y|^2} + 2 \frac{\langle x-y, \nu(x) \rangle \langle x-y, \nu(y) \rangle}{|x-y|^4} \right] h(y) \phi(y) d\sigma(y) \right. \\ &\quad \left. - \int_{\partial D} \frac{\langle x-y, \nu(x) \rangle}{|x-y|^2} \gamma(y) h(y) \phi(y) d\sigma(y) \right\} + O(\varepsilon^2) \\ &= \frac{\partial}{\partial \nu} \mathcal{S}_D \phi(x) + \varepsilon \frac{\partial}{\partial \nu} [\mathcal{D}_D(h\phi) - \mathcal{S}_D(\gamma h\phi)](x) + O(\varepsilon^2). \end{aligned} \quad (3.38)$$

Then we have $M_\varepsilon = M + \varepsilon M_h + O(\varepsilon^2)$, where the operator M_1 on $L_0^2(\partial D) \times L_0^2(\partial\Omega)$ is defined by:

$$M_h := \begin{pmatrix} \mathcal{K}_D^{(1)} & -h' \frac{\partial}{\partial T} \mathcal{S}_\Omega + h \mathcal{S}_\Omega^{(1)} \\ \frac{\partial}{\partial \nu_\Omega} [\mathcal{D}_D(h\cdot) - \mathcal{S}_D(\gamma h\cdot)] & 0 \end{pmatrix}. \quad (3.39)$$

So, the systems (3.28) and (3.29) imply that

$$\begin{pmatrix} \phi_\varepsilon \\ \psi_\varepsilon \end{pmatrix} = \begin{pmatrix} \phi \\ \psi \end{pmatrix} + \varepsilon \begin{pmatrix} \phi_h \\ \psi_h \end{pmatrix} + O(\varepsilon^2), \quad (3.40)$$

where $\begin{pmatrix} \phi_h \\ \psi_h \end{pmatrix}$ is given by

$$\begin{pmatrix} \phi_h \\ \psi_h \end{pmatrix} = -M^{-1} M_h \begin{pmatrix} \phi \\ \psi \end{pmatrix}. \quad (3.41)$$

Thus, using the representation formula and the same calculus, we have also the

asymptotic expansion of the solution u : for $x \in \partial\Omega$:

$$u_\varepsilon(x) = u(x) + \varepsilon(\mathcal{S}_D\phi_1(x) + \mathcal{S}_\Omega\psi_1(x) + \mathcal{D}_D(h\phi)(x) - \mathcal{S}_D(\gamma h\phi)(x)) + O(\varepsilon^2). \quad (3.42)$$

We denote by \tilde{u}_h the function $\mathcal{S}_D\phi_1 + \mathcal{S}_\Omega\psi_1$ in Ω and denote by u_h the function $\tilde{u} + \mathcal{D}_D(h\phi) - \mathcal{S}_D(\gamma h\phi)$. From (3.41), we have on ∂D ,

$$\frac{\partial \tilde{u}_h}{\partial \nu} \Big|_- + \mathcal{K}_D^{(1)}\phi - h' \frac{\partial}{\partial T} \mathcal{S}_\Omega\psi + h\mathcal{S}_\Omega^{(1)}\psi = 0, \quad (3.43)$$

and on $\partial\Omega$,

$$\frac{\partial \tilde{u}_h}{\partial \nu} \Big|_- + \frac{\partial}{\partial \nu} [\mathcal{D}_D(h\phi) - \mathcal{S}_D(\gamma h\phi)] = 0. \quad (3.44)$$

(3.44) implies that

$$\frac{\partial u_h}{\partial \nu} = 0 \quad \text{on } \partial\Omega. \quad (3.45)$$

By (3.25) and the fact that $\frac{\partial}{\partial T}u = 0$ on ∂D , we have,

$$\begin{aligned} 0 &= \frac{\partial}{\partial T} h \frac{\partial u}{\partial T}(x), \\ &= \frac{\partial}{\partial T} h \frac{\partial}{\partial T} \mathcal{S}_D\phi(x) + h'(x) \frac{\partial}{\partial T} \mathcal{S}_\Omega\psi(x) + h(x) \frac{\partial^2}{\partial T^2} \mathcal{S}_\Omega\psi(x), \\ &= \frac{\partial}{\partial T} h \frac{\partial}{\partial T} \mathcal{S}_D\phi(x) + h'(x) \frac{\partial}{\partial T} \mathcal{S}_\Omega\psi(x) \\ &\quad + h(x) \int_{\partial\Omega} \left[\frac{-1}{|x-y|^2} + 2 \frac{\langle x-y, \nu(x) \rangle^2}{|x-y|^4} + 2\gamma(x) \frac{\langle x-y, \nu(x) \rangle}{|x-y|^2} \right] \psi(y) d\sigma(y), \\ &= \frac{\partial}{\partial T} h \frac{\partial}{\partial T} \mathcal{S}_D\phi(x) + h'(x) \frac{\partial}{\partial T} \mathcal{S}_\Omega\psi(x) - h(x) \mathcal{S}_\Omega^{(1)}\psi(x) + 2\gamma(x) h(x) \frac{\partial}{\partial \nu} \mathcal{S}_\Omega\psi(x), \end{aligned}$$

which implies

$$-h' \frac{\partial}{\partial T} \mathcal{S}_\Omega\psi + h\mathcal{S}_\Omega^{(1)}\psi = \frac{\partial}{\partial T} h \frac{\partial}{\partial T} \mathcal{S}_D\phi + 2\gamma h \left(\frac{1}{2}I - \mathcal{K}_D^* \right) \phi \quad (3.46)$$

A similar calculus give us: for $x \in \partial D$

$$\begin{aligned} & \frac{\partial}{\partial T} h \frac{\partial}{\partial T} \mathcal{S}_D \phi(x) \\ &= \int_{\partial D} \left[h'(x) \frac{\langle x-y, T(x) \rangle}{|x-y|^2} + h(x) \left(\frac{-1}{|x-y|^2} + \frac{2\langle x-y, \nu(x) \rangle^2}{|x-y|^4} + 2\gamma(x) \frac{\langle x-y, \nu(x) \rangle}{|x-y|^2} \right) \right] \phi(y) d\sigma(y). \end{aligned} \quad (3.47)$$

Thus,

$$\begin{aligned} & \mathcal{K}_D^{(1)} \phi(x) - h' \frac{\partial}{\partial T} \mathcal{S}_\Omega \psi(x) + h \mathcal{S}_\Omega^{(1)} \psi(x) \\ &= \int_{\partial D} \left[-\frac{\langle \nu(x), \nu(y) \rangle}{|x-y|^2} + 2 \frac{\langle x-y, \nu(x) \rangle \langle x-y, \nu(y) \rangle}{|x-y|^4} \right] h(y) \phi(y) d\sigma(y) \\ & - \int_{\partial D} \frac{\langle x-y, \nu(x) \rangle}{|x-y|^2} \gamma(y) h(y) \phi(y) d\sigma(y) + \gamma(x) h(x) \phi(x) \end{aligned} \quad (3.48)$$

By the continuity of the normal derivative of double layer potentials and the jump relation, we have, for $x \in \partial D$,

$$\begin{aligned} & \frac{\partial}{\partial \nu} \Big|_- [\mathcal{D}_D(h\phi) - \mathcal{S}_D(\gamma h\phi)](x) \\ &= \int_{\partial D} \left[-\frac{\langle \nu(x), \nu(y) \rangle}{|x-y|^2} + 2 \frac{\langle x-y, \nu(x) \rangle \langle x-y, \nu(y) \rangle}{|x-y|^4} \right] h(y) \phi(y) d\sigma(y) \\ & + \frac{1}{2} \gamma(x) h(x) \phi(x) - \int_{\partial D} \frac{\langle x-y, \nu(x) \rangle}{|x-y|^2} \gamma(y) h(y) \phi(y) d\sigma(y). \end{aligned} \quad (3.49)$$

Using (3.43), (3.48) and (3.49), we have,

$$\frac{\partial u_h}{\partial \nu} \Big|_- = \frac{\partial \tilde{u}_h}{\partial \nu} \Big|_- + \frac{\partial}{\partial \nu} \Big|_- [\mathcal{D}_D(h\phi) - \mathcal{S}_D(\gamma h\phi)] = 0. \quad (3.50)$$

It means u_h is the solution to the following equation:

$$\begin{cases} \Delta u_h = 0 & \text{in } D \cup (\Omega \setminus \bar{D}), \\ \frac{\partial u_h}{\partial \nu}|_- = 0 & \text{on } \partial D, \\ u_h|_+ - u_h|_- = -h\phi & \text{on } \partial D, \\ \frac{\partial u_h}{\partial \nu} = 0 & \text{on } \partial\Omega, \\ \int_{\partial\Omega} u_h d\sigma = 0. \end{cases} \quad (3.51)$$

3.5 Inclusion reconstruction

3.5.1 Optimization algorithm

In this section, we consider a numerical scheme to reconstruct the domain contained in a subset $\Omega_0 \subset \Omega$ with $\text{dist}(\partial\Omega_0, \partial\Omega) \geq \delta_0 > 0$, using finitely many measurements. The scheme is based on minimizing the functional

$$J(u) = \frac{1}{2} \int_{\partial\Omega} \sum_{i=1}^P |u - u_{meas}^{(i)}|^2 d\sigma,$$

where $u_{meas}^{(i)}$ are the measured Dirichlet data corresponding to the i -th Neumann data and where u is the solution to (3.1) associated to the current domain $D \subset \Omega_0$. In our numerical simulations, $P = 2$, we use two linearly independent Neumann data: $f_1 = \langle e_1, \nu \rangle$ and $f_2 = \langle e_2, \nu \rangle$, where (e_1, e_2) is the canonical basis of \mathbb{R}^2 .

We assume that our domain D is star shaped and its boundary ∂D can be described by the Fourier series:

$$\partial D = \{X_0 + r(\theta) \begin{pmatrix} \cos \theta \\ \sin \theta \end{pmatrix} | \theta \in [0; 2\pi)\}, \quad r = \sum_{n=-N}^N c_n f_n, \quad (3.52)$$

where $C = \begin{pmatrix} c_{-N} \\ c_{-N+1} \\ \vdots \\ c_N \end{pmatrix} \in \mathbb{R}^{2N+1}$, $f_n(\theta) = \cos(n\theta)$ for $0 \leq n \leq N$ and $f_n(\theta) = \sin(n\theta)$ for $-N \leq n < 0$.

Using (3.51) and integration by parts, we have the expressions of the shape derivative corresponding to each Fourier coefficient, for $-N \leq n \leq N$,

$$\frac{\partial J}{\partial c_n} = \int_{\Omega \setminus D} \nabla w \nabla u_h dX, \quad (3.53)$$

where $h(\theta) = f_n(\theta) \langle \begin{pmatrix} \cos \theta \\ \sin \theta \end{pmatrix}, \nu \rangle$ and w is the solution of the following equation,

$$\begin{cases} \Delta w = 0 & \text{in } \Omega \setminus \overline{D}, \\ \frac{\partial w}{\partial \nu} = 0 & \text{on } \partial D \\ \frac{\partial w}{\partial \nu} = u - u_{meas} & \text{on } \partial \Omega. \end{cases} \quad (3.54)$$

The formula (3.53) is also valid for the shape derivative corresponding to the displacement of X_0 , in these cases, $h = \langle e_i, \nu \rangle$, $i = 1, 2$.

Those expressions are the basis of the following iterative algorithm:

1. Chose an initial domain D_0 .
2. For each iteration, $i > 0$:
 - (a) Calculate the solution to (3.1) u_i , associated to the domain D_i for which the boundary ∂D_i is calculated by (3.52).
 - (b) Calculate the shape derivatives $\frac{\partial J}{\partial x_1}$, $\frac{\partial J}{\partial x_2}$ and $\frac{\partial J}{\partial c_n}$ for all $-N \leq n \leq N$.
 - (c) Update the parameters of the domain $X_{i+1} = X_i - \alpha \nabla_{X_0} J(X_i, C_i)$ and $C_{i+1} = C_i - \alpha \nabla_C J(X_i, C_i)$ with $\alpha > 0$.
 - (d) If the updated domain is not entirely in Ω or if R becomes negative, reduce the size of α .
3. When $J(X_i, C_i)$ becomes smaller than a fixed threshold, we stop.

3.6 Numerical examples

The setting of all numerical tests is as follows:

- We use FreeFem++ for our numerical experiments.
- Ω is a centered ellipse defined by the equation: $\frac{x_1^2}{4^2} + \frac{x_2^2}{3^2} \leq 1$.
We also tried another case with $\partial\Omega_2 = \{[4 + 0.8(\cos\theta + \sin\theta) - (\cos 2\theta + \sin 2\theta)](\cos\theta, \sin\theta), \theta \in [0, 2\pi)\}$.
- We use two linearly independent Neumann data: $f_1 = \langle e_1, \nu \rangle$ and $f_2 = \langle e_2, \nu \rangle$, where (e_1, e_2) is the canonical basis of \mathbb{R}^2 .
- The multifrequency conductivity follows the model (3.3) with $\kappa_1 = 3$, $\kappa_2 = 2$, $\kappa_3 = 1$ and ω are integers from 1 to 8.
- Only the first eigenvalues are taken into consideration, and their apriori estimations are settled as $\widetilde{\lambda}_1^+ = \frac{3}{4}$, $\widetilde{\lambda}_1^- = \frac{1}{4}$ respectively in all cases.
- In the algorithm to reconstruct u_0 and the conductivity profile, the initial guess of u_0 is the function \mathfrak{f} , solution to the equation (3.12).
- The initial estimation of domain D is a centered disk with a radius $\frac{1}{2}$.
- We consider the first 15 Fourier coefficients: $N = 15$.
- We use P1 finite elements for the numerical resolution of the PDEs.
- At each iteration, we remesh the domain to adapt to the new predicted position and shape of the domain.
- The algorithms stop if $J < 10^{-5}$ or the number of iterations exceed 500. All of the cases here have executed 500 iterations.

We present here several numerical simulations of the algorithm. We first present, in the following Table (3.1), the precision of our reconstruction method of u_0 and the reconstructed coefficients κ_1 , κ_2 , κ_3 in Table (3.2). Here, errors are the L^2 -norm of the difference $u_{0reconstruct} - u_0$: $error(u_{0reconstruct}) := \sqrt{\int_{\partial\Omega} |u_{0reconstruct} - u_0|^2 dx}$. We show in the following figures the targets and the reconstruction result. We calculate also the relative symmetric difference $|D_i \Delta D_{target}| / |D_{target}|$ during the iterations, and we draw the curves of the symmetric difference to $\log(u_i)$. We finally give the relative symmetric difference of

•	ellipse	square	near-boundary	small-central	in Ω_2
$f = f_1$	0.04707	0.11973	0.00956	0.00502	0.04208
$f = f_2$	0.01583	0.09905	0.02436	0.00893	0.08556

Table 3.1 – Errors between $u_{0reconstruct}$ and u_0

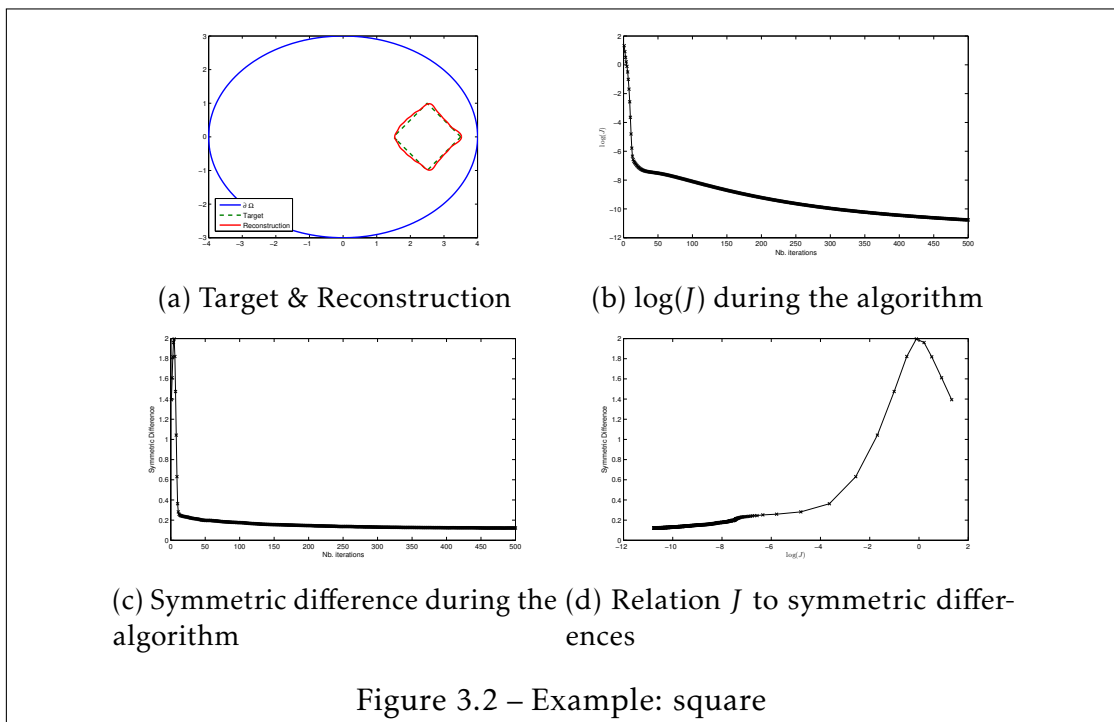
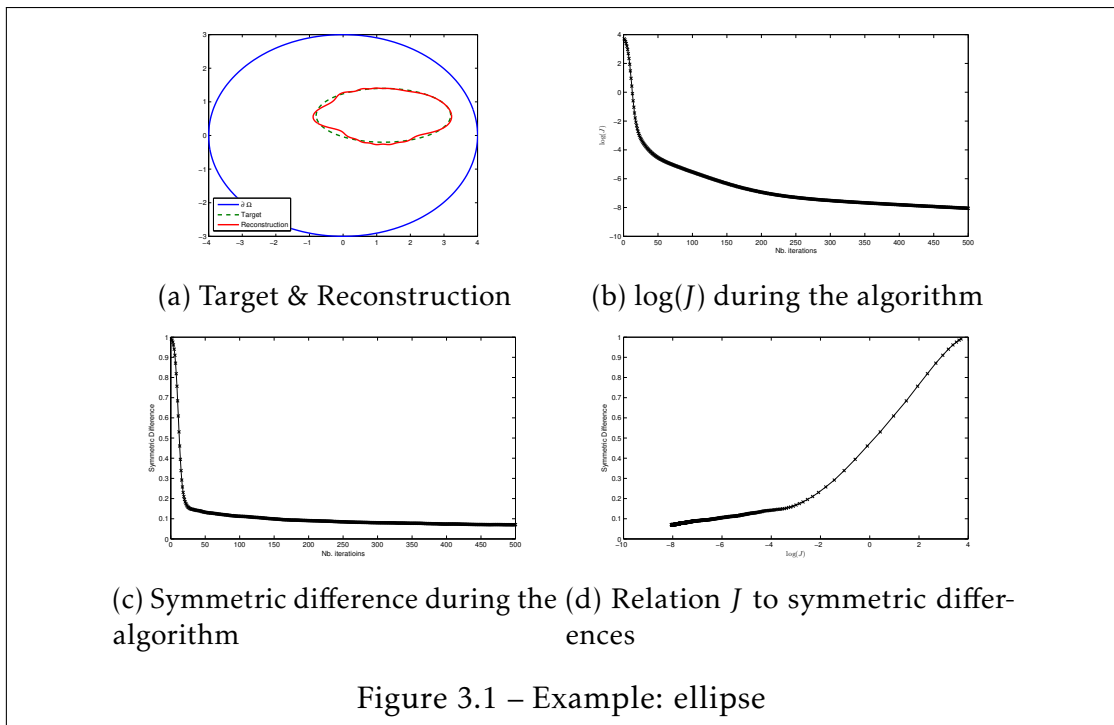
•	real value	ellipse	square	near-boundary	small-central	in Ω_2
κ_1	3	2.80971	3.36482	3.00287	6.65418	2.89787
κ_2	2	1.79063	2.34197	1.96926	5.14671	1.86579
κ_3	1	1.00212	0.987247	0.999658	1.13223	1.00446

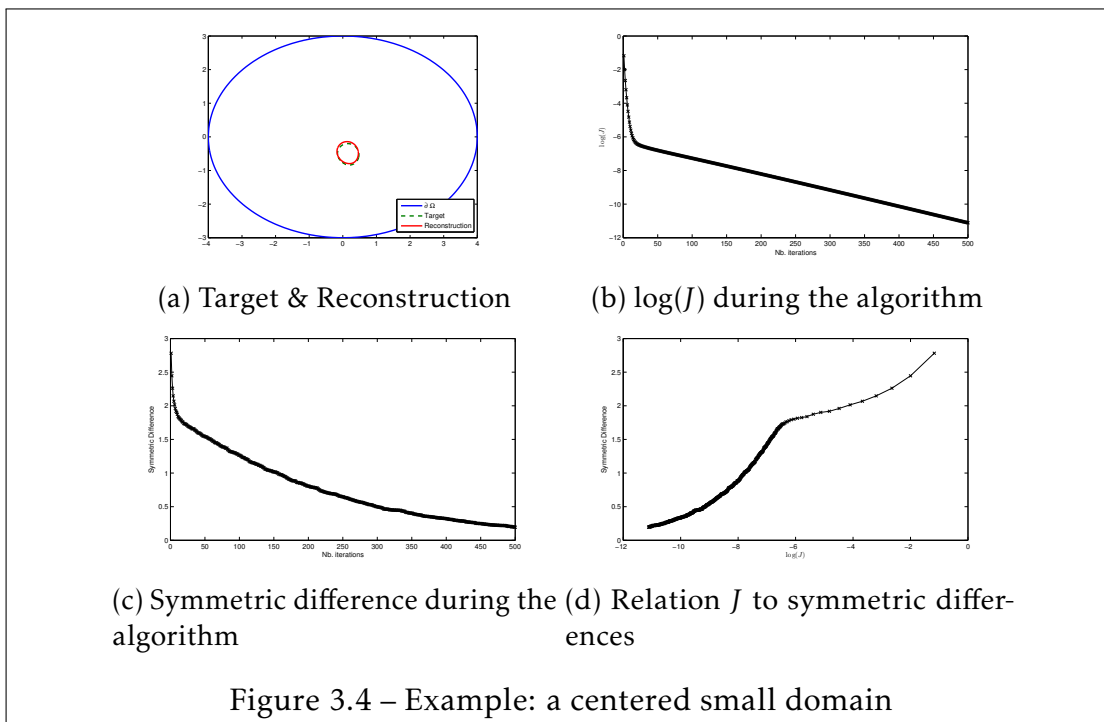
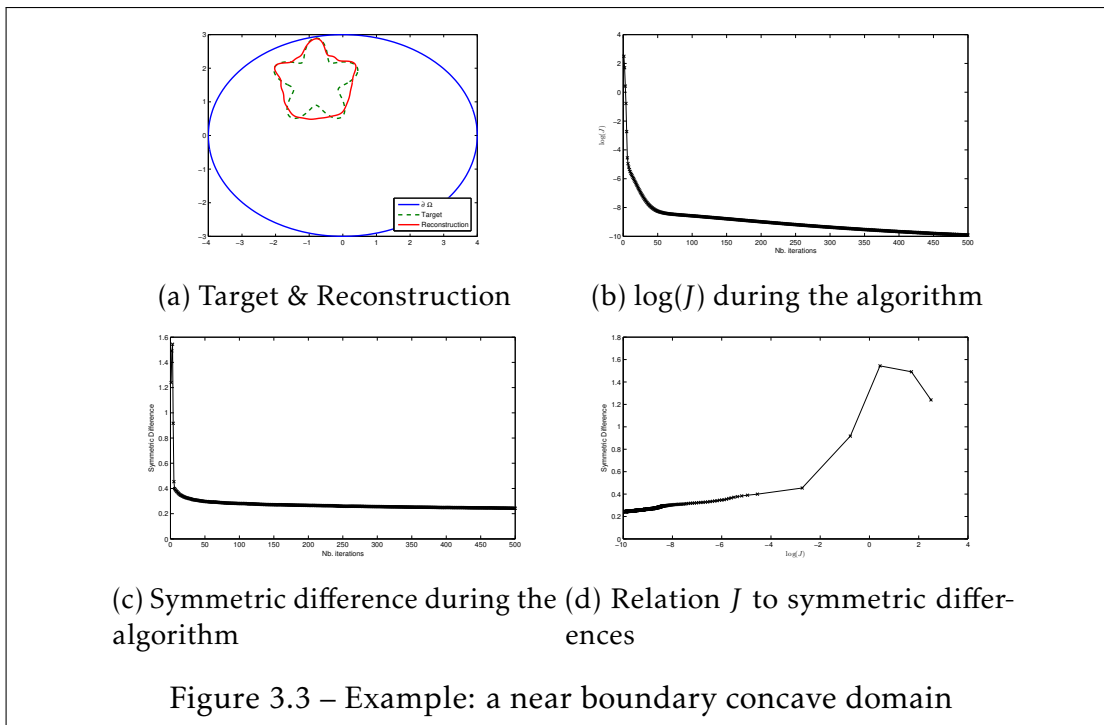
Table 3.2 – Reconstructs conductivity coefficients

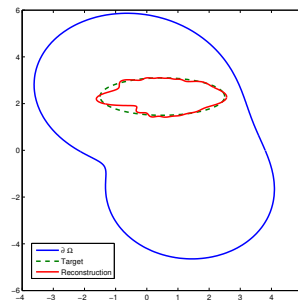
each case in Table 3.3.

•	ellipse	square	near-boundary	small-central	in Ω_2
$ D_i \Delta D_{target} / D_{target} $	0.07055	0.12187	0.24299	0.19471	0.120597

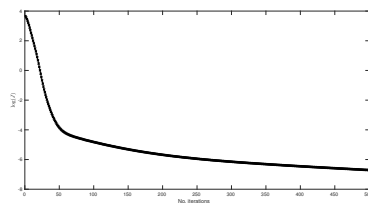
Table 3.3 – Relative symmetric difference



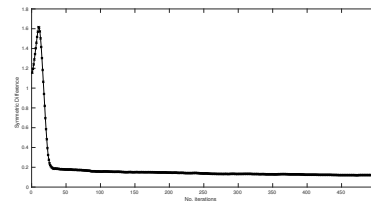




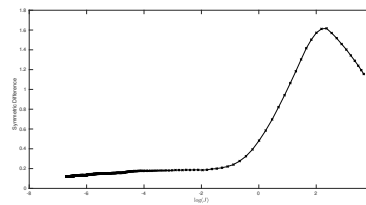
(a) Target & Reconstruction



(b) $\log(J)$ during the algorithm



(c) Symmetric difference during the algorithm



(d) Relation J to symmetric differences

Figure 3.5 – Example: The case in Ω_2

Mathematical model of electroreception

4.1 Introduction

Some species of fish have the ability to recognize the environment around them by generating a weak electrical field at different frequencies. They possess an electric organs, which can generate an electric field, and their skins are sensitive to nearby electric fields. Their central nervous systems can identify objects by analyzing the input electrical impulsion generated by themselves and the received electrical signals from their skin. From the mathematical point of view the electric waves can be described by Maxwell equations in the quasi-static regime, and the behavior of the electrical field in the neighborhood of the fish leads to an inverse conductivity problem with a finite number of excitations at different frequencies, and a finite number of boundary measurements.

To identify its targets the weakly electric fish solves an inverse problem that has many similarities with the studied multifrequency electric impedance tomography problem in the previous chapter. Recall this latter method is a recent imaging technique of biological tissues where one tries to take advantage of the dependence of the conductivity on the frequency [10, 19]. Indeed, most biological tissues exhibit frequency dependent conductivities, when excited by electric waves with frequencies ranging roughly around 10kHz [57]. Experiments

indicate that the electric fish sends out electric waves at different frequencies, to gather information around its environment. Assuming that the target is a different fish, our objective here is to explain how a weakly electric fish might identify it. The proposed inverse problem has many potential bio-inspired applications in underwater robotics [51, 34].

In this chapter we are interested in the case where the fish and the target fish occupy respectively the bounded domains $\Omega \subset \mathbb{R}^d$, $d = 2, 3$, and $D \subset \mathbb{R}^d \setminus \overline{\Omega}$. We assume that the conductivity distribution around the fish, is given by

$$\gamma(x, \omega) = 1 + (k(\omega) - 1)\chi_D(x),$$

with χ_D denotes the characteristic function of D , 1 is the conductivity of the background, $k(\omega) : \mathbb{R}_+ \rightarrow \mathbb{C} \setminus \overline{\mathbb{R}_-}$, is the conductivity of the target fish target, and ω the frequency of the electric wave u produced by the fish. Recently shape recognition and classification methods have been applied on small volume targets [20, 17]. In the present work we adapt the method developed in [10] to the weakly electric fish inverse problem. We take advantage of multifrequency measurements and combine unique continuation techniques for meromorphic complex functions with a clever spectral representation of u involving eigenfunctions of the variational Poincaré operator, to reconstruct the conductivity map γ . The spectral decomposition can be written in the form

$$u(x, \omega) = u_0(x) + u_f(x, k(\omega)),$$

where the function u_0 is independent of the frequency ω , and represents the limiting solution when the contrast $k(\omega)$ tends to ∞ . In fact u_0 is exactly the electric potential when we substitute the target fish by a perfect conductor with the same shape and position! Then, it is not surprising that one can uniquely identify D from only one boundary measurement $u_0|_{\partial\Omega}$. The problem of determining D from $u_0|_{\partial\Omega}$ has been studied in many works, and optimal stability estimates have been already derived (see e.g.[4]).

In this chapter, we are concerned with the multifrequency inverse inclusion problem in unbounded domain. We first describe the mathematical model

of electroreception. After introducing the weighted Sobolev space $\mathcal{W}^{1,-1}(\mathbb{R}^d)$, which is the natural space where we solve the Laplace equation using variational techniques in unbounded domains, we prove the existence and uniqueness of solutions to the direct problem. We then set up a spectral decomposition using a modified variational Poincaré operator on $\mathcal{W}^{1,-1}(\mathbb{R}^d)$. Using the same techniques of reconstruction as in [10], we derive the uniqueness of solutions to the inverse problem, and obtain stability estimates. The numerical validation of our theoretical approach is realized by reconstructing different targets using synthetic data in the next chapter.

This chapter is organized as follows. In the next section, we present the mathematical model of the weakly electric fish. In section 3, we study the well-posedness of the partial differential equation system associated to the forward problem. In section 4, we introduce the Poincaré variational operator, and we study its spectrum. Then, we derive the spectral decomposition of the unique solution to the forward problem in section 5. We derive uniqueness and stability estimates to the inverse problem in section 6. The next chapter is devoted to some numerical illustrations of the obtained theoretical results here. Similar spectral decomposition is used to derive the frequency independent part u_0 in a bounded truncated numerical domain. Then, we introduce an optimization scheme to reconstruct the position and shape of the target fish. Numerical experiments are presented at the end.

4.2 The Mathematical Model

In this section we adapt the mathematical model of the weakly electric fish introduced by Ammari et. al. in [6]. Let $\Omega \subset \mathbb{R}^d$, $d = 2, 3$, be an open connected and bounded region, which represents the electric fish. We suppose that $\partial\Omega$ is of class $\mathcal{C}^{1,\alpha}$ for some $\alpha \in (0, 1]$. We denote by Ω_e the exterior of Ω , that is $\Omega_e := \mathbb{R}^d \setminus \overline{\Omega}$.

The target fish D is also assumed to be an open connected region in Ω_e . We assume that there exists $\delta > 0$ such that $\text{dist}(\partial\Omega, \partial D) > \delta$. We define a class of inclusions on which we study the uniqueness and stability of the inverse problem. We assume that the inclusion D contains the origin. Let $b_1 = \text{dist}(0, \partial\Omega)$ and let

$b_0 < b_1$. For $m > 2$ and $\varsigma \in (0, 1]$, we define the class of inclusions

$$\mathcal{D} := \left\{ D := \{x \in \mathbb{R}^d : |x| < \Upsilon(\hat{x}), \hat{x} = \frac{x}{|x|}\}; b_0 < \Upsilon(\hat{x}) < b_1 - \delta; \|\Upsilon\|_{C^{2,\varsigma}} \leq m \right\}.$$

We assume that the conductivity is equal to 1 everywhere except in the target D where the conductivity is equal to $k(\omega)$. We denote by $\gamma(x, \omega) := 1 + (k(\omega) - 1)\chi_D$, the conductivity distribution in Ω_e . Let u be the electric voltage produced by the electric fish, satisfying the following system

$$\begin{cases} \Delta u = J_s & \text{in } \Omega, \\ \operatorname{div}[\gamma(x, \omega)\nabla u] = 0 & \text{in } \Omega_e, \\ \partial_\nu u|_- = 0 & \text{on } \partial\Omega, \\ u|_+ - u|_- = \xi \partial_\nu u|_+ & \text{on } \partial\Omega, \\ |u| = O\left(\frac{1}{|x|^{d-1}}\right) & \text{as } |x| \rightarrow \infty, \end{cases} \quad (4.1)$$

where the constant $\xi > 0$ is the effective fish skin thickness, J_s represents the electric current source generated by the fish organs, and ∂_ν designates the derivative with respect to the the outward normal vector ν . We assume that J_s can be written as the sum of Dirac functions

$$J_s = \sum_{j=1}^M \alpha_j \delta_{x_s^{(j)}}, \quad (4.2)$$

where $M \in \mathbb{N} \setminus \{0\}$, $x_s^{(j)} \in \Omega$ and the electric charges $\alpha_j \in \mathbb{R}$ satisfy the neutrality condition,

$$\sum_{j=1}^M \alpha_j = 0. \quad (4.3)$$

Note that the equation (4.1) can also be rewritten as

$$\left\{ \begin{array}{ll} \Delta u = J_s & \text{in } \Omega, \\ \Delta u = 0 & \text{in } \Omega_e \setminus \partial D, \\ \partial_\nu u|_- = 0 & \text{on } \partial\Omega, \\ u|_+ - u|_- = \xi \partial_\nu u|_+ & \text{on } \partial\Omega, \\ u|_+ = u|_- & \text{on } \partial D, \\ \partial_\nu u|_+ = k(\omega) \partial_\nu u|_- & \text{on } \partial D, \\ |u| = O\left(\frac{1}{|x|^{d-1}}\right) & \text{as } |x| \rightarrow \infty. \end{array} \right. \quad (4.4)$$

Assuming that $k(\omega)$ is a given continuous function, the weakly electric fish inverse problem is to recover the shape and the position of the inclusion D from measurements of the voltages $u(x, \omega)$ on the boundary $\partial\Omega$ for $\omega \in (\underline{\omega}, \bar{\omega})$, where $\underline{\omega}, \bar{\omega}$ are fixed constants.

4.3 Well-posedness of the direct problem

In this section, we study the well-posedness of the direct problem (4.1). Firstly, we introduce the Sobolev space $\mathcal{W}^{1,-1}(\Omega_e)$. Secondly, we establish the existence and uniqueness to (4.1) in $\mathcal{W}^{1,-1}(\Omega_e)$.

4.3.1 Sobolev space $\mathcal{W}^{1,-1}(\Omega_e)$

In this subsection, we establish using variational techniques the existence and uniqueness for the Laplace equations with a Robin boundary condition in Ω_e . To overcome the difficulties of integrating by parts in the unbounded exterior domain Ω_e , we introduce the following weighted Sobolev space [59].

Definition 4.3.1. • If $d = 2$,

$$\mathcal{W}^{1,-1}(\Omega_e) := \left\{ u; \frac{u(x)}{(1 + |x|^2)^{1/2} \log(2 + |x|^2)} \in L^2(\Omega_e), \nabla u \in L^2(\Omega_e) \right\}. \quad (4.5)$$

- If $d = 3$,

$$\mathcal{W}^{1,-1}(\Omega_e) := \left\{ u; \frac{u(x)}{(1+|x|^2)^{1/2}} \in L^2(\Omega_e), \nabla u \in L^2(\Omega_e) \right\}. \quad (4.6)$$

Remark 4.3.1. We make the following observations.

- From the boundedness of the weight functions, $\mathcal{W}^{1,-1}(U)$ is identically equal to the usual Sobolev space $H^1(U)$ on any open bounded domain U .
- The space of infinitely differentiable functions with compact support $\mathcal{D}(\Omega_e)$ is dense in the subspace $\mathcal{W}_0^{1,-1}(\Omega_e) := \{u \in \mathcal{W}^{1,-1}(\Omega_e); u|_{\partial\Omega} = 0\}$.
- The functions $v \in \mathcal{W}^{1,-1}(\Omega_e)$ satisfy the following decay behavior far from Ω

$$v(x) = O\left(\frac{1}{|x|^{d-2}}\right), \quad |x| \rightarrow +\infty. \quad (4.7)$$

In particular, the constant functions belong to $\mathcal{W}^{1,-1}(\Omega_e)$ when $d = 2$.

If $d = 2$, we introduce the space

$$\mathcal{L}_{-1}^2(\Omega_e) := \left\{ u : \frac{u(x)}{(1+|x|^2)^{1/2} \log(2+|x|^2)} \in L^2(\Omega_e) \right\}.$$

We state now a useful compact embedding result involving these weighted Sobolev spaces.

Lemma 4.3.1. *The embedding $\mathcal{W}^{1,-1}(\Omega_e) \rightarrow \mathcal{L}_{-1}^2(\Omega_e)$ is compact.*

The proof follows the same approach used in [1].

Proof. If the embedding $\mathcal{W}^{1,-1}(\mathbb{R}^2) \rightarrow \mathcal{L}_{-1}^2(\mathbb{R}^2)$ is compact, then it is also compact for any connected domain $O \subset \mathbb{R}^2$. So, without loss of generality, we only consider the case $O = \mathbb{R}^2$.

Letting $u \in \mathcal{D}(\mathbb{R}^2)$, we have

$$u(\rho, \theta) = - \int_{\rho}^{\infty} \frac{\partial u}{\partial r}(r, \theta) dr, \quad (4.8)$$

where (r, θ) are the polar coordinates.

Then,

$$\frac{|u(\rho, \theta)|^2}{(1 + \rho^2)(\log(2 + \rho^2))^2} \leq C \frac{1}{\rho^2(\log(\rho))^2} \int_{\rho}^{\infty} \left| \frac{\partial u}{\partial r} u(r, \theta) \right|^2 dr, \quad (4.9)$$

for $\rho \geq \rho_0 > 0$.

Denoting by B_R^c the exterior of the ball $B_R = B(0, R)$, we have,

$$\begin{aligned} & \int_{B_R^c} \frac{|u(x)|^2}{(1 + |x|^2) \log(2 + |x|^2)^2} dx \\ & \leq C \int_0^{2\pi} d\theta \int_R^{\infty} \frac{1}{\rho(\log(\rho))^2} \int_{\rho}^{\infty} \left| \frac{\partial u}{\partial r} u(r, \theta) \right|^2 dr d\rho \\ & \leq C \frac{1}{\log(R)} \|u\|_{\mathcal{W}^{1,-1}(\mathbb{R}^2)} \end{aligned} \quad (4.10)$$

By density, this inequality holds for any $u \in \mathcal{W}^{1,-1}(\mathbb{R}^2)$. Let $(u_i)_{i \in \mathbb{N}}$ be a bounded sequence in $\mathcal{W}^{1,-1}(\mathbb{R}^2)$. To prove that this sequence is a precompact in $\mathcal{L}_{-1}^2(\mathbb{R}^2)$, it is sufficient to show

- i) for $\varepsilon > 0$, there exists R such that $\|u_i\|_{\mathcal{L}_{-1}^2(B_R^c)} < \varepsilon$ for all i .
- ii) for any bounded part $\mathcal{O} \subset \mathbb{R}^2$, $(u_i|_{\mathcal{O}})_{i \in \mathbb{N}}$ is a precompact.

The first point is a direct consequence of the previous inequality. The second point can be obtained by applying the Rellich-Kondrachov Theorem. Thus, the result of the lemma follows. \square

4.3.2 Well-posedness

In this subsection we establish the existence and uniqueness to (4.1) in $\mathcal{W}^{1,-1}(\Omega_e)$.

Lemma 4.3.2. *If $d = 2$, let $\alpha > 0$. Then there exist $\beta > 0$ such that $\forall u \in \mathcal{W}^{1,-1}(\Omega_e)$,*

$$\int_{\Omega_e} |\nabla u|^2 dx + \alpha \int_{\partial\Omega} u^2 d\sigma \geq \beta \|u\|_{\mathcal{L}_{-1}^2(\Omega_e)}^2. \quad (4.11)$$

Proof. We suppose by a contradiction argument that (4.11) is not true. The opposite of the statement of the lemma implies that there exists a sequence $(u_m)_{m \in \mathbb{N}}$ with $u_m \in \mathcal{W}^{1,-1}(\Omega_e)$, $\|u_m\|_{\mathcal{W}^{1,-1}(\Omega_e)} = 1$, such that

$$\int_{\Omega_e} |\nabla u_m|^2 dx + \alpha \int_{\partial\Omega} u_m^2 d\sigma < \frac{1}{m} \|u_m\|_{\mathcal{L}^2_{-1}(\Omega_e)}^2. \quad (4.12)$$

From the previous compact imbedding result, there is a subsequence, which we always denote by $(u_m)_{m \in \mathbb{N}}$, convergent in $\mathcal{L}^2_{-1}(\Omega_e)$. Moreover, (4.12) implies that $(\nabla u_m)_{m \in \mathbb{N}}$ converges to 0 in $L^2(\Omega_e)$. So, the sequence $(u_m)_{m \in \mathbb{N}}$ converges to a constant in $\mathcal{W}^{1,-1}(\Omega_e)$. We deduce again from relation (4.12) that the trace of u_m converge to 0, thus the sequence $(u_m)_{m \in \mathbb{N}}$ converges to 0, which is in contradiction with the normalization assumption. \square

Theorem 4.3.1. *Let $\alpha > 0$, f be in the dual space $(\mathcal{W}^{1,-1}(\Omega_e))^*$, and $g \in H^{-1/2}(\partial\Omega)$. Then, the following Laplace equation with Robin boundary condition*

$$\begin{cases} -\Delta u = f & \text{in } \Omega_e, \\ u - \alpha \partial_\nu u = g & \text{on } \partial\Omega. \end{cases} \quad (4.13)$$

admits a unique weak solution in $\mathcal{W}^{1,-1}(\Omega_e)$.

Proof. A variational formulation to (4.13) is given by

$$\begin{aligned} & \forall v \in \mathcal{W}^{1,-1}(\Omega_e), \\ & \int_{\Omega_e} \nabla u \nabla v dx + \frac{1}{\alpha} \int_{\partial\Omega} u v d\sigma = \int_{\Omega_e} f v dx + \frac{1}{\alpha} \int_{\partial\Omega} g v d\sigma \end{aligned} \quad (4.14)$$

It follows from the trace theorem that the left-hand side is a bounded bilinear form and the right-hand side is a bounded linear form. We study separately the dimension two and dimension three cases for the coercivity of the bilinear form.

- i) If $d = 2$, the coercivity is a direct consequence of lemma 4.3.2.
- ii) If $d = 3$, we deduce from Theorem 2.5.13 in [59], that there exists a constant $c > 0$ such that $\forall u \in \mathcal{W}^{1,-1}(\Omega_e)$,

$$\|u\|_{\mathcal{W}^{1,-1}(\Omega_e)} \leq c \|\nabla u\|_{L^2(\Omega_e)} \quad (4.15)$$

Then, the left-hand side bilinear form in (4.14) is coercive. Thus, the result follows from the Lax-Milgram Theorem. \square

From the previous theorem, and without considering the asymptotic behavior $u(x) = O(\frac{1}{|x|^{d-1}})$ as $|x| \rightarrow \infty$, we have the existence of solutions to (4.1) up to a constant. In order to establish the uniqueness of the solution, we will give necessary conditions on the trace of the interior and exterior solutions $u|_{\partial\Omega_-}$ and $u|_{\partial\Omega_+}$ respectively, such that the exterior solution satisfies the desired asymptotic behavior.

We split the equation (4.1) into two parts, the interior part

$$\begin{cases} \Delta u_i = J_s & \text{in } \Omega, \\ \frac{\partial u_i}{\partial \nu} = 0 & \text{on } \partial\Omega, \\ \int_{\partial\Omega} u_i d\sigma = 0, \end{cases} \quad (4.16)$$

and the exterior part

$$\begin{cases} \operatorname{div}[(1 + (k(\omega) - 1)\chi_D)\nabla u] = 0 & \text{in } \Omega_e, \\ u = \xi \partial_\nu u + u_i + c_u & \text{on } \partial\Omega, \\ |u| = O(\frac{1}{|x|^{d-1}}) & \text{as } |x| \rightarrow \infty \end{cases} \quad (4.17)$$

where c_u is a constant depending on u that has to be fixed. It is clear that there exists a unique solution u_i to (4.16). For a given constant c_u theorem (4.3.1) guarantee the existence and uniqueness of solution to (4.17) in $\mathcal{W}^{1,-1}(\Omega_e)$. Next, we show that the decay $O(\frac{1}{|x|^{d-1}})$ of the exterior solution as $|x| \rightarrow +\infty$ will determine uniquely the constant c_u .

Lemma 4.3.3. *Assume that c_u is given. Then, the decay $O(\frac{1}{|x|^{d-1}})$ at infinity implies*

$$\frac{1}{|\partial\Omega|} \int_{\partial\Omega} u d\sigma = c_u. \quad (4.18)$$

Proof. Recall the variational formulation for (4.14) with $f = 0$ and $g = u_i + c_u$.

$$\begin{aligned} \forall v \in \mathcal{W}^{1,-1}(\Omega_e), \\ \int_{\Omega_e} \gamma(x) \nabla u \nabla v dx + \frac{1}{\xi} \int_{\partial\Omega} (u - c_u) v d\sigma = \frac{1}{\xi} \int_{\partial\Omega} u_i v d\sigma. \end{aligned}$$

We further distinguish two different cases:

i) $d = 2$.

Since the constants belong to $\mathcal{W}^{1,-1}(\Omega_e)$, by taking $v = 1$ in the previous variational formulation we obtain the desired result.

ii) $d = 3$.

Let B_R be a ball centered at 0 with radius $R > 0$, and assume that R is large enough such that $\overline{\Omega} \subset B_R$. Multiplying (4.17) by 1 and integrating by parts lead to

$$\frac{1}{\xi} \int_{\partial\Omega} (u - c_u) d\sigma = R^2 \int_{S^2} \partial_\nu u(Rt) dt,$$

where S^2 is the unit sphere in \mathbb{R}^3 . Since u is harmonic in Ω_e and decays as $O(\frac{1}{|x|^2})$ when $|x| \rightarrow +\infty$, by expanding it in the spherical harmonic basis [59], we can easily obtain that $\partial_\nu u(Rt) = O(\frac{1}{R^3})$ as $R \rightarrow +\infty$ uniformly in $t \in S^2$. Consequently, the right hand term in the previous inequality tends to zero as $R \rightarrow +\infty$, which achieves the proof of the lemma. □

Taking into account the results of lemma 4.3.3, we can rewrite the represent part of the system (4.1) as follows

$$\begin{cases} \operatorname{div}[(1 + (k(\omega) - 1)\chi_D)\nabla u] = 0 & \text{in } \Omega_e, \\ u - \frac{1}{|\partial\Omega|} \int_{\partial\Omega} u d\sigma - \xi \partial_\nu u = u_i & \text{on } \partial\Omega, \\ |u| = O(\frac{1}{|x|^{\beta-1}}) & \text{as } |x| \rightarrow +\infty, \end{cases} \quad (4.19)$$

where u_i is the unique solution to the system (4.16).

Let

$$\mathcal{W}_\diamond^{1,-1}(\Omega_e) = \left\{ u \in \mathcal{W}^{1,-1}(\Omega_e); |u| = O\left(\frac{1}{|x|^{d-1}}\right) \text{ as } |x| \rightarrow +\infty \right\}. \quad (4.20)$$

Then, the following is the main result of this subsection.

Theorem 4.3.2. *The forward problem (4.1) has a unique solution in $\mathcal{W}_\diamond^{1,-1}(\Omega_e)$.*

Proof. Multiplying the equation (4.19) by v in $\mathcal{W}_\diamond^{1,-1}(\Omega_e)$ and integrating by parts we obtain the following variational formulation

$$\begin{aligned} \forall v \in \mathcal{W}^{1,-1}(\Omega_e), \\ \int_{\Omega_e} \gamma(x) \nabla u \nabla v dx + \frac{1}{\xi} \int_{\partial\Omega} (u - \oint_{\partial\Omega} u)(v - \oint_{\partial\Omega} v) d\sigma = \frac{1}{\xi} \int_{\partial\Omega} u_i v d\sigma, \end{aligned}$$

where $\oint_{\partial\Omega} u d\sigma = \frac{1}{|\partial\Omega|} \int_{\partial\Omega} u d\sigma$.

We claim that the left-hand bilinear form is coercive. In fact, when $d = 3$ we deduce from [59], that the term $\int_{\Omega_e} \nabla u \nabla v dx$ is coercive on $\mathcal{W}^{1,-1}(\Omega_e)$. When $d = 2$ it is proved in [26] that the term $\int_{\Omega_e} \nabla u \nabla v dx$ is also coercive on $\mathcal{W}_\diamond^{1,-1}(\Omega_e)$.

Then, by Lax-Milgram Theorem we obtain the desired result. □

We introduce the fundamental solution Γ to the Laplace operator in \mathbb{R}^d .

Definition 4.3.2. *Denoting by ω_d the area of the unit sphere in \mathbb{R}^d , the fundamental solution to the Laplace operator is given by*

$$\Gamma(x, y) = \begin{cases} \frac{1}{2\pi} \ln(|x - y|) & d = 2, \\ -\frac{1}{\omega_d} |x - y|^{2-d} & d \geq 3. \end{cases} \quad (4.21)$$

A direct consequence of theorem 4.3.1 is the following corollary.

Corollary 4.3.1. *Let $y \in \Omega_e$ be fixed. Then, there exists a unique solution to the system*

$$\begin{cases} \Delta G(x, y) = \delta_y & \text{in } \Omega_e, \\ G - \xi \frac{\partial G}{\partial \nu} = 0 & \text{on } \partial\Omega, \\ G - \Gamma \in \mathcal{W}^{1,-1}(\Omega_e). \end{cases} \quad (4.22)$$

The singular function $G(x, y)$ is the Green function of the Laplace operator in Ω_e with the Robin boundary condition.

4.4 The Poincaré Variational Problem

In this section, we introduce the Poincaré variational problem by following the approach in [10],[26]. We denote by $\mathcal{W}_\diamond^{1,-1}(\Omega_e)$, the subspace of functions $v \in \mathcal{W}^{1,-1}(\Omega_e)$ satisfying $|v(x)| = O(\frac{1}{|x|^{d-1}})$ as $|x| \rightarrow \infty$. It follows from [59], [26] that the space $\mathcal{W}_\diamond^{1,-1}(\Omega_e)$ endowed with the scalar product

$$\langle u, v \rangle_{\mathcal{W}_\diamond^{1,-1}(\Omega_e)} := \int_{\Omega_e} \nabla u \nabla v dx$$

is a Hilbert space. Thus, the following bilinear form defines also an equivalent scalar product on $\mathcal{W}_\diamond^{1,-1}(\Omega_e)$,

$$a(u, v) := \int_{\Omega_e} \nabla u \nabla v dx + \frac{1}{\xi} \int_{\partial\Omega} \bar{u} \bar{v} d\sigma,$$

where $\bar{u} := u - \frac{1}{|\partial\Omega|} \int_{\partial\Omega} u d\sigma$.

For $u \in \mathcal{W}_\diamond^{1,-1}(\Omega_e)$, we infer from the Riesz Theorem that there exist a unique $Tu \in \mathcal{W}_\diamond^{1,-1}(\Omega_e)$ such that for all $v \in \mathcal{W}_\diamond^{1,-1}(\Omega_e)$,

$$\int_{\Omega_e} \nabla Tu \nabla v dx + \frac{1}{\xi} \int_{\partial\Omega} \overline{Tu} \bar{v} d\sigma = \int_D \nabla u \nabla v dx. \quad (4.23)$$

It is easy to obtain that the operator $T : \mathcal{W}_\diamond^{1,-1}(\Omega_e) \rightarrow \mathcal{W}_\diamond^{1,-1}(\Omega_e)$ is self-adjoint and bounded. The spectral problem for T reads as: Find $(w, \lambda) \in \mathcal{W}_\diamond^{1,-1}(\Omega_e) \times \mathbb{R}$,

$w \neq 0$, such that $\forall v \in \mathcal{W}_\diamond^{1,-1}(\Omega_e)$,

$$\lambda \int_{\Omega_e} \nabla w \nabla v dx + \frac{\lambda}{\xi} \int_{\partial\Omega} \bar{w} \bar{v} d\sigma = \int_D \nabla w \nabla v dx. \quad (4.24)$$

We remark that all functions $w \in H_0^1(D)$ are eigenfunctions of T corresponding to the eigenvalue $\lambda = 1$. As those eigenfunctions equal to 0 on $\partial\Omega$, they have not any contribution in the spectral decomposition which will be introduced later, we consider from now on the eigenvalues $\lambda \neq 1$.

Integrating by parts, we can obtain that an eigenfunction w is harmonic in D and in $D' := \Omega_e \setminus \bar{D}$, and on ∂D , we have the transmission and boundary conditions

$$w|_{\partial D}^+ = w|_{\partial D}^-, \quad \partial_\nu w|_{\partial D}^+ = (1 - \frac{1}{\lambda}) \partial_\nu w|_{\partial D}^-, \quad w|_{\partial\Omega} - \xi \partial_\nu w|_{\partial\Omega} = \frac{1}{|\partial\Omega|} \int_{\partial\Omega} w d\sigma, \quad (4.25)$$

where $w|_{\partial D}^\pm(x) = \lim_{t \rightarrow 0} w(x \pm t\nu(x))$ for $x \in \partial D$. In other words, w is a solution to (4.1) for $k = 1 - \frac{1}{\lambda} < 0$, and $J_s = 0$.

We define the space \mathfrak{h}_\diamond as the spaces of the harmonic functions in D and in D' which are continuous across ∂D , with a Robin boundary condition $\bar{u} = \xi \partial_\nu u$ on $\partial\Omega$ and the asymptotic behavior $|u| = O(\frac{1}{|x|^{d-1}})$ as $|x| \rightarrow \infty$, and with a finite energy semi-norm

$$\|u\|_{\mathfrak{h}_\diamond}^2 := \int_{\Omega_e} |\nabla u|^2 dx + \frac{1}{\xi} \int_{\partial\Omega} |\bar{u}|^2 dx. \quad (4.26)$$

We remark that $T\mathfrak{h}_\diamond \subset \mathfrak{h}_\diamond$, thus T defines a bounded operator from \mathfrak{h}_\diamond into \mathfrak{h}_\diamond . We note always by T the restriction of T on \mathfrak{h}_\diamond .

We define now, with this kernel G , the single layer potential $S_D : H^{-1/2}(\partial D) \rightarrow \mathfrak{h}_\diamond$ and the Poincaré operator $K_D^* : H^{-1/2}(\partial D) \rightarrow H^{-1/2}(\partial D)$.

Definition 4.4.1. Let $\phi \in H^{-1/2}(\partial D)$, we define, for $x \in \Omega_e$

$$S_D[\phi](x) = \int_{\partial D} G(x, y) \phi(y) d\sigma(y), \quad (4.27)$$

and, for $x \in \partial D$,

$$K_D^*[\phi](x) = \int_{\partial D} \frac{\partial}{\partial \nu_x} G(x, y) \phi(y) d\sigma(y). \quad (4.28)$$

K_D^* is a compact operator on $L^2(\partial D)$ (see lemma 2.13 in [7]). Since the function G and the Laplace Green's function in the whole space have equivalent weak singularities as $x \rightarrow y$ (see Lemma 2.14 in [8] for the proof's sketch and section 2.5.5 in [59] for the regularity), we have the same jump relations through the boundary ∂D , that is,

$$\partial_\nu S_D[\phi]_\pm(x) = (\pm \frac{1}{2}I + K_D^*)[\phi](x). \quad (4.29)$$

Now, we state the characterization of the spectrum of T .

Theorem 4.4.1. *The variational Poincaré operator T has the following decomposition,*

$$T = \frac{1}{2}I + K, \quad (4.30)$$

where K is a compact, self-adjoint operator. Let w_n^\pm , $n \geq 1$ be the eigenfunctions associated to the eigenvalues $(\lambda_n^\pm)_{n \geq 1}$, we have the following formula via the min-max principle.

$$\begin{aligned} \lambda_1^- &= \min_{0 \neq w \in \mathfrak{H}_\circ} \frac{\int_D |\nabla w(x)|^2 dx}{\int_{\Omega_e} |\nabla w(x)|^2 dx + \frac{1}{\xi} \int_{\partial\Omega} |\bar{w}|^2 dx} \\ \lambda_n^- &= \min_{0 \neq w \in \mathfrak{H}_\circ, w \perp w_1^-, \dots, w_{n-1}^-} \frac{\int_D |\nabla w(x)|^2 dx}{\int_{\Omega_e} |\nabla w(x)|^2 dx + \frac{1}{\xi} \int_{\partial\Omega} |\bar{w}|^2 dx} \\ &= \min_{F_n \subset \mathfrak{H}_\circ, \dim(F_n) = n} \max_{w \in F_n} \frac{\int_D |\nabla w(x)|^2 dx}{\int_{\Omega_e} |\nabla w(x)|^2 dx + \frac{1}{\xi} \int_{\partial\Omega} |\bar{w}|^2 dx}, \end{aligned} \quad (4.31)$$

and similarly

$$\begin{aligned}
\lambda_1^+ &= \max_{0 \neq w \in \mathfrak{H}_\diamond} \frac{\int_D |\nabla w(x)|^2 dx}{\int_{\Omega_e} |\nabla w(x)|^2 dx + \frac{1}{\xi} \int_{\partial\Omega} |\bar{w}|^2 d\sigma} \\
\lambda_n^+ &= \max_{0 \neq w \in \mathfrak{H}_\diamond, w \perp w_1^+, \dots, w_{n-1}^+} \frac{\int_D |\nabla w(x)|^2 dx}{\int_{\Omega_e} |\nabla w(x)|^2 dx + \frac{1}{\xi} \int_{\partial\Omega} |\bar{w}|^2 dx} \\
&= \max_{F_n \subset \mathfrak{H}_\diamond, \dim(F_n) = n} \min_{w \in F_n} \frac{\int_D |\nabla w(x)|^2 dx}{\int_{\Omega_e} |\nabla w(x)|^2 dx + \frac{1}{\xi} \int_{\partial\Omega} |\bar{w}|^2 dx}. \tag{4.32}
\end{aligned}$$

Proof. We define the operator $K : \mathfrak{H}_\diamond \rightarrow \mathfrak{H}_\diamond$, for all $v \in \mathfrak{H}_\diamond$,

$$2\left(\int_{\Omega_e} \nabla K u \nabla v dx + \frac{1}{\xi} \int_{\partial\Omega} \overline{K u} \bar{v} d\sigma \right) = \int_D \nabla u \nabla v dx - \int_{D'} \nabla u \nabla v dx - \frac{1}{\xi} \int_{\partial\Omega} \bar{u} \bar{v} d\sigma. \tag{4.33}$$

We observe that K is bounded and self-adjoint. A direct calculation shows that

$$T = \frac{1}{2}I + K. \tag{4.34}$$

It is shown in [7] that the single layer potential $S_D : H^{-1/2}(\partial D) \rightarrow H^{1/2}(\partial D)$ is invertible in dimension three, and we can modify S_D slightly to show the invertibility in dimension two.

Integrating by parts in the right-hand side (4.33), and using the jump relation (4.29), we find

$$\int_{\Omega_e} \nabla K u \nabla v dx + \frac{1}{\xi} \int_{\partial\Omega} \overline{K u} \bar{v} d\sigma = \int_{\partial D} K_D^* [S_D^{-1}[u|_{\partial D}]] v d\sigma. \tag{4.35}$$

Since K_D^* is compact the operator K is compact.

From Fredholm's alternative, T is a Fredholm operator of index 0, and the spectral decomposition (4.31), (4.32) follows from the min-max principle. \square

Corollary 4.4.1. *If $u \in \mathfrak{H}_\diamond$, then u has the spectral decomposition.*

$$u(x) = \sum_{n=1}^{\infty} u_n^\pm w_n^\pm(x), \quad (4.36)$$

where

$$u_n^\pm = \int_{\Omega_e} \nabla u \nabla w_n^\pm dx + \frac{1}{\xi} \int_{\partial\Omega} \bar{u} \bar{w}_n^\pm dx. \quad (4.37)$$

4.5 Spectral decomposition of the solution $u(x, \omega)$

Theorem 4.5.1. *Let $u(x, \omega)$ be the unique solution to the system (4.1). Then, the following decomposition holds:*

$$\begin{aligned} u(x, \omega) &= u_0(x) + u_f(x, k(\omega)) \\ &= u_0(x) + \frac{1}{\xi} \sum_{n=1}^{\infty} \frac{\int_{\partial\Omega} u_i w_n^\pm d\sigma}{1 + \lambda_n^\pm(k(\omega) - 1)} w_n^\pm(x), \quad x \in \Omega_e, \end{aligned} \quad (4.38)$$

where $u_0 \in \mathcal{W}_\diamond^{1,-1}(\Omega_e)$ is the unique solution to the system:

$$\begin{cases} \Delta v = 0 & \text{in } \Omega_e \setminus \bar{D}, \\ \nabla v = 0 & \text{in } D, \\ v - \int_{\partial\Omega} v d\sigma = \xi \partial_\nu v + u_i & \text{on } \partial\Omega, \\ |v| = O\left(\frac{1}{|x|^{d-1}}\right) & \text{as } |x| \rightarrow \infty, \end{cases} \quad (4.39)$$

and $u_i \in L^2(\Omega)$ is the unique solution to the equation:

$$\begin{cases} \Delta v = J_s & \text{in } \Omega, \\ \partial_\nu v = 0 & \text{on } \partial\Omega, \\ \int_{\partial\Omega} v d\sigma = 0. \end{cases} \quad (4.40)$$

Proof. Let u_\emptyset be the unique solution to

$$\begin{cases} \Delta v = J_s & \text{in } \Omega, \\ \partial_\nu v|_- = 0 & \text{on } \partial\Omega, \\ \int_{\partial\Omega} v|_- d\sigma = 0, & \\ \Delta v = 0 & \text{in } \Omega_e, \\ v|_+ - \int_{\partial\Omega} v|_+ d\sigma - v|_- = \xi \partial_\nu v|_+ & \text{on } \partial\Omega, \\ |v| = O\left(\frac{1}{|x|^{d-1}}\right) & \text{as } |x| \rightarrow \infty. \end{cases} \quad (4.41)$$

Denote $u := u - u_\emptyset$, u is therefore harmonic in D and in $\Omega_e \setminus \bar{D}$. Moreover, it satisfies

$$u|_+ - \int_{\partial\Omega} u|_+ d\sigma = \xi \partial_\nu u|_+ \text{ on } \partial\Omega.$$

Then $u \in \mathfrak{H}_\circ$, and admits the following spectral decomposition:

$$u(x) = \sum_{n=1}^{\infty} u_n^\pm w_n^\pm(x), \quad (4.42)$$

where

$$u_n^\pm = \int_{\Omega_e} \nabla u \nabla w_n^\pm dx + \frac{1}{\xi} \int_{\partial\Omega} \bar{u} \bar{w}_n^\pm d\sigma. \quad (4.43)$$

Otherwise, u is the unique solution to

$$\begin{cases} -\operatorname{div}(\gamma(x, \omega) \nabla u) = \operatorname{div}(\gamma(x, \omega) \nabla u_\emptyset) & \text{in } \Omega_e, \\ u - \xi \partial_\nu u = \frac{1}{|\partial\Omega|} \int_{\partial\Omega} u d\sigma & \text{on } \partial\Omega, \\ |u| = O\left(\frac{1}{|x|^{d-1}}\right) & \text{as } |x| \rightarrow \infty. \end{cases} \quad (4.44)$$

Multiplying the first equation in (4.44) by w_n^\pm , and integrating by parts over Ω_e , we have

$$u_n^\pm = \frac{\int_{\Omega_e} \operatorname{div}(\gamma(x, \omega) \nabla u_\emptyset) w_n^\pm dx}{1 + \lambda_n^\pm (k(\omega) - 1)}. \quad (4.45)$$

The term $\int_{\Omega_e} \operatorname{div}(\gamma(x, \omega) \nabla u_\emptyset) w_n^\pm dx$ can be understood as a dual product between $\operatorname{div}(\gamma(x, \omega) \nabla u_\emptyset) \in (\mathcal{W}^{1,-1}(\Omega_e))^*$ and $w_n^\pm \in \mathcal{W}^{1,-1}(\Omega_e)$. It can be simplified

by means of integration by parts:

$$\begin{aligned}
& \int_{\Omega_e} \operatorname{div}(\gamma(x, \omega) \nabla u_\emptyset) w_n^\pm dx \\
&= - \int_{\Omega_e} \gamma(x, \omega) \nabla u_\emptyset \nabla w_n^\pm dx - \int_{\partial\Omega} \partial_\nu u_\emptyset w_n^\pm d\sigma \\
&= - \int_{\Omega_e} \nabla u_\emptyset \nabla w_n^\pm dx - (k(\omega) - 1) \int_D \nabla u_\emptyset \nabla w_n^\pm dx - \frac{1}{\xi} \int_{\partial\Omega} (u_\emptyset|_+ - u_\emptyset|_-) w_n^\pm d\sigma \\
&= - \int_{\Omega_e} \nabla u_\emptyset \nabla w_n^\pm dx - (k(\omega) - 1) \int_D \nabla u_\emptyset \nabla w_n^\pm dx - \frac{1}{\xi} \int_{\partial\Omega} (\overline{u_\emptyset|_+} - \overline{u_\emptyset|_-}) \overline{w_n^\pm} d\sigma \\
&= - \left[\frac{1}{\lambda_n^\pm} + (k(\omega) - 1) \right] \int_D \nabla u_\emptyset \nabla w_n^\pm dx + \frac{1}{\xi} \int_{\partial\Omega} \overline{u_\emptyset|_-} w_n^\pm d\sigma, \tag{4.46}
\end{aligned}$$

where $\overline{u_\emptyset|_-}$ is exactly the unique solution to (4.40), it means, $\overline{u_\emptyset|_-} = u_i$.

Thus, it follows that

$$u_n^\pm = - \frac{\int_D \nabla u_\emptyset \nabla w_n^\pm dx}{\lambda_n^\pm} + \frac{\int_{\partial\Omega} u_i w_n^\pm d\sigma}{\xi [1 + \lambda_n^\pm (k(\omega) - 1)]}. \tag{4.47}$$

Let $\tilde{u}_0 \in \mathfrak{h}_\diamond$ be the unique solution to the system

$$\begin{cases} \Delta \tilde{u}_0 = 0 & \text{in } \Omega_e \setminus \bar{D}, \\ \nabla \tilde{u}_0 = \nabla u_\emptyset & \text{in } D, \\ \tilde{u}_0 - \xi \frac{\partial \tilde{u}_0}{\partial \nu} = \frac{1}{|\partial\Omega|} \int_{\partial\Omega} \tilde{u}_0 d\sigma & \text{on } \partial\Omega, \\ |\tilde{u}_0| = O\left(\frac{1}{|x|^{d-1}}\right) & \text{as } |x| \rightarrow \infty. \end{cases} \tag{4.48}$$

Since w_n^\pm is an eigenfunction of T and $\tilde{u}_0 \in \mathfrak{h}_\diamond$, we have

$$\int_D \nabla u_\emptyset \nabla w_n^\pm dx = \lambda_n^\pm \left[\int_{\Omega_e} \nabla \tilde{u}_0 \nabla w_n^\pm dx + \frac{1}{\xi} \int_{\partial\Omega} \overline{\tilde{u}_0} \overline{w_n^\pm} d\sigma \right], \tag{4.49}$$

which gives

$$u_n^\pm = - \left[\int_{\Omega_e} \nabla \tilde{u}_0 \nabla w_n^\pm dx + \frac{1}{\xi} \int_{\partial\Omega} \overline{\tilde{u}_0} \overline{w_n^\pm} d\sigma \right] + \frac{\int_{\partial\Omega} u_i w_n^\pm d\sigma}{\xi [1 + \lambda_n^\pm (k(\omega) - 1)]}. \tag{4.50}$$

On the other hand a simple calculations yields

$$u_\emptyset - \tilde{u}_0 = u_0. \quad (4.51)$$

Combining (4.50) and (4.51), the decomposition (4.38) follows. \square

Corollary 4.5.1. *Let $x \in \partial\Omega$. Then the function $k \mapsto u_f(x, k)$ is meromorphic in \mathbb{C} . The poles of $u_f(x, k)$ are the real values solutions to the equations*

$$1 + \lambda_n^\pm(k - 1) = 0, \quad n \geq 1 \quad (4.52)$$

where λ_n^\pm are the eigenvalues of the variational Poincaré operator T .

The poles of $u_f(x, k)$ in the previous corollary are given by $k_n^\pm = (1 - \frac{1}{\lambda_n^\pm}) \in \mathbb{R}_-$, and they can be ordered as follows:

$$k_1^- \leq k_2^- \leq \dots < -1 < \dots \leq k_2^+ \leq k_1^+ < 0 \quad (4.53)$$

We remark that -1 is the only accumulation point of the sequence of poles, it means k_n^\pm tends to -1 as $n \rightarrow \infty$.

4.6 Uniqueness and stability estimates

We establish our uniqueness and stability estimates by modifying slightly the proofs in sections 3 and 4 of [10], we invite readers to consult [10] for detail proofs.

The weakly electric fish inverse problem has a unique solution within the class \mathcal{D} , and we have the following stability estimates.

Theorem 4.6.1. *Let D and \tilde{D} be two inclusions in \mathcal{D} . Denote by u and \tilde{u} respectively the solution of (4.1) with the inclusion D (resp. \tilde{D}). Let*

$$\varepsilon = \sup_{x \in \partial\Omega, \omega \in [\underline{\omega}, \bar{\omega}]} |u - \tilde{u}|.$$

Then, there exist constants C and $\tau \in (0, 1)$, such that the following estimate holds:

$$|D\Delta\tilde{D}| \leq C \left(\frac{1}{\ln(\varepsilon^{-1})} \right)^\tau. \quad (4.54)$$

Here, Δ denotes the symmetric difference and the constants C and τ depend only on J_s, Ω, \mathcal{D} and $\Sigma = \{k(\omega); \omega \in (\underline{\omega}, \bar{\omega})\}$.

Moreover, if the boundaries are analytic, we have a Hölder-type stability estimate.

Theorem 4.6.2. *Assume that $d = 2$, and let D and \tilde{D} be two analytic inclusions in \mathcal{D} . Denote by u and \tilde{u} respectively the solution of (4.1) with the inclusion D (resp. \tilde{D}). Let*

$$\varepsilon = \sup_{x \in \partial\Omega, \omega \in [\underline{\omega}, \bar{\omega}]} |u - \tilde{u}|.$$

Then, there exist constants C and $\tau' \in (0, 1)$, such that the following estimate holds:

$$|D\Delta\tilde{D}| \leq C\varepsilon^{\tau'}. \quad (4.55)$$

Here, Δ denotes the symmetric difference and the constants C and τ depend only on J_s, Ω, \mathcal{D} and Σ .

Numerical identification of the target fish

In this chapter, we develop a numerical scheme to determine the position and shape of the target fish. Regarding the decay of the solution of (4.1) as $|x| \rightarrow +\infty$, we first reduce the computational domain by taking a Dirichlet boundary condition on a large disk B containing the fish Ω and the inclusion D . In fact we will show that a similar spectral decomposition holds in the truncated problem. Using this spectral decomposition, our numerical algorithm splits into two main steps. The first step is to retrieve the frequency dependent part in the spectral decomposition, and the second step is to reconstruct the inclusion from the Cauchy data of u_0 on $\partial\Omega$ obtained in the first step. Precisely, we recover the fish target by using an optimization scheme that minimizes a given energy functional on the boundary $\partial\Omega$ with respect to the inclusion shape.

5.1 The mathematical model in a truncated domain

In order to implement the numerical identification method, we need to reduce the system (4.1) to a bounded domain. Let B be a centered disk large enough such that it contains the electric fish Ω and the target fish D . We substitute (4.1) by the system

$$\left\{ \begin{array}{ll} \Delta \tilde{u} = J_s & \text{in } \Omega, \\ \operatorname{div}[\gamma(x, \omega) \nabla \tilde{u}] = 0 & \text{in } B \setminus \overline{\Omega}, \\ \partial_\nu \tilde{u}|_- = 0 & \text{on } \partial\Omega, \\ \tilde{u}|_+ - \tilde{u}|_- = \xi \partial_\nu \tilde{u}|_+ & \text{on } \partial\Omega, \\ \tilde{u} = 0 & \text{on } \partial B, \\ \int_{\partial B} \partial_\nu \tilde{u} d\sigma = 0. \end{array} \right. \quad (5.1)$$

Here, we always suppose that J_s is taken in the form (4.2) and the electric charges always satisfy (4.3). Then it follows from the standard theory to elliptic partial differential equations that (5.1) admits a unique solution in

$$W_0 := \left\{ u \in H^1(B \setminus \overline{\Omega}) \cup H^1(\Omega), u = 0 \text{ on } \partial B, \int_{\partial B} \partial_\nu \tilde{u} d\sigma = 0 \right\}.$$

We introduce the equivalent scalar product on W_0 and the associated variational Poincaré operator \tilde{T} .

$$\tilde{a}(u, v) := \int_{B \setminus \overline{\Omega}} \nabla u \nabla v dx + \frac{1}{\xi} \int_{\partial\Omega} \tilde{u} \tilde{v} d\sigma.$$

For $u \in W_0$, by the Riesz theorem, there exists a unique $\tilde{T}u \in W_0$ such that for all $v \in W_0$,

$$\int_{B \setminus \overline{\Omega}} \nabla \tilde{T}u \nabla v dx + \frac{1}{\xi} \int_{\partial\Omega} \tilde{T}u v d\sigma = \int_D \nabla u \nabla v dx. \quad (5.2)$$

We introduce also the space \mathfrak{H}_\diamond the functions in W_0 , which are harmonic in D and in $B \setminus (\overline{\Omega \cup D})$, and which satisfy the zero Robin boundary condition $u - \xi \partial_\nu u = 0$ on $\partial\Omega$.

Then, \tilde{T} has similar spectral elements denoted $(w_n^\pm, \tilde{\lambda}_n^\pm)$ than T .

We follow the analysis in the unbounded case to derive a similar spectral decomposition for \tilde{u} .

Theorem 5.1.1. *Let $\tilde{u}(x, \omega)$ be the unique solution to the system (5.1).*

Then the following decomposition holds, for $x \in B \setminus \overline{\Omega}$,

$$\begin{aligned} \tilde{u}(x, \omega) &= \tilde{u}_0(x) + u_f(x, k(\omega)) \\ &= \tilde{u}_0(x) + \frac{1}{\xi} \sum_{n=1}^{\infty} \frac{\int_{\partial\Omega} \tilde{u}_i \tilde{w}_n^{\pm} d\sigma}{1 + \tilde{\lambda}_n^{\pm}(k(\omega) - 1)} \tilde{w}_n^{\pm}(x), \end{aligned} \quad (5.3)$$

where $u_0 \in W_0$ is the unique solution to the system:

$$\begin{cases} \Delta v = 0 & \text{in } B \setminus \overline{(\Omega \cup D)}, \\ \nabla v = 0 & \text{in } D, \\ v - \int_{\partial\Omega} v d\sigma = \xi \partial_\nu v + u_i & \text{on } \partial\Omega, \\ v = 0 & \text{on } \partial B, \\ \int_{\partial B} \partial_\nu v d\sigma = 0, \end{cases} \quad (5.4)$$

and $u_i \in L^2(\Omega)$ is the unique solution to the equation:

$$\begin{cases} \Delta v = J_s & \text{in } \Omega, \\ \partial_\nu v = 0 & \text{on } \partial\Omega, \\ \int_{\partial\Omega} v d\sigma = 0. \end{cases} \quad (5.5)$$

5.2 Retrieval of the frequency independent part

We consider M frequencies of measurements $\omega_1, \omega_2, \dots, \omega_M$. Since $1/2$ is the unique accumulation point of the eigenvalues $(\tilde{\lambda}_n^{\pm})_{n \in \mathbb{N}}$, we only consider the N_f first eigenvalues as unknowns, and we approximate the others eigenvalues by $1/2$. In fact it has been shown in [56] that if D is C^β with $\beta \geq 2$ then for any $\alpha > -2\beta + 3$, we have

$$|\tilde{\lambda}_n^{\pm} - 1/2| = o(n^\alpha), \quad n \rightarrow +\infty.$$

If the boundary of D is C^∞ smooth, then the eigenvalues will decay faster than any power order. Recently H. Kang and his collaborators have showed the exponential convergence of the eigenvalues in the case of analytic inclusions

[21]. Therefore, we make the following approximation, for $x \in \Omega$, $1 \leq p \leq M$,

$$\tilde{u}(x, \omega_p) \approx \tilde{u}_0(x) + \sum_{n=1}^{N_f} \frac{v_n^\pm(x)}{1 + \tilde{\lambda}_n^\pm(k(\omega_p) - 1)} + \frac{2}{k(\omega_p) + 1} v_{N_f+1}(x), \quad (5.6)$$

where

$$v_n^\pm(x) = \frac{1}{\xi} \int_{\partial\Omega} \tilde{u}_i \tilde{w}_n^\pm d\sigma \tilde{w}_n^\pm(x),$$

and

$$v_{N_f+1}(x) = \frac{1}{\xi} \sum_{n>N_f} \int_{\partial\Omega} \tilde{u}_i \tilde{w}_n^\pm d\sigma \tilde{w}_n^\pm(x).$$

By a simple integration by parts, we have, for all $n \in \mathbb{N}$,

$$\frac{1}{\xi} \int_{\partial\Omega} \tilde{u}_i \tilde{w}_n^\pm d\sigma = \int_{B \setminus \bar{\Omega}} \nabla \tilde{u}_0 \nabla \tilde{w}_n^\pm dx + \frac{1}{\xi} \int_{\partial\Omega} \tilde{u}_0 \tilde{w}_n^\pm d\sigma, \quad (5.7)$$

where \tilde{u}_0 is the unique solution in W_0 to

$$\begin{cases} \Delta \tilde{u}_0 = 0 & \text{in } B \setminus \bar{\Omega}, \\ \tilde{u}_0 - \int \tilde{u}_0 d\sigma - \xi \partial_\nu \tilde{u}_0 = \tilde{u}_i & \text{on } \partial\Omega, \\ \tilde{u}_0 = 0 & \text{on } \partial B \\ \int_{\partial B} \partial_\nu \tilde{u}_0 d\sigma = 0. \end{cases} \quad (5.8)$$

So, the function $\sum_{n=1}^{\infty} v_n^\pm$ is the orthogonal projection of the function \tilde{u}_0 on the space \mathfrak{H}_ξ .

On the other hand \tilde{u}_0 satisfies, for all $n \in \mathbb{N}$, $n \geq 1$

$$\begin{aligned}
& \int_{B \setminus \bar{\Omega}} \nabla \tilde{u}_0 \nabla \tilde{w}_n^\pm dx + \frac{1}{\xi} \int_{\partial \Omega} \tilde{u}_0 \tilde{w}_n^\pm d\sigma \\
&= \int_{B \setminus (\bar{\Omega} \cup D)} \nabla \tilde{u}_0 \nabla \tilde{w}_n^\pm dx + \frac{1}{\xi} \int_{\partial \Omega} \tilde{u}_0 \tilde{w}_n^\pm d\sigma \\
&= - \int_{\partial \Omega} \tilde{u}_0 \partial_\nu \tilde{w}_n^\pm d\sigma + \frac{1}{\xi} \int_{\partial \Omega} \hat{u}_0 \tilde{w}_n^\pm d\sigma - \int_{\partial D} \tilde{u}_0 \partial_\nu \tilde{w}_n^\pm d\sigma \\
&= -\tilde{u}_0 \int_{\partial D} \partial_\nu \tilde{w}_n^\pm d\sigma = 0.
\end{aligned} \tag{5.9}$$

As $\tilde{u}_\emptyset - \tilde{u}_0 \in \mathfrak{H}_\diamond$, the orthogonal projection of \tilde{u}_\emptyset on the space \mathfrak{H}_\diamond is $\tilde{u}_\emptyset - \tilde{u}_0$.

Then, the formula (5.6) becomes

$$\begin{aligned}
\tilde{u}(x, \omega_p) &\approx \frac{k(\omega_p) - 1}{k(\omega_p) + 1} \tilde{u}_0(x) + \frac{2}{k(\omega_p) + 1} \tilde{u}_\emptyset(x) \\
&\quad + \sum_{n=1}^{N_f} \left(\frac{1}{1 + \tilde{\lambda}_n^\pm(k(\omega_p) - 1)} - \frac{2}{k(\omega_p) + 1} \right) v_n^\pm(x).
\end{aligned} \tag{5.10}$$

The previous equation can be formulated using the following matrix.

For $x \in \partial \Omega$, we define the vectors

$$\tilde{U}(x, \omega_1, \dots, \omega_M) = (\tilde{u}(x, \omega_j)),$$

$$V(x) = (\tilde{u}_0(x), v_1^+(x), v_1^-(x), \dots, v_{N_f}^+(x), v_{N_f}^-(x)),$$

and

$$L(\tilde{\lambda}_1^\pm, \dots, \tilde{\lambda}_{N_f}^\pm, \omega_1, \dots, \omega_M) = (L_i)_{1 \leq i \leq M}, \text{ where}$$

$$L_i(x) = \left(q_0(\omega_i), q(\widetilde{\lambda}_1^+, \omega_i), q(\widetilde{\lambda}_1^-, \omega_i), \dots, q(\widetilde{\lambda}_{N_f}^+, \omega_i), q(\widetilde{\lambda}_{N_f}^-, \omega_i) \right).$$

Here

$$\begin{aligned} \tilde{u}(x, \omega) &= \tilde{u}(x, \omega) - \frac{2}{k(\omega) + 1} \tilde{u}_0(x), \\ q_0(\omega) &= \frac{k(\omega) - 1}{(k(\omega) + 1)}, \quad \text{and} \quad q(\widetilde{\lambda}, \omega) = \frac{1}{1 + \widetilde{\lambda}(k(\omega) - 1)} - \frac{2}{k(\omega) + 1}. \end{aligned}$$

The matrix formulation of (5.10) becomes then

$$\tilde{U}^T(x, \omega_1, \omega_2, \dots, \omega_M) \approx L(\widetilde{\lambda}_1^\pm, \dots, \widetilde{\lambda}_{N_f}^\pm, \omega_1, \dots, \omega_M) V^T(x). \quad (5.11)$$

So, the vector V can be obtained by the formula,

$$V^T(x) \approx (L^T L)^\dagger L^T \tilde{U}^T(x, \omega_1, \dots, \omega_M). \quad (5.12)$$

where $(L^T L)^\dagger$ is the pseudo-inverse of the matrix $L^T L$. The conditioning of the matrix $(L^T L)^\dagger$ depends on the distance between the frequency sampling values ω_0 . The approximate $\tilde{u}_0(x)$ is then given by the first coefficient of the vector $V(x)$.

5.3 Identification of the target fish

In this section, we consider a numerical scheme to identify the inclusion $D \in \mathcal{D}$ from the knowledge of $\tilde{u}_0|_{\partial\Omega}$ recovered in the previous section. The scheme is based on minimizing the functional

$$J(D) = \frac{1}{2} \int_{\partial\Omega} \sum_{i=1}^P |\tilde{u}_0 - \tilde{u}_{meas}^{(i)}|^2 d\sigma + \varepsilon_T \int_{\partial D} d\sigma,$$

where \tilde{u} is the solution to (5.4). P designs the total number of measurements, we take here $P = 10$. For $1 \leq i \leq 10$, we use the fact that the electric fish can swim around the target, $\tilde{u}_{meas}^{(i)}$ is the measured Dirichlet data corresponding to the case while the electric fish locate in the i -th position. These quantities are

obtained in the previous step by retrieving the frequency dependent part from the multifrequency measurements. The term $\varepsilon_T \int_{\partial D} d\sigma$ represents the Tikhonov regularization.

5.3.1 Shape derivative

Let D_ε be the perturbed domain, given by

$$\partial D_\varepsilon = \{\tilde{x} : \tilde{x} = x + \varepsilon h(x)\nu(x), x \in \partial D\}, \quad (5.13)$$

where $h \in C^1(\partial D)$ and ν denote the unit outward normal vector.

Theorem 5.3.1. *We denote by \tilde{u}_0 and by $\tilde{u}_{0,\varepsilon}$ respectively the solutions to the equation (5.4) with the inclusion D (resp. D_ε). Then, the following relation holds, for $x \in \partial\Omega$,*

$$\tilde{u}_{0,\varepsilon}(x) = \tilde{u}_0(x) + \varepsilon \tilde{u}_h(x) + o(\varepsilon), \quad (5.14)$$

where \tilde{u}_h is the solution to the following equation

$$\left\{ \begin{array}{ll} \Delta v = 0 & \text{in } B \setminus \overline{(\Omega \cup D)}, \\ \nabla v = 0 & \text{in } D, \\ v = -h\partial_\nu \tilde{u}_0|_+ & \text{on } \partial D, \\ v - \int v d\sigma - \xi \partial_\nu v = 0 & \text{on } \partial\Omega, \\ v = 0 & \text{on } \partial B, \\ \int_{\partial B} \partial_\nu v d\sigma = 0, & \end{array} \right. \quad (5.15)$$

Proof. The result can be proved using layer potential techniques by following the proof of Theorem 3.1 in [11]. \square

5.4 Gradient descent algorithms

We assume that our domain D is star shaped and centered at the origin. So its boundary ∂D can be described by the Fourier series:

$$\partial D = \left\{ r(\theta) \begin{pmatrix} \cos \theta \\ \sin \theta \end{pmatrix} \mid \theta \in [0; 2\pi) \right\}, \quad r = \sum_{n=-N}^N c_n f_n, \quad (5.16)$$

where $C = \begin{pmatrix} c_{-N} \\ c_{-N+1} \\ \vdots \\ c_N \end{pmatrix} \in \mathbb{R}^{2N+1}$, $f_n(\theta) = \cos(n\theta)$ for $0 \leq n \leq N$ and $f_n(\theta) = \sin(n\theta)$ for $-N \leq n < 0$.

Using (5.15) and integration by parts, we deduce the expressions of the shape derivatives corresponding to each Fourier coefficient, for $-N \leq n \leq N$,

$$\frac{\partial J}{\partial c_n} = \int_{B \setminus \overline{\Omega \cup D}} \nabla w \nabla \tilde{u}_n dx + \varepsilon_T \int_{\partial D} \kappa h d\sigma, \quad (5.17)$$

where $h(\theta) = f_n(\theta) \left\langle \begin{pmatrix} \cos \theta \\ \sin \theta \end{pmatrix}, \nu \right\rangle$, κ represents the curvature of ∂D and w is the solution of the following equation

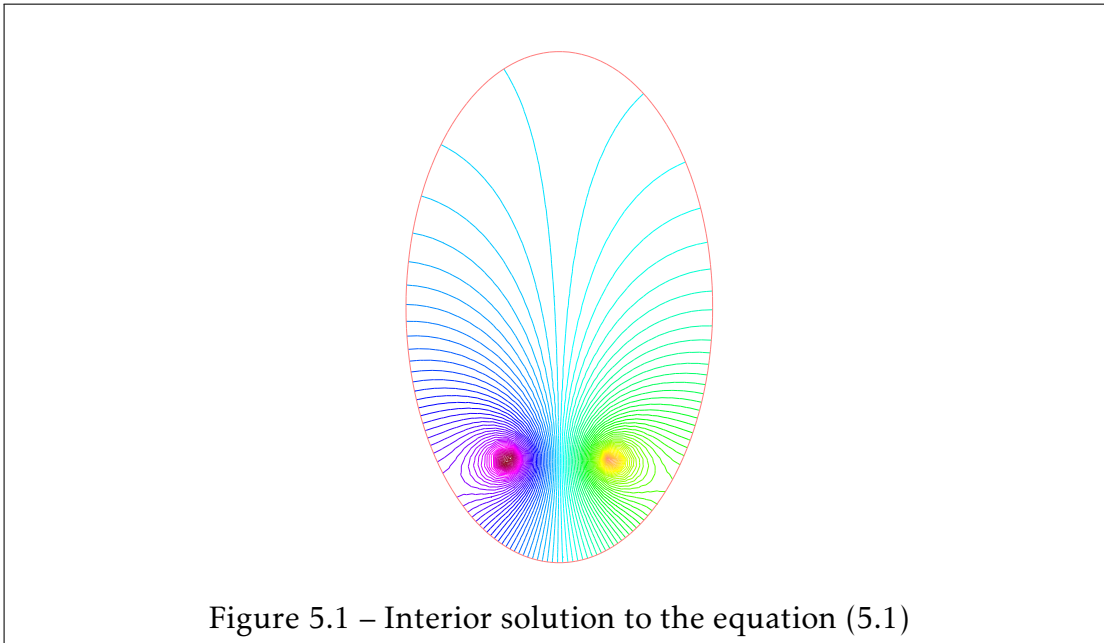
$$\begin{cases} \Delta w = 0 & \text{in } B \setminus \overline{\Omega \cup D}, \\ \partial_\nu w = 0 & \text{on } \partial D, \\ \partial_\nu w = \tilde{u} - \tilde{u}_{meas} & \text{on } \partial \Omega, \\ w = 0 & \text{on } \partial B. \end{cases} \quad (5.18)$$

Now, we are ready to introduce our iterative algorithm:

1. Calculate the interior solution \tilde{u}_i .
2. Using (5.12), retrieval of the frequency independent part \tilde{u}_0 from the multifrequency measurements. We get the Dirichlet data $(\hat{u}_{meas}^{(i)})_{1 \leq i \leq P}$.
3. Chose an initial domain D_0 .

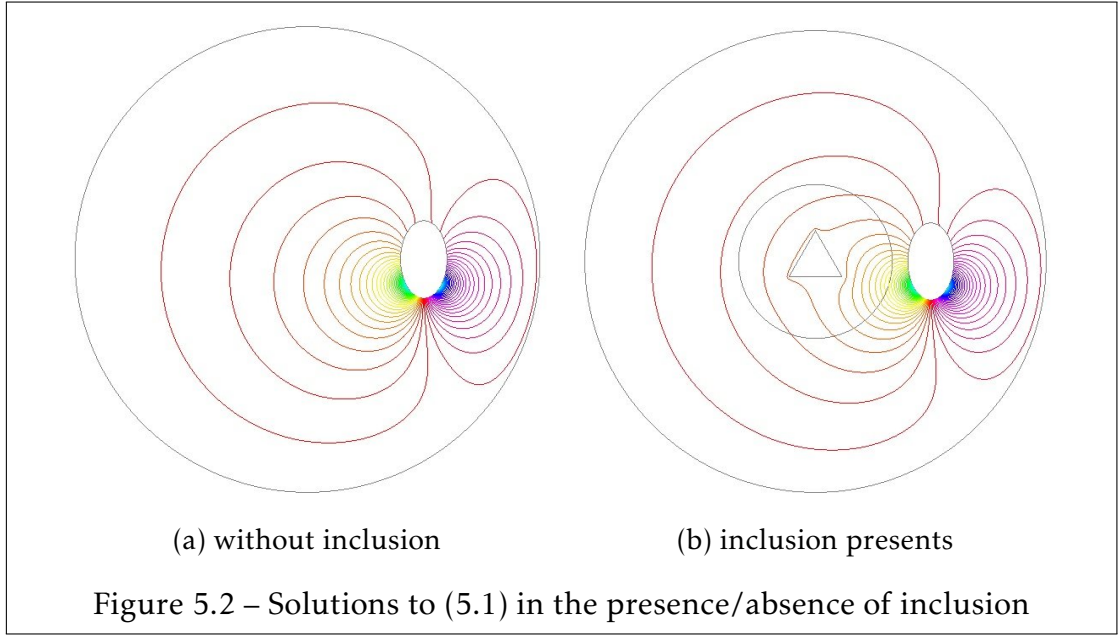
4. For each iteration, $j > 0$:
 - (a) Using (5.4) associated to the domain D_j for which the boundary ∂D_j is obtained from (5.16).
 - (b) Calculate the shape derivatives $\frac{\partial J}{\partial c_n}$ for all $-N \leq n \leq N$ by (5.17).
 - (c) Update the parameters of the domain $C_{j+1} = C_j - \alpha \nabla_C J(C_j)$ with $\alpha > 0$.
 - (d) If the updated domain boundary touches $\partial \Omega$ or if $J(C_{j+1}) > J(C_j)$, reduce the size of α .
5. When $|\nabla J(C_j)|$ becomes smaller than a fixed threshold, we stop.

5.5 Numerical experiments

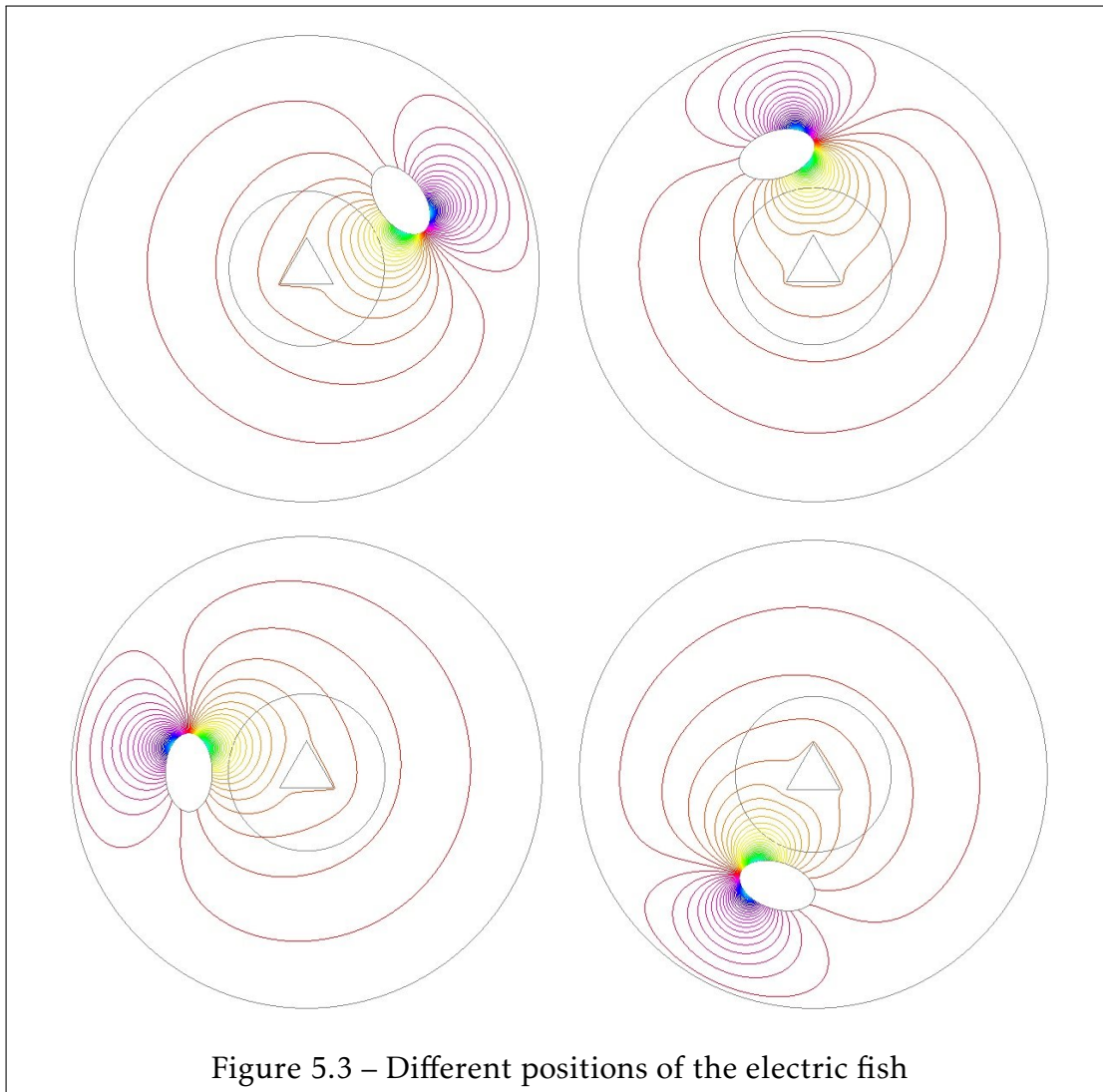


The setting of all numerical tests is as follows:

- We use FreeFem++ for our numerical experiments [42].
- B is a centered ball with the radius $R_B = 30$.



- Ω is an ellipse defined by the equation: $\frac{x^2}{3^2} + \frac{y^2}{4^2} \leq 1$.
- We assume that source function is given by a dipole type source, that means, in the formula (4.2), $M = 2$, $\alpha_1 = 100$, $\alpha_2 = -100$, $x_s^{(1)} = (-3, 1)$, and $x_s^{(2)} = (-3, -1)$.
The interior solution is illustrated in Figure 5.1.
- We profit the fact that the electric fish can swim around the target. We chose $P = 10$ different locations to measure the multifrequency electric potentials, those 10 positions are equi-distributed on the circle with a radius 15. Figure 5.3 shows the 4 locations of them.
- The multifrequency conductivity follows the model $k(\omega) = k_r + in\omega_0$ with $k_r = 5$, $\omega_0 = 0.5$ and n are integers from 0 to 7 [6].
- Only the first eigenvalues are taken into consideration, and their apriori estimations are settled as $\widetilde{\lambda}_1^+ = \frac{3}{4}$, $\widetilde{\lambda}_1^- = \frac{1}{4}$ respectively in all cases.
- The initial estimation of domain D is a centered disk with a radius $\frac{1}{2}$.
- We consider the first 9 Fourier coefficients: $N = 9$.



- We set the Tikhonov regularization coefficient $\varepsilon_T = 0.01$.
- We use P1 finite elements for the numerical resolution of the PDEs.
- At each iteration, we remesh the domain to adapt to the new predicted shape of the domain.
- The algorithms stop if $|\nabla J| < 10^{-6}$ or the number of iterations exceed 100.

We present here several numerical simulations of the algorithm. We first present in Table (5.1), errors in the reconstruction method of \tilde{u}_0 . Here, errors are the

•	ellipse	triangle	star	displaced disk
measure 1	0.10132	0.06892	0.01411	0.05330
measure 2	0.07466	0.07384	0.03364	0.05010
measure 3	0.01637	0.05302	0.07036	0.04712
measure 4	0.00910	0.04580	0.05242	0.04388
measure 5	0.03460	0.06548	0.02822	0.03792
measure 6	0.06959	0.08078	0.03558	0.03408
measure 7	0.05795	0.06175	0.02743	0.03585
measure 8	0.02060	0.03240	0.03819	0.03891
measure 9	0.00675	0.02760	0.07660	0.04054
measure 10	0.03074	0.03623	0.05292	0.04663

Table 5.1 – Errors between $\tilde{u}_{0reconstruct}$ and \tilde{u}_0

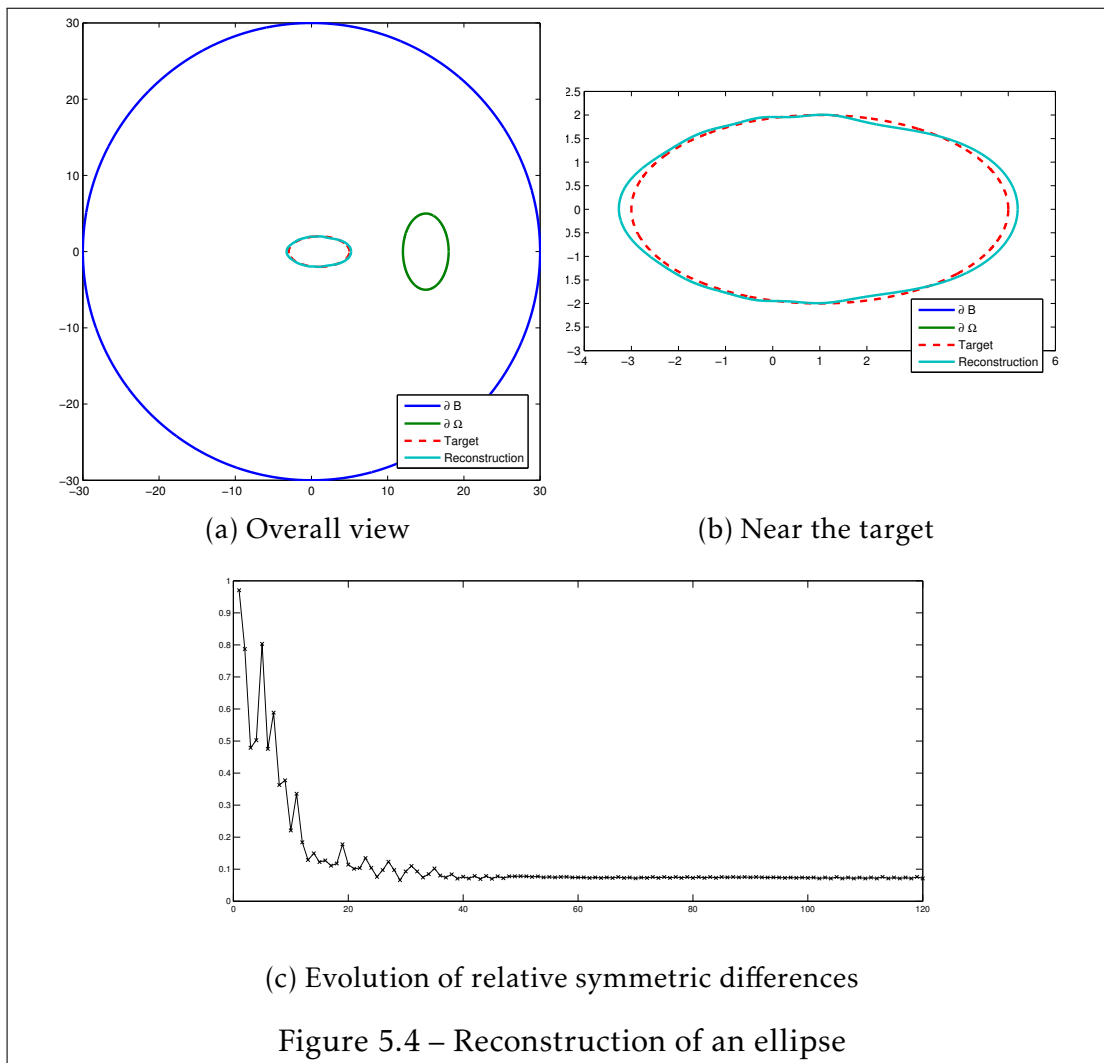
•	ellipse	triangle	star	displaced disk
$ D_i \Delta D_{target} / D_{target} $	0.07128	0,1988	0.4232	0.16805

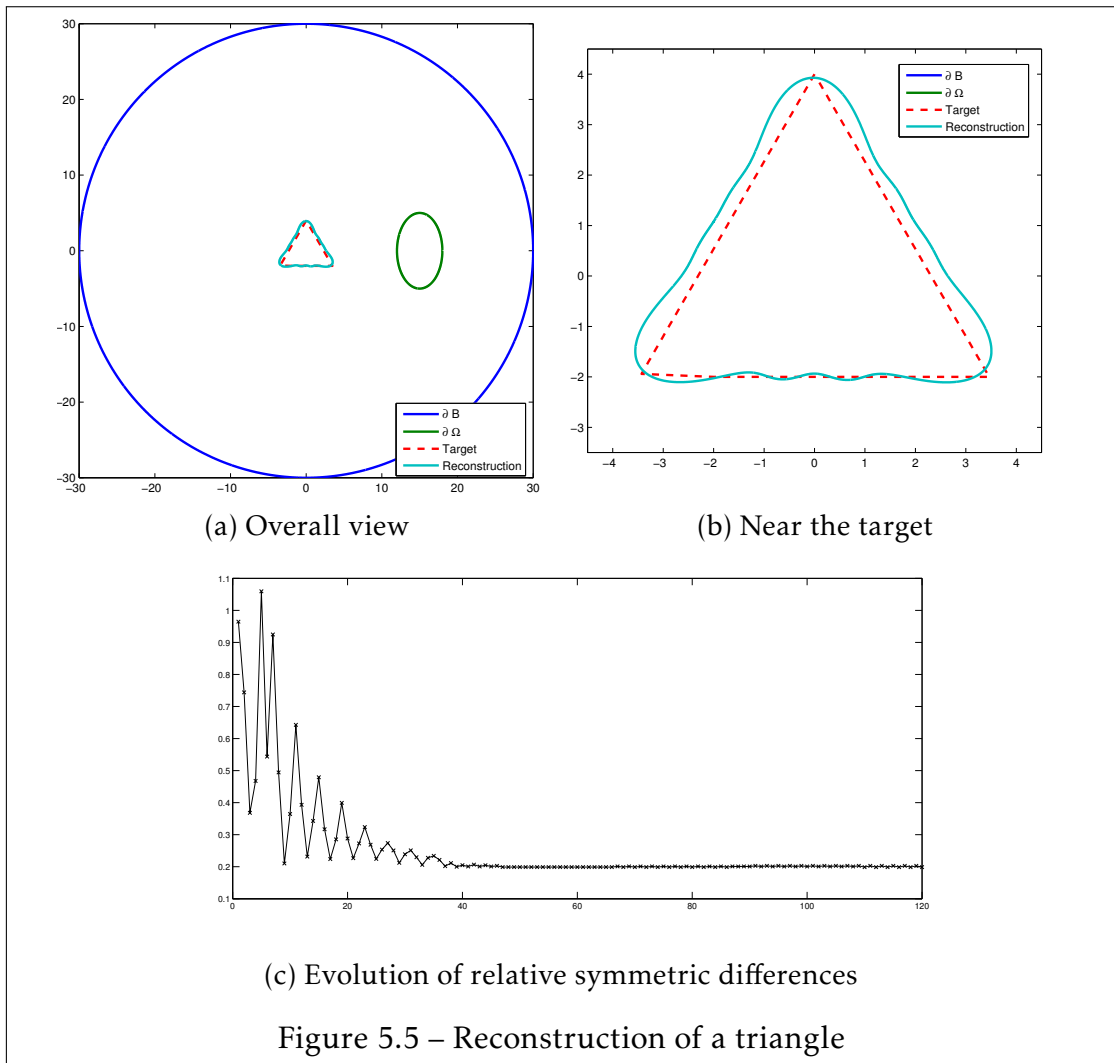
Table 5.2 – Relative symmetric difference

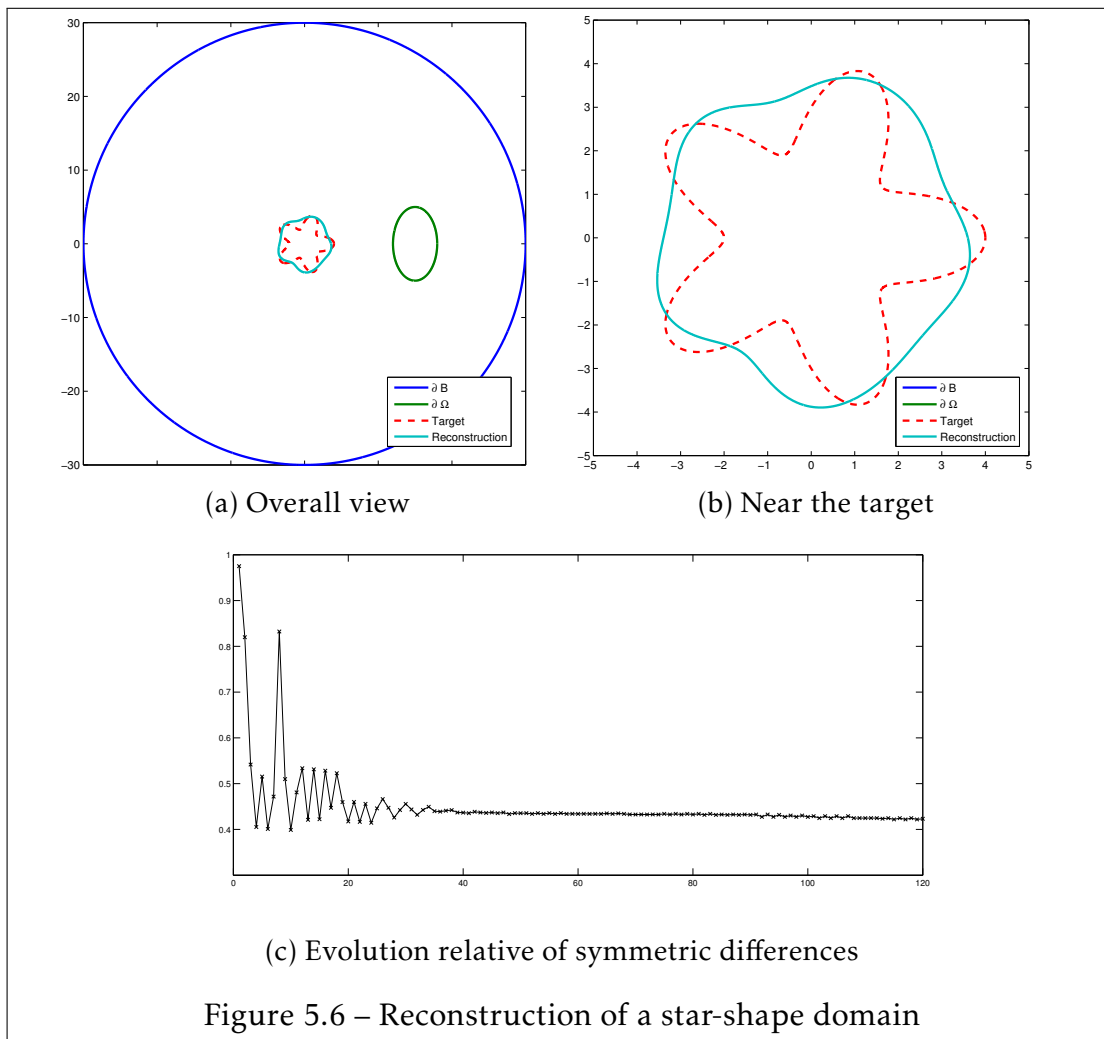
L^2 -norm of the difference $\tilde{u}_{0reconstruct} - \tilde{u}_0$:

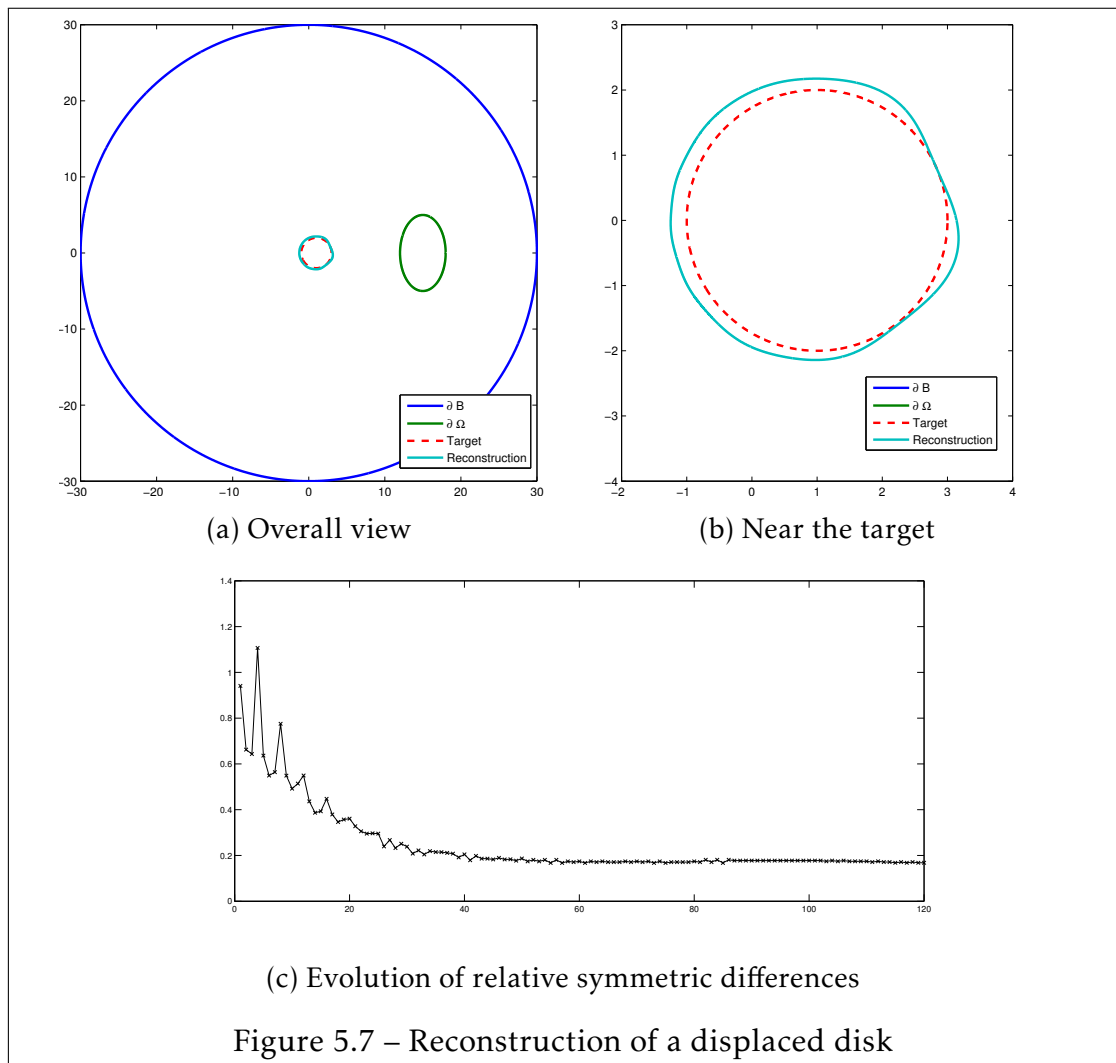
$$error(\tilde{u}_{0reconstruct}) := \sqrt{\int_{\partial\Omega} |\tilde{u}_{0reconstruct} - \tilde{u}_0|^2 d\sigma}.$$

We show in the following figures the targets and the reconstruction result. We calculate also the relative symmetric difference $|D_i \Delta D_{target}|/|D_{target}|$ during the iterations, and we draw the curves of the symmetric difference to the numbers of iterations. We finally give the relative symmetric difference of each case in Table 5.2.









Spectrum of Neumann-Poincaré operator for two close-to-touching inclusions

In a composite medium that contains close-to-touching inclusions, the pointwise values of the gradient of the voltage potential may blow up as the distance δ between some inclusions tends to 0 and as the conductivity contrast degenerates. In [27], the authors showed that the blow-up rate of the gradient is related to how the eigenvalues of the associated Neumann-Poincaré operator converge to $\pm 1/2$ as $\delta \rightarrow 0$, and on the regularity of the contact. Here, we consider two connected 2-D inclusions, at a distance $\delta > 0$ from each other. When $\delta = 0$, the contact between the inclusions is of order $m \geq 2$. We numerically determine the asymptotic behavior of the first eigenvalue of the Neumann-Poincaré operator, in terms of δ and m , and we check that we recover the estimates obtained in [26].

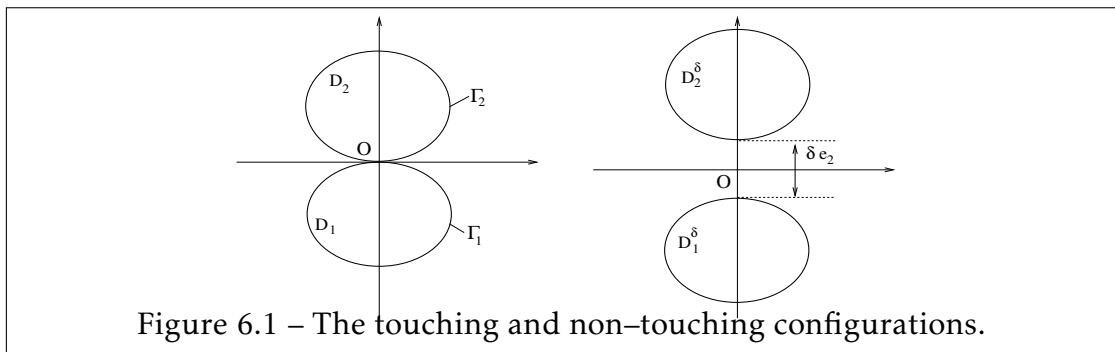
6.1 Eigenvalues of the Neumann-Poincaré operator for two inclusions

Let $D_1, D_2 \subset \mathbb{R}^2$ be two bounded, smooth inclusions separated by a distance $\delta > 0$. We assume that D_1 and D_2 are translates of two reference touching inclusions

$$D_1 = D_1^0 + (0, \delta/2) \quad D_2 = D_2^0 + (0, -\delta/2).$$

We assume that D_1^0 lies in the lower half-plane $x_1 < 0$, D_2^0 in the upper half-plane, and that they meet at the point 0 tangentially to the x_1 -axis (see Figure 6.1). We make the following additional assumptions on the geometry:

- A1. The inclusions D_1^0 and D_2^0 are strictly convex and only meet at the point 0.
- A2. Around the point 0, ∂D_1^0 and ∂D_2^0 are parametrized by 2 curves $(x, \psi_1(x))$ and $(x, -\psi_2(x))$ respectively. The graph of ψ_1 (resp. ψ_2) lies below (resp. above) the x -axis.
- A3. The boundary ∂D_i^0 of each inclusion is globally $C^{1,\alpha}$ for some $0 < \alpha \leq 1$.
- A4. The function $\psi_1(x) + \psi_2(x)$ is equivalent to $C|x|^m$ as $x \rightarrow 0$, where $m \geq 2$ is a fixed integer and C is a positive constant.



Let $a(X)$ be a piecewise constant function that takes the value $0 < k \neq 1$ in each inclusion and 1 in $\mathbb{R}^2 \setminus \overline{D_1 \cup D_2}$, that is $a(X) = 1 + (k - 1)\chi_{D_1 \cup D_2}(X)$, where $\chi_{D_1 \cup D_2}$ is the characteristic function of $D_1 \cup D_2$. Given a harmonic function H , we denote u the solution to the PDE

$$\begin{cases} \operatorname{div}(a(X)\nabla u(X)) = 0 & \text{in } \mathbb{R}^2 \\ u(X) - H(X) \rightarrow 0 & \text{as } |X| \rightarrow \infty. \end{cases} \quad (6.1)$$

Since H is harmonic in the whole space the regularity of u at a fixed value k , only depends on the smoothness of the inclusions and of their distribution [41].

One can express u in terms of layer potentials [59, 14]

$$u(X) = S_1\varphi_1(X) + S_2\varphi_2(X) + H(X), \quad (6.2)$$

where S_i denotes the single layer potential on ∂D_i , defined for $\varphi \in H^{-1/2}(\partial D_i)$ by

$$S_i\varphi(X) = \frac{1}{2\pi} \int_{\partial D_i} \ln|X - Y| \varphi(Y) d\sigma(Y).$$

Denoting the conductivity contrast by $\lambda = \frac{k+1}{2(k-1)} \in]-\infty, -1/2[\cup]1/2, +\infty[$, and expressing the transmission conditions satisfied by u , one sees that the layer potential $\varphi = (\varphi_1, \varphi_2) \in H^{-1/2}(\partial D_1) \times H^{-1/2}(\partial D_2)$ satisfies the system of integral equations

$$(\lambda I - K_\delta^*) \begin{pmatrix} \varphi_1 \\ \varphi_2 \end{pmatrix} = \begin{pmatrix} \partial_{\nu_1} H|_{\partial D_1} \\ \partial_{\nu_2} H|_{\partial D_2} \end{pmatrix}, \quad (6.3)$$

where $\nu_i(X)$ denotes the outer normal at a point $X \in \partial D_i$. The operator K_δ^* is the Neumann-Poincaré operator for the system of two inclusions

$$K_\delta^* \begin{pmatrix} \varphi_1 \\ \varphi_2 \end{pmatrix} = \begin{pmatrix} K_1^* & \partial_{\nu_1} S_2|_{\partial D_1} \\ \partial_{\nu_2} S_1|_{\partial D_2} & K_2^* \end{pmatrix} \begin{pmatrix} \varphi_1 \\ \varphi_2 \end{pmatrix}, \quad (6.4)$$

where the integral operators K_i^* are defined on $H^{-1/2}(\partial D_i)$ by

$$K_i^*\varphi(X) = \frac{1}{2\pi} \int_{\partial D_i} \frac{(X - Y) \cdot \nu_i(X)}{|X - Y|^2} \varphi(Y) d\sigma(Y).$$

In such a system of inclusions, for a fixed contrast $|\lambda| > 1/2$, the gradient of the potential is bounded pointwise [28, 52, 14] *independently of* δ . This is an important fact from the point of view of material sciences, where one would like to control the ‘hot spots’ where gradients may become large [30]. The pointwise control of the gradients is also particularly pertinent in the context of solid mechanics. For instance, the constitutive laws of classical models of plasticity or fracture involve pointwise values of the stress tensor. Similar qualitative results hold in this case [53].

However, the gradients may blow up when both $\delta \rightarrow 0$ and the material coefficients inside the inclusions degenerate [28]. How the bounds depend on the inter-inclusion distance in the case of perfectly conducting inclusions was studied in [62, 23]. Several works study the blow-up rate of the gradient in terms of both parameter $\delta \rightarrow 0$, and $|\lambda| \rightarrow 1/2$ when the inclusions are discs. In this case, the voltage potential u can be represented by a series, that lends itself to a precise asymptotic analysis [9, 16, 15, 25, 30, 54]. In particular, optimal upper and lower bounds on ∇u were obtained in [9, 16, 13].

In a recent work [26], we have used the above integral representation to derive bounds on ∇u , as we had observed that in (6.3) the parameters λ and δ are decoupled since K_δ^* does not depend on λ . Following [48, 49], we showed that K_δ^* has a spectral decomposition in the space of single layer potentials. We showed that its spectrum splits into two families of ordered eigenvalues $\lambda_n^{\delta,\pm}$ which satisfy

$$\lambda_n^{\delta,+} = -\lambda_n^{\delta,-} \quad \text{and} \quad 0 < \lambda_n^{\delta,+} < 1/2.$$

Consequently, denoting by $\varphi_n^{\delta,\pm}$ the associated eigenvectors, the solution to (6.3) can be expressed as

$$\varphi = \begin{pmatrix} \varphi_1 \\ \varphi_2 \end{pmatrix} = \sum_{n \geq 1} \frac{\left\langle \varphi_n^{\delta,\pm}, \begin{pmatrix} \partial_{\nu_1} H|_{\partial D_1} \\ \partial_{\nu_2} H|_{\partial D_2} \end{pmatrix} \right\rangle}{\lambda - \lambda_n^{\delta,\pm}} \varphi_n^{\delta,\pm}. \quad (6.5)$$

This formula indicates that the singularities of u are triggered by the fact that

$\lambda - \lambda_n^{\delta, \pm}$ may become small. Indeed, $\lambda \rightarrow \pm 1/2$ as k tends to 0 or to $+\infty$, whereas we have shown that $\lambda_n^{\delta, \pm} \rightarrow \pm 1/2$ as $\delta \rightarrow 0$ [26].

We do not know if the expansion (6.5) holds in a pointwise sense, except in the case of discs [27], where we can then directly relate the bounds on ∇u to the asymptotic behavior of the eigenvalues. One of the difficulties is that K_δ^* is not self-adjoint. One can nevertheless symmetrize the operator [48]: The expansion (6.5) holds in the sense of the following inner-product on the space $H^{-1/2}(\partial D_1) \times H^{-1/2}(\partial D_2)$

$$\begin{aligned} \langle \varphi, \psi \rangle_S &= \langle -S[\varphi], \psi \rangle_{L^2} \\ &:= - \int_{\partial D_1} S_1[\varphi_1] \psi_1 - \int_{\partial D_2} S_2[\varphi_2] \psi_2, \end{aligned} \tag{6.6}$$

for which K_δ^* becomes a compact self-adjoint operator, which therefore has a spectral decomposition. Moreover, this implies that the eigenvalues of K_δ^* can be obtained via a min-max principle known as the Poincaré variational problem (in the terminology of [48]). It consists in optimizing the ratio

$$J(u) = \frac{\int_{D_1 \cup D_2} |\nabla u|^2}{\int_{\mathbb{R}^2 \setminus \overline{D_1 \cup D_2}} |\nabla u|^2},$$

among all functions $u \in W^{1,2}(\mathbb{R}^2)$ whose restriction to $D = D_1 \cup D_2$ and to $D' = \mathbb{R}^2 \setminus \overline{D_1 \cup D_2}$ is harmonic.

Consider the weighted Sobolev space

$$\mathcal{W}_0^{1,-1}(\mathbb{R}^2) := \left\{ \begin{array}{l} \frac{u(X)}{(1 + |X|^2)^{1/2} \log(2 + |X|^2)} \in L^2(\mathbb{R}^2) \\ \nabla u \in L^2(\mathbb{R}^2), u(X) = o(1) \text{ as } |X| \rightarrow \infty \end{array} \right\},$$

equipped with the scalar product $\int_{\mathbb{R}^2} \nabla u \cdot \nabla v$ [59]. We have shown in [26] that the spectrum of K_δ^* is related to the spectrum of the operator T_δ defined for

$u \in W_0^{1,-1}(\mathbb{R}^2)$ by

$$\forall v \in W_0^{1,-1}(\mathbb{R}^2), \quad \int_{\mathbb{R}^2} \nabla T_\delta u(X) \cdot \nabla v(X) = \int_{D_1 \cup D_2} \nabla u(X) \cdot \nabla v(X).$$

This operator is self adjoint, satisfies $\|T_\delta\| \leq 1$. Proposition 4 and Lemmas 1 and 2 in [26] show that its eigenvalues can be grouped in two families $\beta_n^{\delta,+} \subset [0, 1/2]$, and $\beta_n^{\delta,-} \subset [1/2, 1]$, which are symmetric with respect to $1/2$. The values $\beta_0^{\delta,-} = 1$ is an eigenvalue of T_δ , with associated eigenspace

$$\text{Ker}(I - T_\delta) = \{v|_{D'} \equiv 0, v|_D \in H_0^1(D)\}.$$

Due to the symmetry, $\beta_0^{\delta,+} = 0$ is also an eigenvalue, and its eigenspace is

$$\text{Ker}(T_\delta) = \{v|_{D'} \in \mathcal{W}_0^{1,-1}(D'), v|_D \equiv 0\} \cup \mathbb{R} w_0,$$

where w_0 is defined by

$$\begin{cases} \Delta w_0(X) = 0 & \text{in } D', \\ w_0(X) = C_j & \text{on } \partial D_j \quad j = 1, 2, \\ \int_{\partial D_j} \frac{\partial w_0}{\partial \nu} = (-1)^j & j = 1, 2. \end{cases} \quad (6.7)$$

The constants $C_1, C_2 \in \mathbb{R}$ are chosen so that $w_0 \in \mathcal{W}_0^{1,-1}(\mathbb{R}^2)$.

All the other eigenvalues $\beta_n^{\delta,+}$ are given by the following min-max principle

$$\begin{aligned} \beta_n^{\delta,+} &= \min_{u \in W_0^{1,-1}(\mathbb{R}^2), \perp w_0, w_1^{\delta,+}, \dots, w_n^{\delta,+}} \frac{\int_D |\nabla u(X)|^2 dX}{\int_{\mathbb{R}^2} |\nabla u(X)|^2 dX} \\ &= \max_{F_n \subset W_0^{1,-1}(\mathbb{R}^2)} \min_{u \in F_n} \frac{\int_D |\nabla u(X)|^2 dX}{\int_{\mathbb{R}^2} |\nabla u(X)|^2 dX} \\ &\quad \dim(F_n) = n + 1 \end{aligned}$$

The eigenvalues of T_δ are related to the $\lambda_n^{\delta,\pm}$'s by

$$\beta_n^{\delta,\pm} = 1/2 - \lambda_n^{\delta,\pm}.$$

The min-max characterization of T_δ allows to derive an asymptotic expansion of the eigenvalues of the Neumann-Poincaré operator (see [26], Theorem 1) as $\delta \rightarrow 0$.

Theorem 6.1.1. *For two close to touching inclusions with contact of order m , the eigenvalues of the Neumann-Poincaré operator K_δ^* split in two families $(\lambda_n^\pm)_{n \geq 1}$, with*

$$\begin{cases} \lambda_n^+ \sim 1/2 - c_n^+ \delta^{\frac{m-1}{m}} + o(\delta^{\frac{m-1}{m}}) \\ \lambda_n^- \sim -1/2 + c_n^- \delta^{\frac{m-1}{m}} + o(\delta^{\frac{m-1}{m}}) \end{cases} \quad (6.8)$$

where $(c_n^\pm)_{n \geq 1}$ are increasing sequences of positive numbers, that only depend on the shapes of the inclusions, and that satisfy $c_n^\pm \sim n$ as $n \rightarrow \infty$.

In this work, we consider a numerical approximation of the spectral problem for T_δ so as to give a numerical validation of the rates of convergence of $\lambda_1^{\delta,+}$ as $\delta \rightarrow 0$. The first eigenvalue $\lambda_1^{\delta,+}$ is of importance in applications since it is related to the spectral radius of the operator K_δ^* , and gives the rate of convergence of Neumann series that appears in solving the integral equation (6.3) [61].

In Section 2, we show that the asymptotic behavior of the eigenvalues of T_δ can be estimated by the eigenvalues of an operator of similar type, but defined on a ball B_R that contains the inclusions. In fact, by considering the auxiliary spectral problem in a large ball B_R , we reduce the computation to a bounded domain.

In Section 3, we explain how we discretized the latter spectral problem, by choosing a basis of functions which are harmonic polynomials on each inclusion, extended as harmonic functions in $B_R \setminus \overline{D_1 \cup D_2}$. Finally, numerical results for $\beta_1^{\delta,+}$ with different contact orders m are presented in Section 4.

6.2 Comparison of T_δ with an operator defined on a bounded domain

Let $R > 2$ be large enough, so that $D_1 \cup D_2 \subset B_{R/2}$ when $\delta < \delta_0$. It follows from the Riesz Theorem that for any $u \in H_0^1(B_R)$, there exists a unique $B_\delta u \in H_0^1(B_R)$ such that

$$\forall v \in H_0^1(B_R), \quad \int_{B_R} \nabla B_\delta u(X) \cdot \nabla v(X) = \int_{D_1 \cup D_2} \nabla u(X) \cdot \nabla v(X).$$

The operator B_δ maps $H_0^1(B_R)$ into itself, and it is easily seen to satisfy $\|B_\delta\| \leq 1$. The argument in [26] concerning T_δ shows that B_δ is self adjoint and of Fredholm type, thus has a spectral decomposition. Let $b_n^{\delta, \pm}$ denote its eigenvalues.

Theorem 6.2.1. *Let $n \geq 1$. There exists a constant C independent of δ and n such that*

$$\frac{1}{C} b_n^{\delta, +} \leq \beta_n^{\delta, +} \leq C b_n^{\delta, +}. \quad (6.9)$$

Proof: Let $f \in H^{1/2}(\partial D)$ and let $u_f \in W_0^{1,-1}(\mathbb{R}^2)$ and $v_f \in H_0^1(B_R)$ denote the functions which are harmonic in $\mathbb{R}^2 \setminus D$ and in $B_R \setminus D$ respectively, which are also harmonic in D , and which satisfy $u_f = v_f = f$ on ∂D . We will show that there exists a constant $C > 0$ independent of δ and n such that for all $f \in H^{1/2}(\partial D) \setminus \{0\}$,

$$\frac{1}{C} \frac{\int_D |\nabla v_f|^2}{\int_{B_R} |\nabla v_f|^2} \leq \frac{\int_D |\nabla u_f|^2}{\int_{\mathbb{R}^2} |\nabla u_f|^2} \leq C \frac{\int_D |\nabla v_f|^2}{\int_{B_R} |\nabla v_f|^2}. \quad (6.10)$$

The statement of the theorem follows then from the min-max principle for the operators T_δ and B_δ .

To prove (6.10), we first note that since u_f and v_f are harmonic in D and coincide on ∂D , $u_f \equiv v_f$ on ∂D , so that

$$\int_D |\nabla u_f|^2 = \int_D |\nabla v_f|^2. \quad (6.11)$$

Since the extension of v_f by 0 outside of B_R is a function of $W_0^{1,-1}(\mathbb{R}^2)$, we see that

$$\int_{\mathbb{R}^2} |\nabla u|^2 \leq \min_{w \in W_0^{1,-1}(\mathbb{R}^2)} \int_{\mathbb{R}^2} |\nabla w|^2 \leq \int_{B_R} |\nabla v|^2,$$

which together with (6.11) proves the right-hand inequality in (6.10).

To prove the other inequality, let χ denote a smooth cut-off function, such that $\chi \equiv 1$ in $B_{R/2}$ and $\chi \equiv 0$ outside B_R . We may also assume that $\|\chi\|_{W^{1,\infty}} \leq 1$. The function $\tilde{u}_f = \chi u_f$ lies in $H_0^1(B_R)$, and there is a constant C that only depends on R such that

$$\int_{B_R \setminus \bar{D}} |\nabla \tilde{u}_f|^2 \leq C \int_{\mathbb{R}^2 \setminus \bar{D}} |\nabla u_f|^2.$$

Since $\tilde{u}_f = u_f = v_f$ on ∂D , it follows from the Dirichlet principle that

$$\int_{B_R \setminus \bar{D}} |\nabla v_f|^2 \leq \int_{B_R \setminus \bar{D}} |\nabla \tilde{u}_f|^2,$$

which combined with (6.11) yields the desired inequality.

6.3 Discretization

In the sequel, we estimate numerically the rate of convergence to 0 of the first non-degenerate eigenvalue $b_1^{\delta,+}$, from which, using Theorem 6.1.1, we will infer the behavior of $\beta_1^{\delta,+}$. To this end, we use the min-max principle to approximate $b_1^{\delta,+}$ by

$$b_{1,N}^{\delta,+} = \min_{u \in V_N} \frac{\int_D |\nabla u(X)|^2 dX}{\int_{B_R} |\nabla u(X)|^2 dX} \quad (6.12)$$

where V_N is a finite dimensional subspace of $H_0^1(B_R)$. We construct approximation spaces V_N in the following fashion Let $X_1 = (x_1 + iy_1) \in D_1, X_2 = (x_2 + iy_2) \in D_2$ and $n \in \mathbb{N}$. Define $\phi_{n,1}^\pm, \phi_{n,2}^\pm : \mathbb{R}^2 \rightarrow \mathbb{C}$ by $\phi_{n,1}(z) = (z - X_1)^n, \phi_{n,2}(z) = (z - X_2)^n$,

where $z = x + iy$. Let $w_m, m \geq 1$ be the $H_0^1(D)$ functions which are harmonic in $B_R \setminus \overline{D}$ and such that

$$\begin{cases} w_{4n-3} = \operatorname{Re}(\phi_{n,1}) & \text{in } D_1 \\ w_{4n-3} = 0 & \text{in } D_2, \end{cases} \quad \begin{cases} w_{4n-2} = \operatorname{Im}(\phi_{n,1}) & \text{in } D_1 \\ w_{4n-2} = 0 & \text{in } D_2, \end{cases}$$

$$\begin{cases} w_{4n-1} = 0 & \text{in } D_1 \\ w_{4n-1} = \operatorname{Re}(\phi_{n,2}) & \text{in } D_2, \end{cases} \quad \begin{cases} w_{4n} = 0 & \text{in } D_1 \\ w_{4n} = \operatorname{Im}(\phi_{n,2}) & \text{in } D_2. \end{cases}$$

We consider a conformal triangulation \mathcal{T} of B_R , which is refined in the neck between the 2 inclusions. The width of the refined zone is chosen so that its thickness is equal to 5δ at its extremities (see for instance Figures (6.2),(6.3) and (6.4)) for the case of two discs. Let $\hat{w}_m, m \geq 1$ denote the H^1 projection of w_m on the space of functions which are piecewise linear on \mathcal{T} . We define V_N as the vector space generated by the functions $\hat{w}_m, m \leq 4N$.

We note that the functions $w_m, m \geq 1$ are linearly independent. Together with the functions $w_{0,1}, w_{0,2}$ in $H_0^1(B_R)$ defined by $\Delta w_{0,i} = 0$ in $B_R \setminus \overline{D}$, and

$$\begin{cases} w_{0,1} = 1 & \text{in } D_1 \\ w_{0,1} = 0 & \text{in } D_2, \end{cases} \quad \begin{cases} w_{0,2} = 0 & \text{in } D_1 \\ w_{0,2} = 1 & \text{in } D_2, \end{cases}$$

they form a basis of $H_0^1(B_R)$. We also note that the functions $w_{0,i}$ are the eigenfunctions of B_δ associated to the degenerate mode $b_0 = 0$. To compute the eigenvalues $b_{1,N}^{\delta,+}$, we form the matrices A and B with entries

$$A_{i,j} = \int_{D_1 \cup D_2} \nabla \hat{w}_i \cdot \nabla \hat{w}_j, \quad B_{i,j} = \int_{B_R} \nabla \hat{w}_i \cdot \nabla \hat{w}_j,$$

and then compute the generalized eigenvalues of the system $AU = \lambda BU$. We have used the software Freefem++ [42] to compute the vectors \hat{w}_m , and Scilab [60] to solve the above matrix eigenvalue problem.

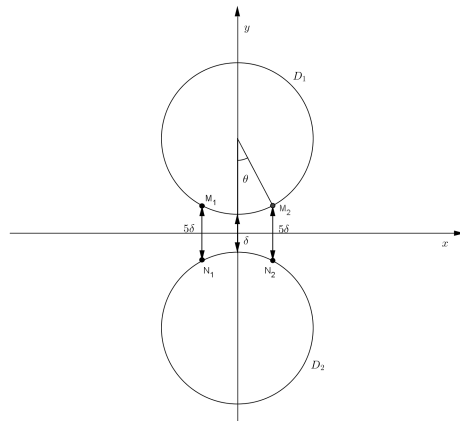


Figure 6.2 – Mesh refinement zone.

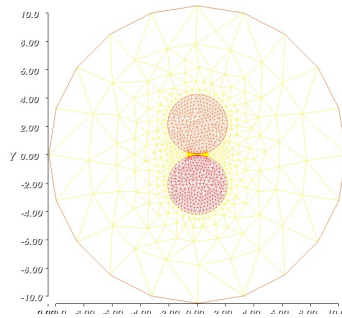
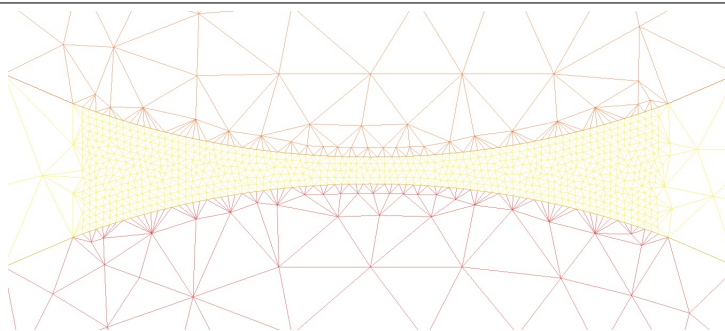
Figure 6.3 – Mesh for $\delta = 1/16$.

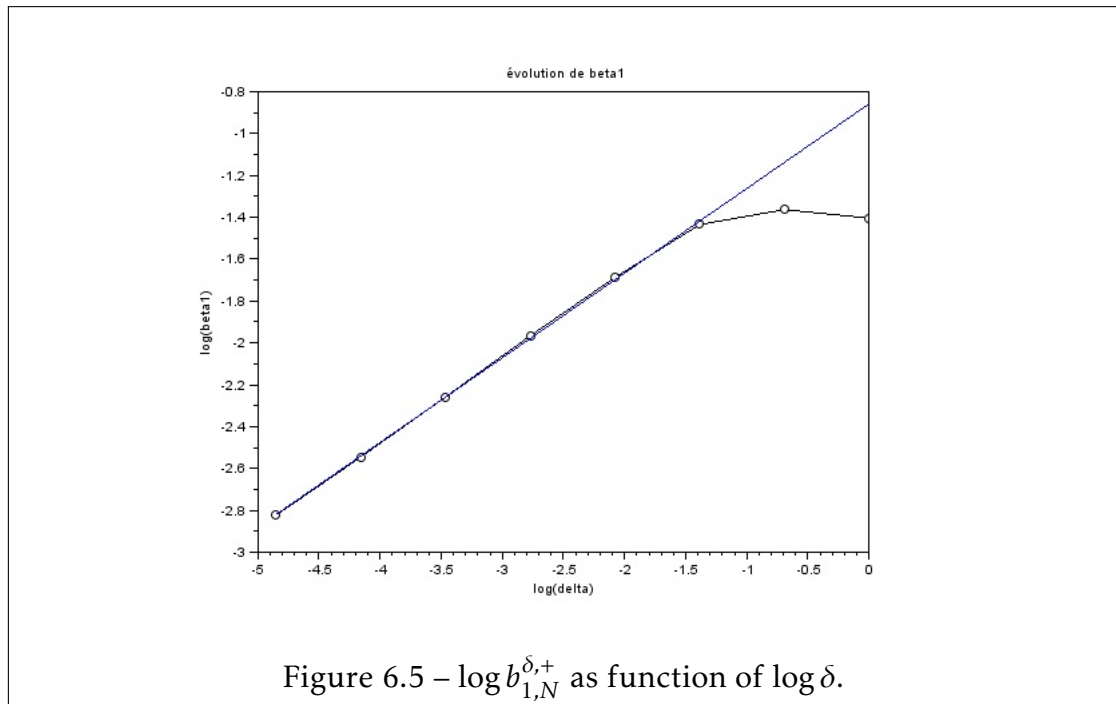
Figure 6.4 – Mesh refinement near the contact point.

6.4 Numerical results

We deduce from Theorems 6.1.1 and 6.2.1 that $\log b_{1,N}^{\delta,+} \sim \log c_1^+ + \frac{m-1}{m} \log \delta$ as δ tends to 0. In this section, we draw the graph of $\log b_{1,N}^{\delta,+}$ as a function of $\log \delta$, and determine numerically its slope $\frac{m-1}{m}$. We first study the case where the inclusions are two discs, and then we perturb the inclusions to have a contact point with higher order.

6.4.1 The case of 2 discs

We start with the case of two discs $D_1 = B_r(0, r + \frac{\delta}{2})$ and $D_2 = B_r(0, r - \frac{\delta}{2})$ with $r = 2$. Here, X_1 and X_2 in the construction of V_N , are chosen to be the centers of the discs D_1 and D_2 .

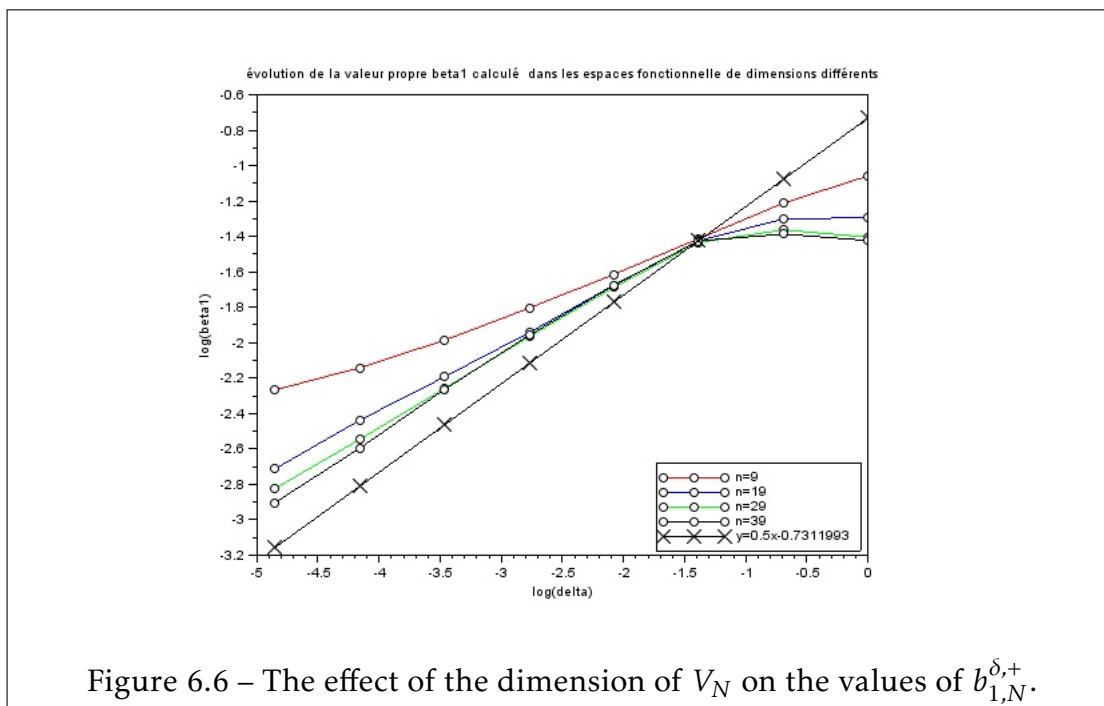


Since the contact of order two, i.e. $\psi_1(x) + \psi_2(x) \sim C|x|^2$ as $x \rightarrow 0$, the theoretical slope is $1/2$. Taking $N = 39$, the graph of $\log b_{1,N}^{\delta,+}$ tends to the line with equation $t = -0.7934156 + 0.4307516s$ (see for instance Figure (6.5)). The equa-

tion of the line is computed using the least squares method.

The dimension of the space V_N is $4N + 2$. Hence, we expect that the numerical slope will tend to the theoretical one when N becomes larger. The following table and graph give how does the numerical slope behave as a function of N , and shows a good agreement with the theoretical predictions.

Values of N	equation of the line approximation
$N = 9$	$t = -1.09526 + 0.2486835s$
$N = 19$	$t = -0.9099896 + 0.3700286s$
$N = 29$	$t = -0.8575362 + 0.4045268s$
$N = 39$	$t = -0.7934156 + 0.4307516s$



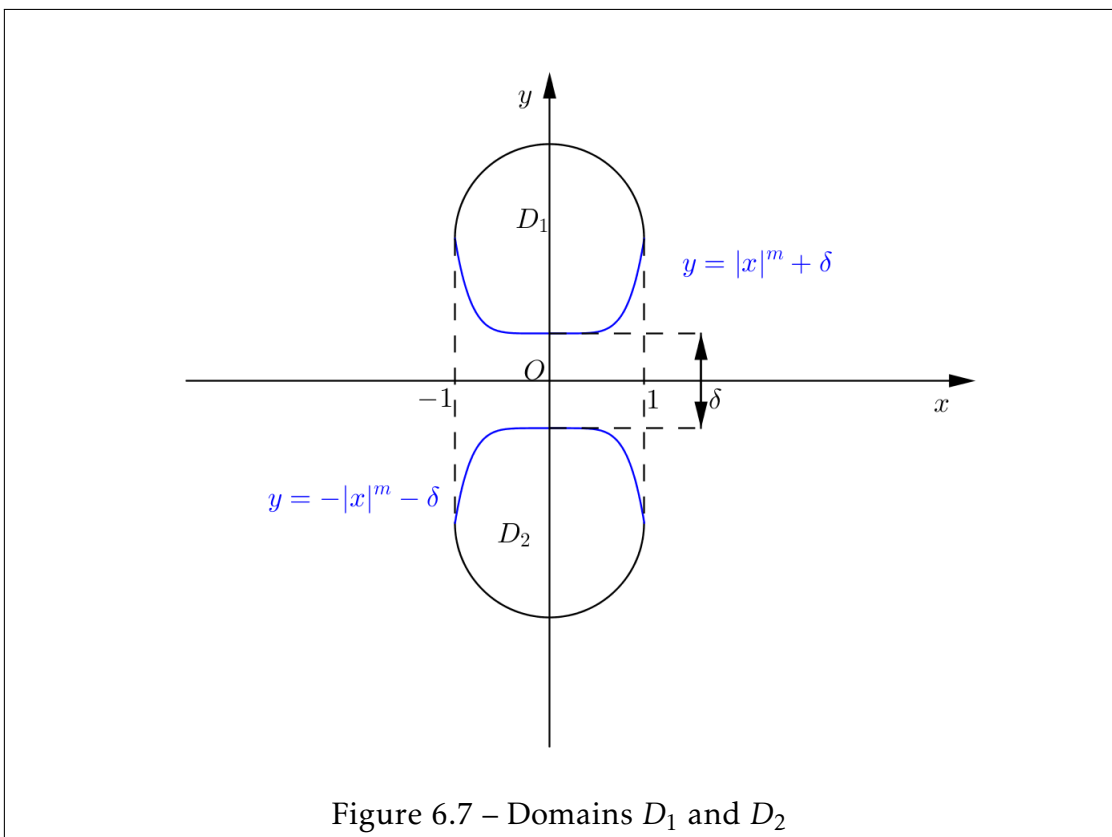
6.4.2 Contact of order m

Now, we consider shapes with different contact orders i.e. $\psi_1(x) + \psi_2(x) \sim C|x|^m$.

Let D_1 and D_2 be the perturbed half discs defined by (see Figure (6.7))

$$D_1 = \{-1 \leq x \leq 1, |x|^m + \delta \leq y \leq 1 + \delta\} \cup \{x^2 + (y - 1 - \delta)^2 \leq 1, y \geq 1 + \delta\},$$

$$D_2 = \{-1 \leq x \leq 1, -|x|^m - \delta \geq y \geq -1 - \delta\} \cup \{x^2 + (y + 1 + \delta)^2 \leq 1, y \leq -1 - \delta\}.$$



The points X_1 and X_2 in the construction of the space V_N , are the centers of the perturbed discs. The following table provide the numerical results for δ between $1/2$ and $1/2^7$, and $N = 39$.

m	Equation of the line	Theoretical slope	Error
$m = 2$	$t = -0.7934156 + 0.4307516s$	$\frac{1}{2} = 0.5$	0.0692484
$m = 6$	$t = -0.1401772 + 0.8003479s$	$\frac{5}{6} \simeq 0.83$	0.03298543
$m = 9$	$t = -0.2357561 + 0.8508496s$	$\frac{8}{9} \simeq 0.89$	0.03803929

We remark that the computed slopes are in a good agreement with the expected theoretical values.

6.5 Conclusion

We have studied the behavior of the eigenvalues of the Neumann-Poincaré operator for two close-to-touching inclusions in dimension two. We have validated numerically the rates of convergence derived in [26]. We continue to study the asymptotic behavior of the spectrum of the Neumann-Poincaré integral operator for two close-to-touching inclusions in dimension three. We also plan to extend the results of [27] to general geometries in dimension two. In dimension three the sizes of the matrices A and B become too large and this may complicate the computation of the generalized eigenvalues. In another line of research, we propose to use an integral equation approach combined with an asymptotic approximation of the kernels of the off-diagonal operators in the system (6.4) around the contact point. We think that this approach is more appropriate to dimension three and larger. We will report related results in future works.

Conclusion

In this Phd thesis, we studied mathematical models of the inverse problem of recovering an inclusion from boundary measurements : the model of electrical impedance tomography (2) and the model of electroreception (4.1). We propose two different approaches to analyze the inverse problem, using either a single measurement or using multifrequency measurements when the conductivity inside the inclusion is frequency dependent. In the latter case, we use a representation of the voltage potential based on the spectral decomposition of the Neumann-Poincaré operator. This led us to also study the asymptotic behavior of the eigenvalues of Neumann-Poincaré operator in the case of two close-to-touching inclusion.

Firstly, we have established the uniqueness of the inclusion recovery problem using a single measurement, under the assumption that the inclusion has a circular shape and we improved the stability estimate result in [37]. Our stability estimate is valid even for non-zero input electrical current. Our numerical simulations show that the Hölder stability coefficient in the stability estimate is close to 1, which indicates that the dependence might actually be Lipschitz.

Secondly, we addressed similar questions in the case of multifrequency measurements. We have shown that the unique solution to equation (3.1) has a spectral decomposition (3.8) on the basis of eigenfunctions of the Neumann-Poincaré operator associated to the inclusion D . Based on this spectral decomposition, we have designed a numerical scheme to reconstruct the frequency profile $k(\omega)$ and the geometry of the inclusion. From our numerical experiments, we remark that the reconstructions of the conductivity inside the inclusion, as a function of the frequency ω , are good in general, except when the inclusion is far from the boundary where the measurements are taken. Our algorithm to reconstruct

the inclusion is however quite costly, and it may take several hours to numerically reconstruct a given shape. In particular, it proved extremely difficult to reconstruct a non-convex shape with this algorithm.

Thirdly, concerning electroreception, we addressed the question of existence and uniqueness of the solution to the forward problem (4.1). We derived a spectral decomposition (4.38) of the voltage potential, using the same analysis as for the EIT model. We derived a numerical algorithm to determine the volume and the shape of the target, assuming that the position of its center and its conductivity profile are known. This algorithm is however also very costly, and to speed up the computations, we reduced the number of Fourier coefficients, that parametrize the shape of the inclusion D .

Finally, we studied the asymptotic behavior of Neumann-Poincaré operator for two close-to-touching inclusions. We designed an original numerical scheme that projects functions on the space of harmonic polynomials. Our numerical simulations show that the convergence rates agree with the theoretical prediction [26], as the interinclusion distance δ tends to 0.

We conclude with a few perspectives that our work opens. Concerning the EIT model under a single measurement (in 2D), it would be quite interesting to generalize our results for the circle to the case of an ellipse or of an analytic shape. This would have an important practical impact in the context of medical imaging for instance. Generalizing the stability estimates in 3D is also challenging, even when the inclusion is simply a ball.

As for the EIT model using multifrequency measurements, it would be worthwhile to obtain more precise estimates on the eigenvalues of Neumann-Poincaré operator and their rate of decay. The case of multiple inclusions also addresses interesting questions. In particular, we would like to find out whether such spectral decompositions could lead to a fast algorithm, that would allow identification of one or several inclusions within a given set of shapes in real time.

Finally, several questions concerning the spectrum of the Neumann-Poincaré operator, in the context of close-to-touching inclusions remain open. In particular, it would be very interesting to study how the blow up of the gradient of the voltage potential depends on the geometry of the contact points in dimension 3.

Bibliography

- [1] Robert A Adams. “Compact Sobolev imbeddings for unbounded domains with discrete boundaries”. In: *Journal of Mathematical Analysis and Applications* 24.2 (1968), pp. 326–333. ISSN: 0022-247X. DOI: [http://dx.doi.org/10.1016/0022-247X\(68\)90034-6](http://dx.doi.org/10.1016/0022-247X(68)90034-6). URL: <http://www.sciencedirect.com/science/article/pii/0022247X68900346>.
- [2] Giovanni Alessandrini. “An identification problem for an elliptic equation in two variables”. In: *Annali di Matematica Pura ed Applicata* 145.1 (), pp. 265–295. ISSN: 1618-1891. DOI: 10.1007/BF01790543. URL: <http://dx.doi.org/10.1007/BF01790543>.
- [3] Giovanni Alessandrini. “Stable determination of conductivity by boundary measurements”. In: *Applicable Analysis* 27.1-3 (1988), pp. 153–172.
- [4] Giovanni Alessandrini et al. “Optimal stability for inverse elliptic boundary value problems with unknown boundaries.” English. In: *Ann. Sc. Norm. Super. Pisa, Cl. Sci., IV. Ser.* 29.4 (2000), pp. 755–806. ISSN: 0391-173X.
- [5] Grégoire Allaire, François Jouve, and Anca-Maria Toader. “Structural optimization using sensitivity analysis and a level-set method”. In: *Journal of computational physics* 194.1 (2004), pp. 363–393.
- [6] Habib Ammari, Thomas Boulier, and Josselin Garnier. “Modeling active electrolocation in weakly electric fish”. In: *SIAM Journal on Imaging Sciences* 6.1 (2013), pp. 285–321.
- [7] Habib Ammari and Hyeonbae Kang. *Polarization and moment tensors: with applications to inverse problems and effective medium theory*. Vol. 162. Springer Science & Business Media, 2007.
- [8] Habib Ammari and Hyeonbae Kang. *Reconstruction of small inhomogeneities from boundary measurements*. 1846. Springer Science & Business Media, 2004.
- [9] Habib Ammari, Hyeonbae Kang, and Mikyoung Lim. “Gradient estimates for solutions to the conductivity problem”. In: *Mathematische Annalen* 332.2 (2005), pp. 277–286.

- [10] Habib Ammari and Faouzi Triki. “Identification of an inclusion in multi-frequency electric impedance tomography”. In: *Communications in Partial Differential Equations* just-accepted (2016).
- [11] Habib Ammari, Faouzi Triki, and Chun-Hsiang Tsou. “Numerical determination of anomalies in multifrequency electrical impedance tomography”. In: *arXiv preprint arXiv:1704.04878* (2017).
- [12] Habib Ammari et al. “Conductivity interface problems. Part I: small perturbations of an interface”. In: *Transactions of the American Mathematical Society* 362.5 (2010), pp. 2435–2449.
- [13] Habib Ammari et al. “Decomposition theorems and fine estimates for electrical fields in the presence of closely located circular inclusions”. In: *Journal of Differential Equations* 247.11 (2009), pp. 2897–2912.
- [14] Habib Ammari et al. “Elliptic estimates in composite media with smooth inclusions: an integral equation approach”. In: *Annales Scientifiques de l’École Normale Supérieure* 48.2 (May 2014), pp. 1–50. URL: <https://hal.archives-ouvertes.fr/hal-00997234>.
- [15] Habib Ammari et al. “Estimates for the electric field in the presence of adjacent perfectly conducting spheres”. In: *Quarterly of applied mathematics* 65.2 (2007), pp. 339–356.
- [16] Habib Ammari et al. “Optimal estimates for the electric field in two dimensions”. In: *Journal de mathématiques pures et appliquées* 88.4 (2007), pp. 307–324.
- [17] Habib Ammari et al. “Shape recognition and classification in electro-sensing”. In: *Proceedings of the National Academy of Sciences* 111.32 (2014), pp. 11652–11657.
- [18] Habib Ammari et al. “Spectral theory of a Neumann–Poincaré-type operator and analysis of cloaking due to anomalous localized resonance”. In: *Archive for Rational Mechanics and Analysis* 208.2 (2013), pp. 667–692.
- [19] Habib Ammari et al. “Spectroscopic imaging of a dilute cell suspension”. In: *Journal de Mathématiques Pures et Appliquées* 105.5 (2016), pp. 603–661. ISSN: 0021-7824. DOI: <https://doi.org/10.1016/j.matpur.2015.11.009>. URL: <http://www.sciencedirect.com/science/article/pii/S0021782415001592>.
- [20] Habib Ammari et al. “Target Identification Using Dictionary Matching of Generalized Polarization Tensors”. In: *Foundations of Computational Mathematics* 14.1 (Feb. 2014), pp. 27–62. ISSN: 1615-3383. DOI: [10.1007/s10208-013-9168-6](https://doi.org/10.1007/s10208-013-9168-6). URL: <https://doi.org/10.1007/s10208-013-9168-6>.

- [21] Kazunori Ando, Hyeonbae Kang, and Yoshihisa Miyanishi. “Exponential decay estimates of the eigenvalues for the Neumann-Poincaré operator on analytic boundaries in two dimensions”. In: *arXiv preprint arXiv:1606.01483* (2016).
- [22] Kari Astala and Lassi Päivärinta. “Calderón’s inverse conductivity problem in the plane”. In: *Annals of Mathematics* (2006), pp. 265–299.
- [23] Ellen Shiting Bao, Yan Yan Li, and Biao Yin. “Gradient estimates for the perfect conductivity problem”. In: *Archive for rational mechanics and analysis* 193.1 (2009), pp. 195–226.
- [24] Bartolomé Barceló, Eugene Fabes, and Jin Keun Seo. “The inverse conductivity problem with one measurement: uniqueness for convex polyhedra”. In: *Proceedings of the American Mathematical Society* 122.1 (1994), pp. 183–189.
- [25] MF Ben Hassen and Eric Bonnetier. “Asymptotic formulas for the voltage potential in a composite medium containing close or touching disks of small diameter”. In: *Multiscale Modeling & Simulation* 4.1 (2005), pp. 250–277.
- [26] Eric Bonnetier and Faouzi Triki. “On the Spectrum of the Poincaré Variational Problem for Two Close-to-Touching Inclusions in 2D”. In: *Archive for Rational Mechanics and Analysis* 209.2 (2013), pp. 541–567. ISSN: 1432-0673. DOI: 10.1007/s00205-013-0636-6. URL: <http://dx.doi.org/10.1007/s00205-013-0636-6>.
- [27] Eric Bonnetier and Faouzi Triki. “Pointwise bounds on the gradient and the spectrum of the Neumann–Poincaré operator: the case of 2 discs”. In: *Contemp. Math* 577 (2012), pp. 81–92.
- [28] Eric Bonnetier and Michael Vogelius. “An elliptic regularity result for a composite medium with “touching” fibers of circular cross-section”. In: *SIAM Journal on Mathematical Analysis* 31.3 (2000), pp. 651–677.
- [29] Liliana Borcea. “Electrical impedance tomography”. In: *Inverse problems* 18.6 (2002), R99.
- [30] B Budiansky and GF Carrier. “High shear stresses in stiff-fiber composites”. In: *Journal of applied mechanics* 51.4 (1984), pp. 733–735.
- [31] Alberto P. Calderón. “On an inverse boundary value problem”. en. In: *Computational & Applied Mathematics* 25 (2006), pp. 133–138. ISSN: 1807-0302. URL: http://www.scielo.br/scielo.php?script=sci_arttext&pid=S1807-03022006000200002&nrm=iso.

- [32] Torsten Carleman. “Über das Neumann-Poincaresche problem für ein Gebiet mit Ecken”. In: (1916).
- [33] David Colton and Rainer Kress. *Inverse acoustic and electromagnetic scattering theory*. Vol. 93. Springer Science & Business Media, 2012.
- [34] Oscar M Curet et al. “Aquatic manoeuvring with counter-propagating waves: a novel locomotive strategy”. In: *Journal of The Royal Society Interface* 8.60 (2011), pp. 1041–1050.
- [35] F. Triki E. Bonnetier and C-H. Tsou. “Eigenvalues of the Neumann-Poincaré operator of 2 inclusions with contact of order m : a numerical study”. In: *Journal of Computational Mathematics* (2017 (to appear)).
- [36] F. Triki E. Bonnetier and C-H. Tsou. “Inverse Conductivity Problem: A stable method to determine discs”. In: *preprint, 2016* ().
- [37] Eugene Fabes, Hyeonbae Kang, and Jin Keun Seo. “Inverse conductivity problem with one measurement: Error estimates and approximate identification for perturbed disks”. In: *SIAM Journal on Mathematical Analysis* 30.4 (1999), pp. 699–720.
- [38] Avner Friedman and Victor Isakov. *On the uniqueness in the inverse conductivity problem with one measurement*. Institute for Mathematics and its Applications (USA), 1988.
- [39] J. Powell G. Alessandrini V. Isakov. “Local Uniqueness in the Inverse Conductivity Problem with One Measurement”. In: *Transactions of the American Mathematical Society* 347.8 (1995), pp. 3031–3041. ISSN: 00029947. URL: <http://www.jstor.org/stable/2154768>.
- [40] C Gabriel, A Peyman, and EH Grant. “Electrical conductivity of tissue at frequencies below 1 MHz”. In: *Physics in medicine and biology* 54.16 (2009), p. 4863.
- [41] David Gilbarg and Neil S Trudinger. *Elliptic partial differential equations of second order*. Springer, 2015.
- [42] F. Hecht. “New development in FreeFem++”. In: *J. Numer. Math.* 20.3-4 (2012), pp. 251–265. ISSN: 1570-2820.
- [43] Victor Isakov. *Inverse problems for partial differential equations*. Vol. 127. Springer, 2006.
- [44] Gunther Uhlmann John Sylvester. “A Global Uniqueness Theorem for an Inverse Boundary Value Problem”. In: *Annals of Mathematics* 125.1 (1987), pp. 153–169. ISSN: 0003486X. URL: <http://www.jstor.org/stable/1971291>.

- [45] Hyeonbae Kang, Mikyoung Lim, and KiHyun Yun. “Asymptotics and computation of the solution to the conductivity equation in the presence of adjacent inclusions with extreme conductivities”. In: *Journal de Mathématiques Pures et Appliquées* 99.2 (2013), pp. 234–249.
- [46] Hyeonbae Kang and Jin Keun Seo. “Inverse Conductivity Problem with One Measurement: Uniqueness of Balls in \mathbb{R}^3 ”. In: *SIAM Journal on Applied Mathematics* 59.5 (1999), pp. 1533–1539. doi: 10.1137/S0036139997324595. eprint: <http://dx.doi.org/10.1137/S0036139997324595>. URL: <http://dx.doi.org/10.1137/S0036139997324595>.
- [47] Hyeonbae Kang, Jin Keun Seo, and Dongwoo Sheen. “The inverse conductivity problem with one measurement: stability and estimation of size”. In: *SIAM Journal on Mathematical Analysis* 28.6 (1997), pp. 1389–1405.
- [48] Dmitry Khavinson, Mihai Putinar, and Harold S Shapiro. “Poincaré’s variational problem in potential theory”. In: *Archive for rational mechanics and analysis* 185.1 (2007), pp. 143–184.
- [49] MG Krein. “Compact linear operators on functional spaces with two norms”. In: *Integral Equations and Operator Theory* 30.2 (1998), pp. 140–162.
- [50] Ohin Kwon, Jin Keun Seo, and Jeong-Rock Yoon. “A real time algorithm for the location search of discontinuous conductivities with one measurement”. In: *Communications on Pure and Applied Mathematics* 55.1 (2002), pp. 1–29. issn: 1097-0312. doi: 10.1002/cpa.3009. URL: <http://dx.doi.org/10.1002/cpa.3009>.
- [51] Vincent Lebastard et al. “Underwater robot navigation around a sphere using electrolocation sense and kalman filter”. In: *Intelligent Robots and Systems (IROS), 2010 IEEE/RSJ International Conference on*. IEEE. 2010, pp. 4225–4230.
- [52] Yan Yan Li and Michael Vogelius. “Gradient estimates for solutions to divergence form elliptic equations with discontinuous coefficients”. In: *Archive for Rational Mechanics and Analysis* 153.2 (2000), pp. 91–151.
- [53] Yanyan Li and Louis Nirenberg. “Estimates for elliptic systems from composite material”. In: *Communications on pure and applied mathematics* 56.7 (2003), pp. 892–925.
- [54] X Markenscoff. “Stress amplification in vanishingly small geometries”. In: *Computational Mechanics* 19.1 (1996), pp. 77–83.
- [55] Isaak D Mayergoyz, Donald R Fredkin, and Zhenyu Zhang. “Electrostatic (plasmon) resonances in nanoparticles”. In: *Physical Review B* 72.15 (2005), p. 155412.

- [56] Yoshihisa Miyanishi and Takashi Suzuki. “Eigenvalues and eigenfunctions of double layer potentials”. In: *Transactions of the American Mathematical Society* (2017).
- [57] Peter Moller. *Electric fishes: history and behavior*. Vol. 17. Chapman & Hall, 1995.
- [58] Adrian I. Nachman. “Reconstructions From Boundary Measurements”. In: *Annals of Mathematics* 128.3 (1988), pp. 531–576. ISSN: 0003486X. URL: <http://www.jstor.org/stable/1971435>.
- [59] Jean-Claude Nédélec. *Acoustic and electromagnetic equations: integral representations for harmonic problems*. Vol. 144. Springer Science & Business Media, 2001.
- [60] Scilab Enterprises. *Scilab: Free and Open Source software for numerical computation*. Scilab Enterprises. Orsay, France, 2012. URL: <http://www.scilab.org>.
- [61] W.L. Wendland. *On the double layer potential. Analysis, Partial Differential Equations and Applications: The Vladimir Maz’ya Anniversary Volume*. Vol. 193. Springer Science & Business Media, 2010, pp. 319–334.
- [62] KiHyun Yun. “Optimal bound on high stresses occurring between stiff fibers with arbitrary shaped cross-sections”. In: *Journal of Mathematical Analysis and Applications* 350.1 (2009), pp. 306–312.

Contents

Abstract	xiii
Remerciements	xv
Avertissement	xvii
Sommaire	xix
List of Tables	xxi
List of Figures	xxiii
Introduction	1
Identification of disks in a two dimensional plane	3
Determination of inclusions using multifrequency measurements . .	4
Determination of inclusions in the model of electric fish	5
Eigenvalues of Neumann-Poincaré operator for two close-to-touching inclusions	6
1 Determination of a disk in a two dimensional plane	7
1.1 Introduction	7
1.2 Main Results	8
1.2.1 Generalities	8
1.2.2 Analysis in complex variables	11
1.2.3 Stability estimate	13
1.2.4 Reconstruction from two measurements	21
2 Numerical determination of disks	23
2.1 Optimization algorithm	23
2.2 Numerical examples	27

3	Determination of inclusions using multifrequency measurements	31
3.1	Introduction	31
3.2	Spectral decomposition	32
3.3	Retrieval the frequency part	36
3.4	Asymptotic expansion	40
3.4.1	Expansions of layer potentials	41
3.5	Inclusion reconstruction	46
3.5.1	Optimization algorithm	46
3.6	Numerical examples	47
4	Mathematical model of electroreception	53
4.1	Introduction	53
4.2	The Mathematical Model	55
4.3	Well-posedness of the direct problem	57
4.3.1	Sobolev space $\mathcal{W}^{1,-1}(\Omega_\epsilon)$	57
4.3.2	Well-posedness	59
4.4	The Poincaré Variational Problem	64
4.5	Spectral decomposition of the solution $u(x, \omega)$	68
4.6	Uniqueness and stability estimates	71
5	Numerical identification of the target fish	73
5.1	The mathematical model in a truncated domain	73
5.2	Retrieval of the frequency independent part	75
5.3	Identification of the target fish	78
5.3.1	Shape derivative	79
5.4	Gradient descent algorithms	80
5.5	Numerical experiments	81
6	Spectrum of Neumann-Poincaré operator for two close-to-touching inclusions	89
6.1	Eigenvalues of the Neumann-Poincaré operator for two inclusions	90
6.2	Comparison of T_δ with an operator defined on a bounded domain	96
6.3	Discretization	97
6.4	Numerical results	100
6.4.1	The case of 2 discs	100
6.4.2	Contact of order m	102
6.5	Conclusion	103
	Conclusion	105
	Bibliography	107

Contents 115

Contents 113

TARGET IDENTIFICATION USING ELECTRORECEPTION

Abstract

Electrolocation is the name given to the sensor ability for certain electric fish robots, which are able to detect electrostatic perturbations caused to the presence of some objects in their neighborhood. This ability to interpret an electrical signal to locate itself in space opens important perspectives, including in the field of biologically inspired robotics. Mathematically, electrolocation is linked to the electric impedance tomography: so it's about a non-linear inverse problem, particularly ill-posed problem. We will, in this Phd, study some methods of reconstruction, which could be obtain robustly some characteristic of the obstacle's shape, rather all of their geometry details. So, it's about to study the stability between the observable part of the obstacles and the errors of measurements.

Keywords: inverse problem, conduction equation, electroreception

IDENTIFICATION D'UNE CIBLE PAR L'ÉLECTRO-LOCALISATION

Résumé

L'électro-localisation est le nom donné aux capacités sensorielles de certains poissons électriques, vivant en eaux troubles, capables de détecter les perturbations électrostatiques dues à la présence d'objets dans leurs voisinages. Cette aptitude à interpréter un signal électrique pour se repérer dans l'espace ouvre l'importance perspectives, notamment dans le domaine de la robotique bio-inspiré. Mathématiquement, l'électro-localisation est proche de la tomographie d'impédance électrique : il s'agit donc d'un problème inverse non linéaire, notoirement mal posé. Nous proposons dans cette thèse d'étudier des méthodes de reconstruction qui permettraient d'obtenir de manière robuste certaines caractéristiques de la forme des obstacles, plutôt que l'ensemble des détails de leurs géométries. Il s'agit donc d'étudier la stabilité de la partie observable des obstacles par rapport à des erreurs dans les mesures.

Mots clés : problème inverse, équation de conduction, électro-localisation

Laboratoire Jean Kuntzmann

Bâtiment IMAG – Université Grenoble Alpes – 700 Avenue Centrale – 38401
Domaine Universitaire de Saint-Martin-d'Hères – France